Carbon-carbon double-bond shift in the biosynthesis of the antibiotic corallopyronin A

CorJ DH*: a shift domain

Dissertation

zur

Erlangung des Doktorgrades (Dr. rer. nat.)

der

Mathematisch-Naturwissenschaftlichen Fakultät

der

Rheinischen Friedrich-Wilhelms-Universität Bonn

vorgelegt von

Diplom-Pharmazeutin (Dipl.-Pharm.)

Friederike Lohr

aus

Haan

Bonn 2014

Angefertigt mit Genehmigung der Mathematisch-Naturwissenschaftlichen Fakultät der Rheinischen Friedrich-Wilhelms-Universität Bonn

1. Referentin	:	Prof. Dr. G. M. König
2. Referent	:	Prof. Dr. M. Gütschow
Tag der Promotion	:	16. Dezember 2015
Erscheinungsdatum	:	2015

Für meine Eltern und Maxim.

Publications

Ö. Erol, T. F. Schäberle, A. Schmitz, S. Rachid, C. Gurgui, M. El Omari, F. Lohr, S. Kehraus, J. Piel, R. Müller, G. M. König; **Biosynthesis of the myxobacterial antibiotic corallopyronin A**. *Chem Bio Chem* 2010, 11, 1253–1265

M. Frizler, F. Lohr, N. Furtmann, J. Kläs, M. Gütschow; **Structural optimization of azadipeptide nitriles strongly increases association rates and allows the development of selective cathepsin inhibitors**. *J Med Chem* 2011, 54, 396–400

M. Frizler, F. Lohr, M. Lüllsdorf, M. Gütschow; **Facing the gem-dialkyl effect in enzyme inhibitor design: preparation of homocycloleucine-based azadipeptide nitriles**. *Chemistry* **2011**, 17, 11419–11423

A. Schmitz, S. Felder, T. Höver, S. Kehraus, F. Lohr, G. M. König, T. F. Schäberle; **Antibiotics from gliding bacteria**. *Phytochem. Rev.* **2013**, 12, 507–516

F. Lohr, I. Jenniches, M. Frizler, M. J. Meehan, M. Sylvester, A. Schmitz, M. Gütschow, P. C. Dorrestein, G. M. König, T. F. Schäberle; **alpha, beta –> beta, gamma double-bond migration in corallopyronin A biosynthesis**. *Chem Sci* **2013**, 4, 4175–4180

T. F. Schäberle, M. Mir Mohseni, F. Lohr, A. Schmitz, G. M. König; **Function of the loading module in CorI and of the O-methyltransferase CorH in vinyl carbamate biosynthesis of the antibiotic corallopyronin A**. *Antimicrob. Agents Chemother.* **2014**, 58, 950–956

T. F. Schäberle, F. Lohr, A. Schmitz, G. M. König; **Antibiotics from Myxobacteria.** DOI:10.1039/C4NP00011K.

Conferences

International VAAM (Vereinigung für angewandte und allgemeine Mikrobiologie)-Workshop **2010** „Biology of bacteria producing natural products“; 26–28 september 2010 in Tübingen, Germany. Poster presentation: “Biosynthesis of the myxobacterial antibiotic corallopyronin A”. Abstract published in program & abstract book International VAAM-Workshop 2010 “Biology of bacteria producing natural products”.

International VAAM (Vereinigung für angewandte und allgemeine Mikrobiologie)-Workshop **2011** „Biology of bacteria producing natural products“; 28–30 september 2011 in Bonn, Germany.

XIV International symposium on marine natural products (MaNaPro) **2013**, 8 ECMNP (European conference on marine natural products); 15–20 september 2013 in La Toja Island, Spain. Poster presentation: “Investigation of the double-bond shift in corallopyronin A biosynthesis”. Abstract published in program & abstract book XIV International symposium on marine natural products.

Internationale DPhG-Doktorandentagung **2014**; 10–12 march 2014 in Wuppertal, Germany. Oral presentation: “Investigation of the double-bond shift in corallopyronin A biosynthesis”. Abstract published in program & abstract book Internationale DPhG-Doktorandentagung 2014.

Workshop

International workshop for young researchers **2013**; 10–12 july 2013 in Lille-Villeneuve d’Ascq, France. Bioinformatics tools for NRPS discovery: from genomic data to the products.

Further professional education

Fortbildungsveranstaltung zur Ausbildung von Projektleitern und Beauftragten für biologische Sicherheit nach §15 (2) und (4) GenTSV **2012**; 25–27 september 2012 at the University of Cologne, Germany.

Danke!

Ich möchte meinen besonderen Dank meiner Doktormutter Frau Professorin König aussprechen, dafür dass sie mich in ihre Arbeitsgruppe aufgenommen hat und mir die Möglichkeit gegeben hat, auf dem vielseitigen Feld der bakteriellen Biosynthese zu arbeiten. Ich möchte ihr sehr dafür danken, dass sie mir während meiner praktischen Arbeit und während des Schreibens der Dissertation immer zur Seite stand, wissenschaftlich und persönlich.

Herrn Professor Gütschow möchte ich zum einen für die erfolgreiche Kooperation im Bereich der hier beschriebenen Synthese und zum anderen für die Bereitschaft zur Übernahme des Coreferats dieser Arbeit danken.

Frau Professorin Wägele und Herrn Professor Wagner danke ich für ihre Bereitschaft Teil der Prüfungskommission zu sein.

Meinem Freund Dr. Maxim Frizler möchte ich an dieser Stelle herzlich für seinen Einsatz bei der Synthese des in dieser Arbeit verwendeten Substrats danken, welche im Rahmen der Kooperation mit dem Arbeitskreis von Professor Gütschow durchgeführt wurde. Ich bin ihm dankbar für etliche wissenschaftliche Diskussionen und für seine liebevolle Unterstützung zu jeder Zeit. Danke.

Bei Herrn Dr. Marc Sylvester (Institut für Biochemie und Molekularbiologie der Uni Bonn) möchte ich mich für die massenspektrometrischen Messungen im Rahmen des „ppant ejection assays“ bedanken.

Herrn Dr. Till Schäberle danke ich für die Betreuung während meiner Promotion, für viele konstruktive Diskussionen und für das Korrekturlesen einiger Teile meiner Arbeit.

Herrn Dr. Stefan Kehraus möchte ich für die Unterstützung bei allen HPLC- und NMR-Fragen und für die Aufnahme von NMR Spektren in der Pharmazeutischen Chemie danken. Vielen Dank auch für das Korrekturlesen einiger Teile meiner Arbeit.

Bei Frau Edith Neu möchte ich mich für die Einführung in das Arbeiten mit Myxobakterien, besonders deren Isolierung und Kultivierung, bedanken. Frau Ekatarina Eguereva danke ich für LC/MS Messungen und Frau Mila Goralski für Tips und Hilfestellungen im S1 Labor. Allen dreien danke ich von Herzen für eine richtig schöne Zeit.

Ich danke Herrn Thomas Kögler für seine Hilfe bei Problemen aller Art mit dem Computer und anderen technischen Geräten.

Den Damen Kirsten Knapp und Annika Orland danke ich für die voranbringende Zusammenarbeit während der Promotion und noch viel mehr für ihre Freundschaft.

Den Herren Alexander Bogdanov, Stephan Felder, Henrik Harms und Peter Hufendiek möchte Danke sagen für die Unterstützung bei HPLC und NMR Fragen, für manches gemeinsam getrunkene Bier und für eine tolle Zeit.

Allen Kollegen und Kolleginnen des Arbeitskreises der Pharmazeutischen Biologie in Bonn danke ich herzlich für die gute Zusammenarbeit, für vielseitige Gespräche und für die ausgewogene Mischung aus lustiger und konzentrierter Arbeitsatmosphäre.

Meiner Mutter danke ich für das Korrekturlesen der Arbeit.

Meinen Eltern und Maxim danke ich für ihren Glauben an mich, der mir immer sicher ist und der alles leicht macht.

Abbreviations

A	Alanine
A domain	Adenylation domain
AT	Acyltransferase
ACP	Acyl-carrier protein
°C	Degree Celsius
1D	One-dimensional
2D	Two-dimensional
∂	NMR chemical shift (ppm)
ε	Extinction coefficient (UV/VIS spectroscopy)
λ	Wavelength (nm)
µ	Micro (10^{-6})
br	Broad
c	Concentration
CID	Collision-induced dissociation
CoA	Coenzyme A
COSY	Correlated spectroscopy
CP	Carrier protein
CYP	Cytochrome
d	Doublet (in connection with NMR data)
D	Aspartat
Da	Dalton
DH	Dehydrogenase domain
DAD	Diode array detector
DCM	Dichloromethane
DEPT	Distortionless enhancement by polarisation transfer
DMAP	4-Dimethylaminopyridine
DMSO	Dimetyhlsulfoxide
DNA	Deoxyribonucleic acid
EDTA	Ethylenediamine-tetraacetic acid

e.g.	„Exempli gratia“ (Latin); for example
EE	Ethylacetat
ER	Enoylreductase v
EtOH	Ethanol
ESI	Electro spray ionisation
et al.	„Et alii“ (Latin); and others
H	Histidine
h	Hour
H/D	Proton/deuterium
HMBC	Heteronuclear multiple-bond correlation
HMG	Hydroxymethylglutaryl
HPLC	High performance liquid chromatography
HSQC	Heteronuclear single quantum correlation
Hz	Hertz
IC_{50}	Inhibitory concentration - concentration of a drug that is required for 50 % inhibition of viral replication, protein binding etc.
i.e.	„Id est“ (Latin); that is
J	Spin-spin coupling constant [Hz]
KR	Ketoreductase domain
KS	Ketosynthase domain
kbp	Kilo base pairs
L	Leucine
L	Litre
log	Decadic logarithm
m	Multiplet (in connection with NMR data)
M	Molar (mol/L)
M_r	Molecular mass
max	Maximum
min	Minute
MeOH	Methanol

MHz	Megahertz
MIC	Minimal inhibitory concentration
MRSA	Methicilline resistant *Staphylococcus aureus*
MS	Mass spectrometry
mult.	Multiplicity
m/z	Mass-to-charge ratio
N	Asparagine
n.d.	Not determined
n.i.	Not investigated
NMR	Nuclear magnetic resonance
No.	Number
NRPS	Nonribosomal peptide synthetase
P	Proline
ppm	Parts per million
PCR	Polymerase chain reaction
PE	Petroleum ether
pH	Potentia hydrogenii
PKS	Polyketide synthase
ppant	Phosphopantethein
pant	Pantethein
q	Quartet (in connection with NMR data)
R	Residue (in combination with chemical structures)
rpm	Rounds per minute
RNA	Ribonucleic acid
RNAP	RNA Polymerase
RP	Reversed phase
rt	Room temperature
R_t	Retention time
s	Singlet (in connection with NMR data)
SAM	S-Adenosyl-L-methionine

SDS	Sodium dodecyl sulfate
SNAC	*N*-acetylcysteamine
t	Triplet (in connection with NMR data)
Taq aquaticus	Thermostable polymerase from the thermophilic bacterium *Thermus*
TEMED	Tetramethylethylendiamin
TFA	Trifluoroacetic acid
Tris	Tris(hydroxymethyl)-aminomethan
UV	Ultraviolet
VIS	Visible

1 Introduction[1]

The increased emergence of bacteria resistant to antibiotics is a serious threat to modern medicine (Schäberle and Hack, 2014). The successful treatment of bacterial infections is in danger, since ever more multi-, and even pan-resistant bacteria evolve. This development is aggravated by the fact that, since the golden age of antibiotics in the 70ies, the number of new antibiotically active drugs introduced into therapy is dramatically dwindling. Therefore, research to identify new putative antibiotics has to be pursued and intensified. Natural products, especially microbe-derived compounds, proved themselves as a good source for antibiotics. Besides the well-known proliferative producer organisms like the streptomycetes and bacilli, currently myxobacteria move into the focus. This group of bacteria synthesises structurally diverse secondary metabolites, distinct from the classes known so far from traditional antibiotic producers. An example for a myxobacterial metabolite successfully introduced into therapy, albeit in another therapeutic area, is the anti-cancer drug ixabepilon, a derivative of the myxobacterial metabolite epothilone, which was launched in 2007 (Thompson, 2007). Interestingly, many myxobacterial compounds showing promising antibacterial activities were identified to date, however none of these was further developed as a drug.

In this review all myxobacterial compounds with antibiotic activity, which could serve as lead structures for future developments are discussed, according to their mode of action.

1.1 Myxobacterial antibiotics that target bacterial RNA polymerase

Bacterial RNA polymerase (RNAP) is an established target for antibiotics (Chopra, 2007; Ho et al., 2009; Mariani and Maffioli, 2009; Villain-Guillot et al., 2007). It is an essential enzyme and well suited for the attack of antibiotics, since the bacterial subunits are highly conserved, but differ from the eukaryotic ones. This way, such antibiotics are highly selective, have a broad-spectrum activity and low toxicity. RNAP-inhibitors in clinical use are the rifamycins, natural products and their derivatives originating from actinomycetes, which are of particular importance in the

[1] The introduction is published in Schäberle et al., 2014; Antibiotics from myxobacteria.

treatment of tuberculosis. Other infections are also amenable to therapy with rifamycins, *e.g.* in infections with *Bacillus anthracis* (inhalation anthrax) a combination therapy using a rifamycin together with ciprofloxacin or doxycycline proved successful in the 2001 anthrax attacks (Srivastava et al., 2011). Fidoxamicin, another RNA synthesis inhibitor was only recently approved for *Clostridium difficile* infections (Artsimovitch et al., 2012).

Up to date four antibiotics and their corresponding derivatives are known from myxobacteria, which inhibit bacterial RNAP, namely corallopyronin A, myxopyronin A, ripostatin A, and sorangicin A.

1.1.1 Corallopyronins and myxopyronins

Corallopyronins were first isolated in 1985 from a *Corallococcus coralloides* strain from Tunisia (Jansen et al., 1985). Corallopyronin A (**I**) has several interesting structural features. A pyrone ring forms the central rigid core of the molecule, to which two conformationally more flexible chains are attached, *i.e.* the lipophilic western chain with three methyl groups, a hydroxyl group, and a diene element, and the eastern chain with one methyl group, an enamide function, and a methyl carbamate moiety. Carbamates are a rarely found structural moiety in secondary metabolites from bacteria.

Three analogues are known, *i.e.* corallopyronin A´ (**III**), corallopyronin B (**II**) and corallopyronin C (**IV**). The double-bond $\Delta^{19,20}$ is *Z*-configurated in corallopyronin A', whereas in the main metabolite corallopyronin A the configuration of this double-bond is *E*. Corallopyronin A´ may be an artefact formed during isolation and storage of corallopyronin A. Corallopyronin B differs from A in the western chain by an additional methylene group, assumed to be derived from the respectively incorporated starter unit, *i.e.* a propionyl instead of an acetyl moiety, during the biosynthesis of this chain (Erol et al., 2010). Corallopyronin C is characterized by a tetrahydrofuran ring in the western chain. However also in this case, it cannot be excluded that corallopyronin C is an artefact of the isolation process, and might be formed through a reaction of the C-24 hydroxyl group of corallopyronin A with the diene motif.

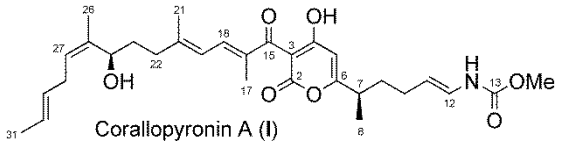

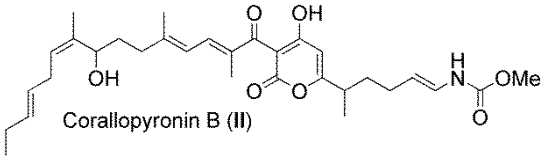

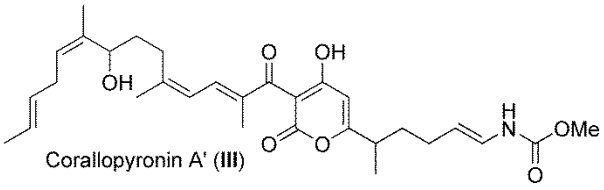

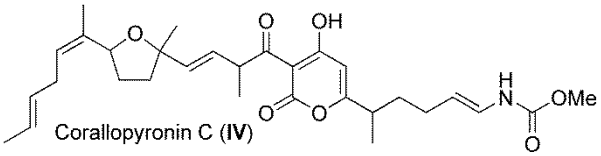

Beside the above mentioned analogues, further structures related to the corallopyronins were published already in 1983, called myxopyronin A (**V**) and B (**VI**) (Kohl et al., 1983). These were isolated from a *Myxococcus fulvus* strain, and share the eastern chain and the central pyrone ring with corallopyronin A, but in the case of the myxopyronins the non-hydroxylated western chain is shorter, and terminated for myxopyronin A at the respective corallopyronin carbon C-24, and for myxopyronin B at the respective corallopyronin-carbon C-25.

Due to their close structural relationship, which is also reflected in the genomic organisation of the recently published biosynthetic gene clusters encoding the corallopyronins (Erol et al., 2010) and the myxopyronins (Sucipto et al., 2013) biosynthesis, these α-pyrone antibiotics can be considered jointly in the following paragraphs. Feeding experiments with ^{13}C-labelled precursors gave first biosynthetic insights (Erol et al., 2010). The resulting labelling pattern allowed the conclusion, that these antibiotics are constructed from two chains, which are interconnected to form the central pyrone motif (Erol et al., 2010; Irschik et al., 1983a, 1985; Kohl et al., 1984; Schmitz et al., 2013). The two chains creating the backbone of the molecules are synthesized by a mixed non-ribosomal peptide synthetase/polyketide synthase (NRPS/PKS) hybrid system (Erol et al., 2010; Sucipto et al., 2013), whereby the PKS is of the *trans*-acyltransferase (AT) type (Piel, 2010). Indeed, 11 intact acetate units and a glycine moiety are incorporated into the corallopyronin A backbone. The methyl groups originate partially from *S*-adenosyl-L-methionine (SAM), but also from acetate, whereby in the latter case C-2 of acetate is incorporated via a β-branching mechanism (Erol et al., 2010). The formation of the methyl carbamate (*i.e.* C-13) unit is most unusual, and until recently only little was known concerning its biosynthesis. Feeding

experiments with [^{13}C]bicarbonate suggested that carbonic acid is the origin of C-13 in corallopyronin A biosynthesis. The published biosynthetic gene cluster (Erol et al., 2010) confirmed the labelling studies and opened up possibilities to analyse specific features of the biosynthesis in detail. Thus, further experimental data for the incorporation of the unusual starter carbonic acid (or its methyl ester) (Schäberle et al., 2014a), as well as for the biochemical basis of an α,β to β,γ double-bond shift in corallopyronin A biosynthesis were obtained. The latter involved a shift of the double bond $\Delta^{10,11}$ in the precursor molecule of corallopyronin A to the $\Delta^{11,12}$ position due to the action of the shift domain DH*, encoded in module 3 of the PKS/NRPS cluster (Kusebauch et al., 2010; Lohr et al., 2013; Moldenhauer et al., 2010).

Total chemical syntheses were successfully performed for myxopyronin A and B in 1998 (Hu et al., 1998), followed by the synthesis of derivatives of myxopyronin B (Doundoulakis et al., 2004; Lira et al., 2007). For the corallopyronins with the more complex western chain it took much longer, but finally in 2012 a complete chemical access to the molecule was published (Rentsch and Kalesse, 2012).

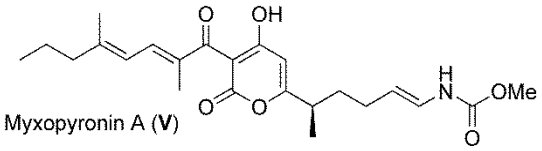

Myxopyronin A (**V**)

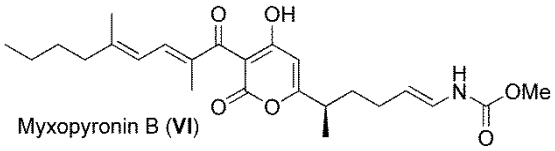

Myxopyronin B (**VI**)

Antibiotic activity of corallopyronins and myxopyronins. Corallopyronin A was assayed toward a series of microorganisms, and showed promising activity against Gram-positive bacteria with MIC values in the range of 0.097 µg/mL (*Staphylococcus aureus*) and 0.39 µg/mL (*Bacillus megaterium*) (Irschik et al., 1985). Corallopyronin B was less active in the same test systems with MIC values of 0.39 µg/mL (*S. aureus*) and 3.1 µg/mL (*B. megaterium*), respectively. Corallopyronin C (respective MICs 0.78 and 6.25 µg/mL) and the double bond isomer corallopyronin A´ (respective MICs 0.78 and 1.56 µg/mL) were much less active. The corallopyronins did not show antibiotic activity against Gram-negative bacteria, apart from the mutant *Escherichia coli* strain tolC, which is a hypersensitive phenotype due to the absence of the efflux protein TolC.

The antibiotic profile of the myxopyronins was comparable, whereby the activity was not as high as that of corallopyronin A. Myxopyronin B performed better than myxopyronin A (MIC MyxA 1.0 and 6.0 µg/mL; MIC MyxB 0.3 and 0.8 µg/mL against *S. aureus* and *B. megaterium*, respectively) (Irschik et al., 1983a). In the initial activity assessments in the 80ies neither activity of the myxopyronins, nor of the corallopyronins was observed against *Mycobacterium phlei* (Irschik et al., 1983a, 1985). Our recent evaluation of corallopyronin A required 64 µg/mL in Müller-Hinton medium and 128 µg/mL of corallopyronin A in Lysogeny Broth medium to inhibit *Mycobacterium smegmatis*. An MIC of 16 µg/mL of corallopyronin A was determined for the sensitive strain *Mycobacterium bovis* Bacillus Calmette-Guérin (BCG), the latter causing animal tuberculosis with only subordinate relevance for human tuberculosis (Ayele et al., 2004; Schiefer et al., 2012). Furthermore, we observed an MIC value of 0.25 µg/mL toward a methicillin resistant (MRSA) strain of *S. aureus* SG 511 (Institute collection of IMMIP, University of Bonn, Germany) (Schmitz, 2013). It should be noted, that the recently determined MICs toward *S. aureus* are much higher as the ones described in 1985, but nevertheless in a very promising range. In our experiments the MIC against *Micrococcus luteus* H78S 1–3 was found to be 0.5 µg/mL while toward *Bacillus subtilis* 168 instead, an MIC of 32 µg/mL was determined (Rentsch and Kalesse, 2012). The low sensitivity of *B. subtilis* towards pyrone antibiotics was also noted in another study, in this case using racemic myxopyronin B, which produced only slight inhibition zones in disk diffusion assays at a concentration of 30 µg/ml (Yakushiji et al., 2013).

The activity of corallopyronin A was further determined against *Wolbachia* species, intracellular bacteria of nematodes (Schiefer et al., 2012). These Gram-negative proteobacteria of the order Rickettsiales are obligate endosymbionts of nematodes, and considered as a novel target for controlling filarial infections like lymphatic filariasis or onchocerciasis (Taylor et al., 2010). As one of a multitude of screened substances, corallopyronin A proved itself to be *in vivo* active. In the model applied, mice were infected with the filarial nematode *Litomosoides sigmodontis*. Beginning the day after the infection, mice were untreated or given intraperitoneal injections containing corallopyronin A (35 mg/kg/day) for 28 days. Five weeks post infection, worms were recovered from the pleural cavity and depletion of *Wolbachia* was

monitored by qPCR. More than 99 % of *Wolbachia* were depleted from *L. sigmodontis* worms after corallopyronin A treatment ($P < 0.0001$ compared with untreated) (Schiefer et al., 2012). This treatment does finally also kill the nematodes, since they are dependent on their bacterial symbionts. It should be emphasised that, the antibiotic is *in vivo* effective against intracellular *Wolbachia* despite the many boundaries, and membranes the drug has to penetrate, like blood vessels, pleura, worm cuticle, worm cells, vesicles, *Wolbachia* inner and outer membranes (Schäberle et al., 2014b; Schiefer et al., 2012). Toxicity in mice was not detected up to the maximum tested of 100 mg/kg (Irschik et al., 1983a).

The low activity against mycobacteria may here be regarded as an advantage of corallopyronin A, since it opens up the possibility to develop a drug for filariasis elimination without concern for cross-resistance development in tuberculosis (Schäberle et al., 2014b; Schiefer et al., 2012).

A report in 2009 stated that no activity was observed for corallopyronin A in a *S. aureus* sepsis model in mice after parenteral dosage, but no experimental details for the respective experiments were given. The authors assumed that the lack of *in vivo* activity was due to high serum protein binding (Haebich and von Nussbaum, 2009). Indeed, in a later study Moy et al. described that the MIC of myxopyronin B toward *S. aureus* increased > 128-fold in the presence of human serum albumin (Moy et al., 2011). In the light of the above discussed *in vivo* experiments, however, corallopyronin A has to be judged as very promising for further development at least as an antinematodal agent targeting intracellular *Wolbachia*.

Mode of action. The mode of action of these natural products was determined by studying, protein, RNA and DNA synthesis in antibiotic treated *S. aureus* cells by adding the radioactive precursors [U-^{14}C]leucine, or [2-^{14}C]uracil, or [U-^{14}C]thymidine. The result of these incorporation experiments showed that thymidine incorporation was not affected, while leucine and uracil incorporation decreased. The reduction of leucine incorporation was clearly delayed with respect to the immediate inhibiting effect on uracil-incorporation. Thus, inhibition of RNA synthesis was suggested as primary target. Consequently, the influence of myxopyronin A directly on the enzyme RNAP of *Thermus thermophilus* was determined in *in vitro* experiments. It was found that myxopyronin A acts specifically on bacterial RNAP, while the corresponding

eukaryotic enzyme was not affected even at the highest concentration tested, *i.e.* up to 200 µg/mL myxopyronin A and 40 µg/mL corallopyronin A, respectively (Irschik et al., 1983a, 1985). Interestingly, corallopyronin A inhibited the growth of rifampin-resistant *S. aureus* (O'Neill et al., 2000). Therefore, it was concluded that corallopyronin A must address a new binding pocket on RNAP and thus represented a novel mode of action. Subsequent X-ray analysis and biochemical data on *T. thermophilus* RNAP complexed with myxopyronin A, and independently of a desmethyl derivative of myxopyronin B, revealed the mode of action of these antibiotics on the molecular level (Belogurov et al., 2008; Mukhopadhyay et al., 2008).

Mukhopadhyay *et al.* showed that myxopyronin A interacts with the RNAP ''switch region'', *i.e.* the hinge that mediates opening and closing of the RNAP active centre cleft (Mukhopadhyay et al., 2008). By this binding the correct interaction of RNAP with the template promoter DNA is prevented. It was further suggested that myxopyronin A acts by inhibiting transcription initiation, since inhibition requires myxopyronin-RNAP-interaction prior to interaction with promoter DNA. Thus, it was proposed that myxopyronin A interferes with the opening and closing of the RNAP clamp by jamming the hinge. Belogurov *et al.* also found desmethyl myxopyronin B binding to the same pocket deep inside the RNA polymerase clamp head domain (Belogurov et al., 2008). Through this binding the interaction with the DNA template in the transcription bubble is disturbed and might compromise binding to, or directly clash with, the melted template DNA strand (Belogurov et al., 2008). Footprinting data showed that promoter DNA is indeed melted, but that its propagation towards the active site is blocked.

The X-ray structures pictured that adjacent to the myxopyronin A binding pocket an additional hydrophobic pocket is situated (Belogurov et al., 2008). This organization may provide an explanation for the decrease of antibiotic activity going along with a decrease in length of the western chain. It seems that a complete jamming of the binding pocket infers more efficient with the hinge region, and consequently results in a better antibiotic activity. Modelling corallopyronin A into *Wolbachia* RNAP indicated that the binding pockets analysed by Mukhopadhyay *et al.*, and by Belogurov *et al.*, for myxopyronins, were completely occupied, explaining the

superior activity of the molecule (Schiefer et al., 2012). Correspondingly, the weaker activity of corallopyronin B, possessing a longer western chain may result in partial repulsion, since this molecule seems already too large.

The detailed knowledge on the binding mode of myxopyronin on RNAP was taken by several studies as a starting point for a structure-based ligand design of novel RNAP inhibitors. Described are either hybrid compounds, which include structural features of the myxopyronins (Sahner et al., 2013; Yakushiji et al., 2013) or molecules with a pyridyl-benzamide skeleton (McPhillie et al., 2011) or so-called squaramide derivatives (Buurman et al., 2012) which are structurally completely different to the respective natural product. All synthesized compounds that were found based on this approach are considerably less active than the natural products.

Besides the RNAP-inhibiting effect, the α-pyrone-containing antibiotics might also possess an additional mechanism of action, since inhibitory effects on fatty acid synthesis were shown for antibiotic agents with an α-pyrone moiety (Giddens et al., 2008). Further, **1** slightly induced the *fabHB* biosensor that is responsive to inhibition of fatty acid biosynthesis (Mariner et al., 2011).

Resistance development. Resistance development is well described for the RNAP-targeting rifamycins (Wehrli and Staehelo, 1971). Likewise resistance can develop against the above described inhibitors of the RNAP switch region by mutations of the RNAP resulting in a change of the respective binding pocket (Mariner et al., 2011; Moy et al., 2011; Srivastava et al., 2011). Despite this observation, it would be worthwhile considering whether the corallopyronin-type antibiotics could be useful in combination therapy, as well known for the rifamycins. In this context it is also of interest – as mentioned above – that there is no concern about cross-resistance in tuberculosis-causing pathogens. Corallopyronin A is now in the focus of a translational project to be developed as a drug for filariasis elimination (Annual report 2012 of the German Centre for Infection Research).

1.1.2 Ripostatins

Ripostatin A–C were isolated from *Sorangium cellulosum* So ce377 (**VII**–**IX**) (Augustiniak et al., 1996; Irschik et al., 1995). Ripostatin A (**VII**) and B (**VIII**) are 14-membered macrolides with three 2,5,8-positioned double-bonds, whereas ripostatin

C (**IX**) is a non-cyclised derivative. All ripostatins have a terminal phenyl ring. Ripostatin A, which occurs in methanolic solution as a mixture of ketone (**VIIa**) and hemiketal (**VIIb**) forms can be chemically transformed into the B form by reduction, and into the C form by base-catalysed elimination (Schleicher and Jamison, 2013). To verify the biosynthetic origin of the ripostatins, feeding experiments with sodium [l-^{13}C]acetate, [1,2-$^{13}C_2$]acetate, [1-^{13}C]propionate, [l-^{13}C]phenylacetate, [$^{13}CH_3$]methionine and [2-^{13}C]phenylalanine were performed. Only phenylalanine was incorporated to result in a phenylethyl moiety (corresponding to the C-19–C-26 segment in **VII**) (Augustiniak et al., 1996), a fact which speaks for a specific adenylation domain involved in the biosynthesis. Carbon C-17, C-18 and C-30 result from a propionate building block, whereas all other carbon atoms in the molecule were acetate derived (Augustiniak et al., 1996). Thus, C-29 has to be incorporated by a β-branching mechanism, comparable to the methyl groups C-21 and C-26 in corallopyronin A biosynthesis. Ripostatins are thus polyketides, largely assembled from acetate, and one unit of each, propionate and phenylalanine. A biosynthetic gene cluster, supposedly a PKS/NRPS cluster, was not yet assigned.

Synthetic chemists showed great interest in the ripostatins. In 2012 four publications dealt with the total synthesis of ripostatin A and B. The overall yields of the three contemporaneous, independent efforts were for ripostatin B 4 % (14 steps in the longest linear sequence (Winter et al., 2012), 0.22 % (18 steps) (Tang and Prusov, 2012a), 3.6 % (21 steps) (Glaus and Altmann, 2012) and for ripostatin A 5 % (14 steps) (Tang and Prusov, 2012b).

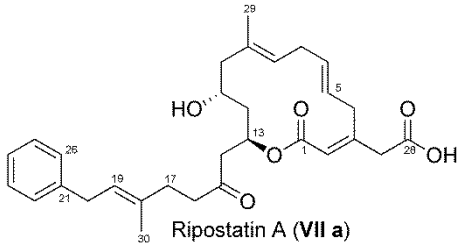

Ripostatin A (**VII a**)

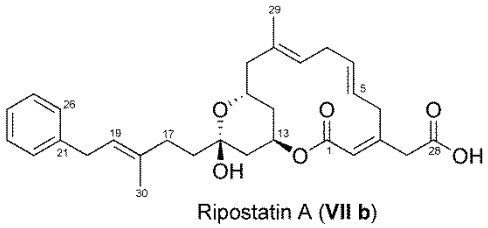

Ripostatin A (**VII b**)

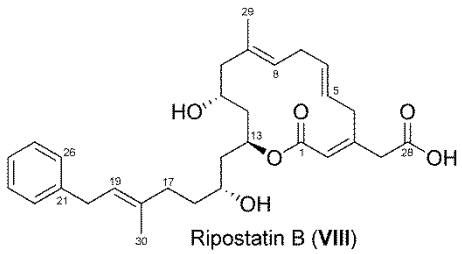

Ripostatin B (**VIII**)

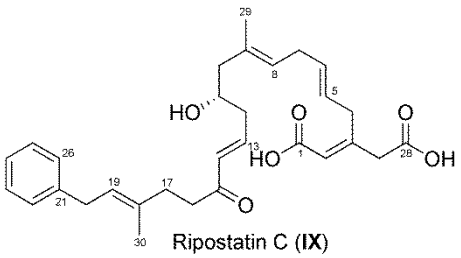

Ripostatin C (**IX**)

Antibiotic activity. The two compounds **VII** and **VIII** showed nearly the same antimicrobial activity against certain Gram-positive bacteria, mainly *S. aureus* strains, and toward *E. coli* tolC with MICs in the range of about 1 µg/mL. Ripostatin B displayed additionally minor activity against several yeasts and fungi (MIC 20 µg/mL against *Nadsonia fulvescens* and 80 µg/mL against *Debaryomyces hansenii*, respectively) (Irschik et al., 1995). The acyclic ripostatin C is biologically inactive (Augustiniak et al., 1996). Furthermore, it was found that no cross-resistance occurs between ripostatins and rifampin or sorangicin (Irschik et al., 1995). Indeed, ripostatin A was effective against rifampin-resistant bacteria harbouring point mutations in the *rpoB* gene sequence coding for their RNAP (Moy et al., 2011). Ripostatin A showed no inhibitory effect on wheat germ RNAP II at a concentration of 20 µg/mL. However, when applied to mouse fibroblasts L929 cells (10 µg/disc) an inhibition zone of 74 mm indicated a toxic effect (Irschik et al., 1995). No other toxicity data are known. Ripostatin A and B, even though being RNAP inhibitors such as the rifamycins, seem to have no activity towards mycobacteria (Irschik et al., 1995).

Mode of action. In *S. aureus* cultures treated with ripostatin A (**VII**) RNA synthesis was completely blocked (Irschik et al., 1995). The antibiotic also inhibited isolated *E. coli* RNAP with an IC_{50} of 0.1 µg/mL (complete inhibition at 50 µg/mL). The earlier assumption that the ripostatin binding site differs from the one of the rifamycins was confirmed by analysing the cross-resistance patterns of mutagenized *E. coli* RNAP with myxopyronin A, corallopyronin A, ripostatin A, and rifampin, respectively. Thus, based on the *Thermus thermophilus* RNAP-myxopyronin A X-ray structure, it was concluded that despite lack of structural similarity between the ripostatins and the α-pyrone antibiotics, both target the RNAP switch region – a binding site different to that of the rifamycin antibacterial agents (Mukhopadhyay et al., 2008).

Overall, there may be a risk of toxicity concerning the ripostatins. Since the published data are not extensive, a detailed *in vitro* evalution would be valuable though.

1.1.3 Sorangicins

The sorangicin antibiotics, as the ripostatins, also originate from a myxobacterial strain of the genus *Sorangium*. Fermentation of *S. cellulosum* So ce12 yielded, by activity based screening, sorangicin A (**X**), the desoxygenated variant sorangicin B (**XI**),

as well as some respective glycosides, called sorangiosides (**XII**,**XIII**) (Irschik et al., 1987; Jansen et al., 1989a, 1989b). Further sorangicin isomers were reported (A_1, A_2, A_3, C_1, C_2, C_3, C_4) (Jansen et al., 1989a). The core structure comprises a large macrocyclic hydroxylacton with seven, in part conjugated carbon-carbon double bonds. Incorporated in the macrocyle are three pyran rings, one trisubstituted dihydro-, and two tetrasubstituted tetrahydro-pyran rings, with one of the latter also being part of a tetrahydro-furan ring.

The corresponding polyketide biosynthetic gene cluster was identified and comprises over 120 kb (Irschik et al., 2010). Comparison to the available genome sequence of strain *S. cellulosum* So ce56 suggested that the gene cluster forms a genetic island, since the flanking genes in So ce12 are located sequentially within the So ce56 genome. Detailed annotation of the seven large PKS-coding genes revealed a *trans*-AT PKS system (Piel, 2010) consisting of 23 modules (Irschik et al., 2010).

Chemical synthesis of the structurally complex molecule sorangicin A was achieved using mild conditions for the critical macrocyclisation, to obtain the macrolactone in the desired configuration (Smith et al., 2009). Further synthetic studies were published, some of which also target partial structures of the sorangicins (Crimmins et al., 2011; Lee et al., 2012; Mohapatra et al., 2010).

Antibiotic activity. Sorangicin A and B, the most abundant metabolites, showed strong inhibitory effects predominantly against Gram-positive bacteria, including mycobacteria, with MIC values from 0.01 µg/mL against *Nocardia corallina* to 0.08 µg/mL toward *Mycobacterium phlei* (Irschik et al., 1987). At higher concentrations also Gram-negative bacteria were inhibited, *e.g.* MIC for *E. coli* was 16 µg/mL for sorangicin A and 6 µg/mL for sorangicin B, respectively (Irschik et al., 1987). Myxobacteria, Gram-negative themselves, are surprisingly very sensitive to sorangicins (MIC *S. cellulosum* So ce14 3 µg/mL). However, the corresponding glycosides are only poorly active, suggesting that this modification might represent the self-resistance mechanism of *S. cellulosum* (Kopp et al., 2007). Sorangicin A was weakly inhibiting different tumor cell lines with an IC_{50} of 15–25 µg/mL, but no obvious toxicity was detectable in mice up to a dosing of 300 mg/kg (Jansen et al., 1989b).

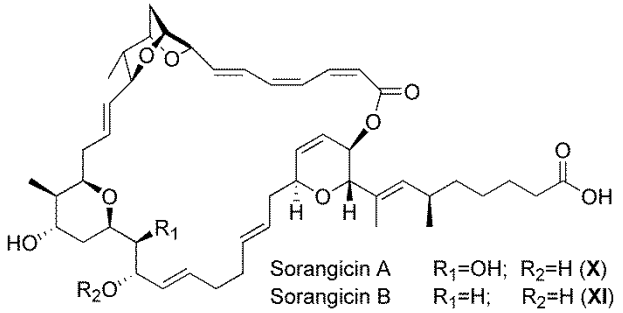

Mode of action. Incubation of bacteria with sorangicin A and labelled precursors for the biosynthesis of biomacromolecules revealed RNA synthesis as the primary target (Irschik et al., 1987). The inhibitory effect was only observed when the compounds were added prior to RNA polymerisation, since after initiation of this process the enzyme was no longer inhibited. The same kind of RNAP interference was described for rifampin. Even though sorangicins lack chemical and structural similarity to the ansamycin rifampin, analysis of the resistance profile of mutated RNAP variants revealed that their RNAP binding pocket overlaps almost completely (Xu et al., 2005). Both antibiotics inhibit transcription by blocking the designated path of the transcript during the elongation process in the RNAP (Campbell et al., 2005). The activity of sorangicin A is, however, not as sensitive to mutations in the RNAP sequence as it is the case for rifampin, even if these alter the shape of the binding pocket. Thus, it was suggested that the conformationally more flexible sorangicin A can adapt to changes in the binding pocket, while the more rigid rifampin cannot (Campbell et al., 2005).
Overall, the sorangicins have to be judged as prime candidates for further development, especially if they would prove superior to rifamycins in future studies.

1.1.4 Etnangien

From the two *Sorangium cellulosum* strains So ce750 and So ce1045 etnangien (**XIV**) was isolated (Irschik et al., 2007a). It is chemically characterized by a 22-membered, polyhydroxylated macrolide ring bearing a polyunsaturated C_{21} carboxylated side chain with two aliphatic hydroxyl groups (Irschik et al., 2007a).
Detailed studies of the etnangien biosynthesis genes from *S. cellulosum* strain So ce56 revealed a complex non-colinear *trans*-AT type PKS which performs the assembly of the etnangien core structure from acetate and malonyl units, which also includes the

methyl branches. Six open reading frames (*etnD–I*) were identified to encode for the biosynthetic assembly line. Five additional genes found in the upstream region of the PKS genes, are encoding for a HMG-CoA depending "β-branching box" (*etnOMNPQ*). Further five genes located in the up- and downstream region adjacent to the PKS genes seem to be involved in the biosynthesis of etnangien, but their distinct functions remain still unclear (*etnABC, etnJK*). To prove the proposed action of the "*β*-branching box", Δ*etnP*-mutants were generated. Analysis of their phenotypes showed that the mutants lost their ability to produce etnangien and proved thereby EtnP to be relevant for etnangien production. The biosynthetic gene cluster exhibits unusual features including split module organisation (module 3, 7, 10 and 14), skipped modules (probably modules 11, 14, 20), programmed module iteration (one of the modules 2–5), and an uncommon starter unit. Succinate was assumed to be the starter molecule, but phylogenetic analysis showed that KS1 belongs to the clade IV-harbouring domains, which accept substrates containing β-OH groups. Thus, the actual starter unit remains to be confirmed (Menche et al., 2008). Likewise, the assumption of skipped modules remains obscure, because sequence data gave no indication for inactivity for any ketosynthase domain in the etnangien assembly line. Menche and Müller, together with their co-workers, predicted the 12 stereogenic centres of etnangien. For this purpose, the amino acid sequences of the core regions of the ketoreductases were analysed, regarding the presence of an aspartate residue, resulting in a D-configured alcohol or the absence of aspartate, suggesting an L-configured secondary alcohol function (Kitsche and Kalesse, 2013). Bioinformatic predictions turned out to match fully with spectroscopic, computational and chemical analysis of the hydroxyl bearing stereogenic centres and also with the spectroscopic determination of the double bond configuration in etnangien (Menche et al., 2008). In 2010 Menche and his group were successful in the total synthesis of etnangien, which proceeded in 23 steps and 0.25 % yield (Menche et al., 2010).

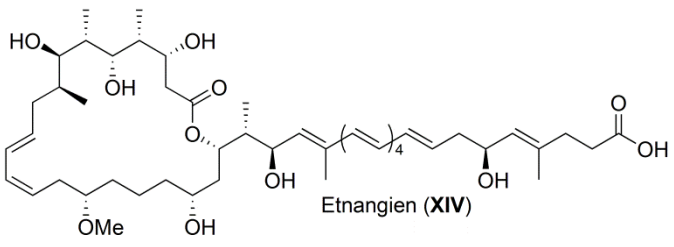

Etnangien (**XIV**)

Antibiotic activity and mode of action. Etnangien is effective against a broad panel of Gram-positive bacteria, some belonging to the Corynebacteria like *Nocardia corallia* and mycobacteria. Of special note is its antibiotic activity against rifampin-resistant *S. aureus* (MIC 0.62 µg/mL) (Irschik et al., 2007a). Investigations of the DNA, RNA and protein synthesis of etnangien-treated *Micrococcus luteus* cells revealed an inhibitory effect on the formation of all of these macromolecules. Inhibition assays using purified RNA (*Ec*RNAP) and DNA polymerase (*Ec*DNAP) and reverse transcriptase (HIVRT) showed comparable dose-effect curves, with a maximal inhibition reached at 60 µg/mL etnangien. The reverse transcriptase of Moloney murine leukemia virus (MuLVRT) was the most sensitive virus with a nearly complete inhibition at 5 µg/mL etnangien. Although, eukaryotic DNA polymerase is a sensitive target for etnangien, only a low toxicity against mammalian cells (IC_{50} of 74 µg/mL against mouse fibroblasts cells L929) was observed (Irschik et al., 2007a). Analogs of entnangien with an absent or a shortened polyene side chain, or a contracted macrocycle lost their antibiotic activity, whereas the activity of the carboxy-methylester analogue was comparable with that of the natural product (Menche et al., 2010). Derivatives with modifications in the highly labile polyene portion of the side chain had no or merely marginal activity (Altendorfer et al., 2012, 2013). These synthetic studies showed that the macrocycle as well as the side chain are essential parts of the pharmacophore.

1.2 Myxobacterial antibiotics targeting bacterial protein biosynthesis

Ribosomes play a key role in all living organisms including microbes, and due to distinct differences in their molecular structure represent an important target for antibacterial agents. A large number of clinically useful antibiotics, *e.g.* aminoglycosides and tetracyclines, target this complex machinery responsible for protein synthesis. A few myxobacterial metabolites were identified, which interfere with this ribonucleoprotein machinery.

1.2.1 Althiomycin

The sulphur-containing antibiotic althiomycin (**XV**) was first isolated in 1957 from a *Streptomyces althioticus* strain (Yamaguchi et al., 1957). However, also members of

the myxobacterial genera *Cystobacter* and *Myxococcus* are producers of this compound (Kunze et al., 1982), as well as the insect pathogen *Serratia marcescens* (Gerc et al., 2012). The major chemical characteristics are an oxime group, a thiazole, thiazoline and a methoxypyrrolinone ring (Sakakibara et al., 1974). The backbone of althiomycin consists of five amino acids (H_2N-Gly-Cys-Ser-Cys-Gly-COOH), whereby the two cysteine residues are part of the thiazoline and the thiazole ring, formed in a heterocyclisation step. These suggestions, drawn by a retro-biosynthetic analysis, were confirmed via the characterisation of the althiomycin biosynthetic gene cluster in *Myxococcus xanthus* DK897 using a genome mining approach (Cortina et al., 2011). Six ORFs (*almEDCABF*, named according to their organisation in the gene cluster) were detected, all of which are involved in althiomycin production, as was proven by LC-MS analysis of knockout mutants (*almABCDF*$^-$). Within the NRPS cluster, *almA* encodes for the loading and the first elongation module, whereas modules 2–5, encoded by *almB* form a mixed-type NRPS/PKS. In a molecular modelling approach, the binding pocket of the A domains of each module showed exact correlation with the amino acids predicted for the backbone of althiomycin. This finding was partially confirmed by feeding experiments with [$^{13}C_3$,^{15}N]-L-serine and [$^{13}C_3$,^{15}N]-L-cysteine. The first step in the assembly of the molecule is the incorporation of glycine, whose amino functionality is oxidized to an oxime by the *N*-oxygenase AlmD. Further building blocks are subsequently the amino acids cysteine, serine, cysteine and glycine, whereby the cyclisation of both cysteine residues takes place directly after introduction of the amino acid in module 1 and 3, respectively. The final elongation step is the condensation of the peptide chain with one malony-CoA unit by the single PKS module (module 5). Keto-enol tautomerisation of the keto group of the C-terminal glycine moiety yields after methylation of the enol form the corresponding methoxy group. The latter reaction is catalysed by the SAM depending methyltransferase AlmC. The formation of the methoxypyrrolinone ring as the final step in althiomycin biosynthesis is not yet fully clarified. It was hypothesized that AlmF, a proline iminopeptidase, is involved in the ring formation after hydrolytic release of the molecule by the thioesterase domain of AlmB. However, this step may also be catalysed by the thioesterase alone (Cortina et al., 2011).

Comparative analysis of the NRPS/PKS biosynthetic gene clusters from *Serratia marcescens* and *Myxococcus xanthus* DK897 showed similarity in the range of 59–72 % on the protein level. The predicted functions of the biosynthetic proteins are comparable with each other, except for the proteins (Alb6 vs. AlmF), encoded by the sixth gene (*alb6* vs. *almF*), which differs completely. Alb6 is predicted to be a type II thioesterase with a proofreading function in between the NRPS/PKS machinery (Gerc et al., 2012), whereas AlmF is proposed to be a proline iminopeptidase and may affect the methoxypyrrolinone formation.

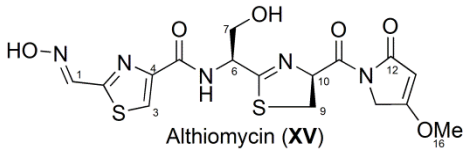

Althiomycin (**XV**)

Antibiotic activity and mode of action

Althiomycin showed antibiotic activity against several Gram-negative and -positive bacteria, *e.g.* an MIC of 6.3 µg/mL against *Klebsiella pneumoniae*, of 1 µg/mL against *E. coli* 1852E PM, of 16 µg/mL against *S. aureus* 853E, and of 0.8 µg/mL against *Corynebacterium diphteriae* was observed (Inami and Shiba, 1986; Zarantonello et al., 2002).

Studies regarding the mode of action of althiomycin were performed with *E. coli* cells. Monitoring the effect of althiomycin on the synthesis of DNA, RNA and proteins revealed that althiomycin primarily inhibits protein synthesis (Fujimoto et al., 1970). This mechanism could be confirmed by a cell free inhibition assay of polypeptide synthesis in a ribosome system, using native mRNA. Further studies suggested that althiomycin effects the peptide bond formation by interfering with the amino acid bound to the A site of the ribosome. However, althiomycin did not inhibit aminoacyl-tRNA synthesis or binding of the aminoacyl-tRNA to ribosomes. No significant inhibition effect of althiomycin on the protein synthesis was observed in rabbit reticulocytes. Thus, a low cytotoxicity and a good selectivity towards prokaryotic cells may be concluded (Fujimoto et al., 1970; Inami and Shiba, 1986).

To evaluate the pharmacophore, several analogues of althiomycin have been synthesised. In bioactivity assays only one of the synthetic althiomycin derivatives, *i.e.* dehydroxymethyl-althiomycin, a molecule without the C-7 hydroxymethylene

function, retained weak antibiotic activity. The MICs for this compound were determined to be 32 µg/mL against *S. aureus* and 16 µg/mL against *E. coli* 1852E PM (Zarantonello et al., 2002). From the synthetic studies it could be deduced that the following chemical features have major impact on the antibiotic activity: (i) the configuration of the C-10 chiral centre of the thiazoline ring, (ii) the methoxypyrrolinone ring, (iii) the oxime moiety, and (iv) the hydroxymethyl group (Inami and Shiba, 1986; Zarantonello et al., 2002).

It was reported that the pharmaceutical industry had some interest in the antibiotic althiomycin (Kirst et al., 1975; Zarantonello et al., 2002), mainly because of its antibiotic effects against Gram-negative bacteria, and despite the fact that its potency toward several clinically relevant Gram-positives is low. Althiomycin is water-insoluble and all efforts to modify the structure resulted in strongly decreased activity. There seems to be no current interest in the molecule, it may however, be worthwhile to explore SAR more extensively to exploit the lead structure offered by this natural product.

1.2.2 Angiolam A

Angiolam A (**XVI**) is a lactam-lactone antibiotic from *Angiococcus disciformis* An d30 (Kohl et al., 1985). Very recently the total synthesis of angiolam A was accomplished. The material synthesized by this 18 step procedure enabled the revision of the absolute configuration and confirmed the C2–C3 double-bond of **XVI** to be *E*-configured (Gieseler and Kalesse, 2014). The 19-membered macrocycle is decorated with methyl, carbonyl and hydroxyl groups and contains a single carbon-carbon double-bond. The side chain is monohydroxylated with three double-bonds including a terminal diene system. To date, no data on the biosynthesis of this molecule are available.

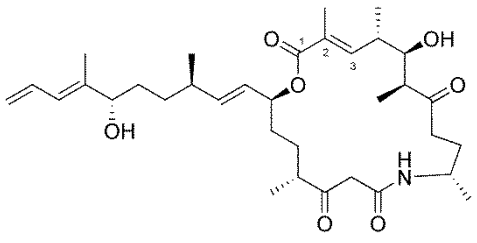

Angiolam A (**XVI**)

Antibiotic activity and mode of action. The antibiotic activity profile was found to be very narrow, in that only some members of the Gram-positive Bacillaceae, including anaerobic *Clostridium perfringens*, were sensitive (MIC of the latter 0.78 µg/mL) (Kohl et al., 1985). Gram-negative bacteria were in general resistant, except of *E. coli* mutants with increased permeability (MIC of 2.5 µg/mL against *E. coli* tolC) (Kohl et al., 1985).

The antibiotic effect was bacteriostatic. This was tested by adding up to 10 µg/mL of angiolam A to growing *Bacillus* cells; the latter were subsequently still able to form colonies. The effect on macromolecule biosynthesis revealed that protein biosynthesis stopped completely 5 minutes after addition of angiolam A. In terms of toxicity to mice, no acute toxicity was observed up to a dosing of 300 mg/kg subcutaneously (*s.c.*) (Kunze et al., 1985).

In general it seems that the antibiotic activity of angiolam A towards only a very few bacteria does not speak for the development of the natural product itself, unless a narrow spectrum of activity is aimed for. It would be worthwhile though, to analyse the activity of analogues for a potentially better profile.

1.2.3 Myxovalargins

Myxovalargins A (**XVII**) and the derivatives myxovalargin B and C were obtained from *Myxococcus fulvus* strain Mx f65 (Irschik et al., 1983b). These compounds are linear peptides consisting of 14 amino acids, and hydrolysis proved that many of these are non-proteinogenic. Among others, *N*-methylalanine, β-hydroxyvaline, agmatine, 3-methylbutyric acid, α,β-dehydrovaline, α,β-dehydroleucine, and (*S*)-β-Tyr are incorporated into myxovalargins. The conversion of L-Tyr into (*S*)-β-Tyr by the catalytic action of the *M. fulvus* Mx f65 derived tyrosine aminomutase was proven (Krug and Müller, 2009), providing this essential precursor for incorporation into the nascent myxovalargin peptide chain. A corresponding gene cluster is not published yet.

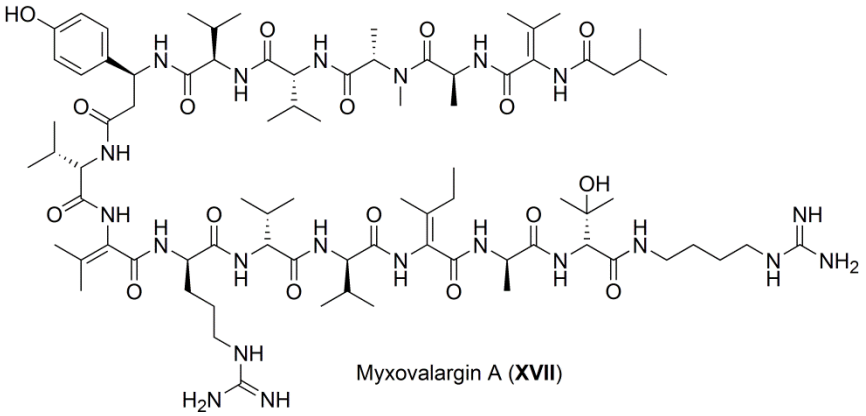

Myxovalargin A (**XVII**)

Antibiotic activity and mode of action. The antibiotic spectrum of myxovalargins (a mixture of the different myxovalargins containing 90 % myxovalargin A was used in the studies) is prominent against Gram-positive bacteria with MICs ranging from 0.3 µg/mL against *Micrococcus luteus* up to 5 µg/mL toward *Corynebacterium mediolanum* (Irschik et al., 1983b). All Gram-negative bacteria were only inhibited at significantly higher concentrations (MIC of 6 µg/mL against *E. coli*).

The mode of action underlying the described antibiotic effects can be separated into two different mechanisms. At low concentrations (below 1 µg/mL) myxovalargin A inhibits instantaneously bacterial protein synthesis, whereas at higher concentrations (above 5 µg/mL), or upon prolonged incubation, cell membranes are damaged (Irschik and Reichenbach, 1985). In a cell free *E. coli* system protein synthesis was only inhibited, if myxovalargin A was added prior to the reaction start. This observation and continuing experiments with ribosomes led to the suggestion that myxovalargin A acts at the A site of the ribosome. Comparable results were not obtained with eukaryotic systems; only very high concentrations led to a partial protein synthesis inhibition. However, in contrast to most afore mentioned myxobacterial antibiotics, myxovalargin A showed cytotoxicity. The LD_{50} for mice (*s.c.*) was 10 mg/kg, and the LD_{100} 30 mg/kg. Due to this toxicity along with the fact that eukaryotic ribosomes were not inhibited, an additional biological effect was proposed. It was found that at higher concentrations myxovalargin A interacted with membranes, resulting in cell lysis. This activity was observed when applying to *Bacillus* cells, but also with erythrocytes, and may be the reason for the toxicity observed in mice (Irschik and Reichenbach, 1985).

Overall, based on the results obtained for myxovalarin A, these compounds seem to be too toxic for an application as an antibiotic. However, it cannot be excluded today that the derivatives B–D or other derivatives will show only minor toxicity.

1.3 Myxobacterial antibiotics targeting the respiratory chain

Two antibiotically active myxobacterial metabolites were found that target the respiratory chain, *i.e.* aurachins and thuggacins. Enzymes of the respiratory chain do not represent a classical target in antibiotic therapy, since these proteins are highly conserved in all organisms. Therefore, the chance of toxicity is high. However, there might be the chance of finding specific inhibitors within the variants described below.

1.3.1 Aurachins

A range of isoprenoid quinoline alkaloids were isolated from *Stigmatella aurantiaca* strain SG a15, and the three main metabolites were named aurachin A (**XVIII**), B (**XIX**) and C (**XX**), while D (**XXI**) and E (**XXII**) are minor products (Kunze et al., 1987). All of these compounds share the quinoline nucleus, in some cases with the nitrogen being present as N-oxide, and are substituted with a sesquiterpene unit. In addition to various *Stigmatella* strains also *Rhodococcus* species were now identified as producers of aurachins (Kitagawa et al., 2013; Nachtigall et al., 2010).

Concerning the biosynthesis, first insights were gained by feeding studies with assumed precursors like ^{13}C- and ^{18}O-labelled anthranilic acid, C-1 and C-2 ^{13}C-enriched acetate and ^{18}O-labelled molecular oxygen (Höfle and Kunze, 2008). It was proven that anthranilic acid is a building block of the aurachins, presenting a biosynthetic bottle neck, since medium supplementation with anthranilic acid increased the yield of aurachins. Unexpectedly, the farnesyl residue was constructed in parallel via different pathways, *i.e.* isoprenoid biosynthesis by the mevalonate and non-mevalonate (methyl-erythritol phosphate/deoxy-xylulose phosphate, MEP/DOXP) pathway, as well as leucine degradation (Höfle and Kunze, 2008). Concerning the decoration of the quinoline alkaloid moiety with an isoprenoid side chain, biochemical investigations showed AuaA to be the responsible enzyme, in that it catalyses the prenylation of 2-methyl-4-hydroxyquinoline in the presence of

farnesyl diphosphate (FPP), thereby yielding aurachin D (**XXI**) (Stec et al., 2011). Aurachin D harbouring the prenylation at position C-3 of the quinoline ring represents the precursor for aurachin C (**XX**), the latter on its part is converted to aurachin B (**XIX**) by a rearrangement of the farnesyl moiety from position C-3 to C-4 of the quinoline ring. Subsequent oxidation and heterocycle formation finally yields aurachin A (**XVIII**). After the involvement of a type II PKS (AuaD) in aurachin biosynthesis was proven (Sandmann et al., 2007), finally in 2011 the group of Rolf Müller identified the corresponding biosynthetic gene cluster, a step which was complicated by the split organisation of the cluster (Pistorius et al., 2011). By analysis of the non-clustered genes involved in the final steps of aurachin biosynthesis, insights in the migration of the prenyl group were obtained. In a sequential reaction first AuaG catalyses epoxidation which is the prerequisite for the following semipinacol rearrangement, enabling migration of the farnesyl group. The ketoreductase AuaH was assumed to subsequently reduce the isomer with the migrated prenyl group and thereby, through aromatisation, the molecule is stabilised (Katsuyama et al., 2012).

Chemical synthesis of aurachin D through a key Conrad-Limpach reaction was established and served for the generation of analogues with cyclic as opposed to acyclic (concerning the oxygen heterocycle in A) analogues. This enabled first SAR studies (Li et al., 2013). Only the geranyl analogue of aurachin D had antibacterial effects comparable to that of the natural product, all other synthesised analogues did not perform as well.

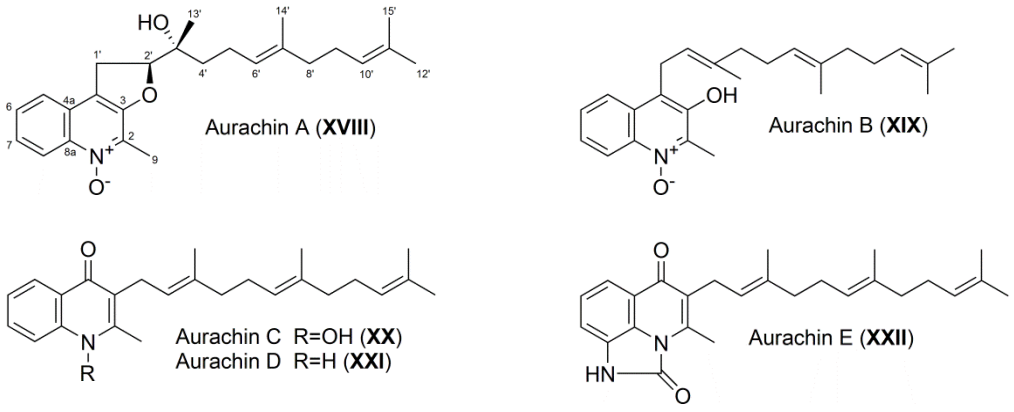

Antibiotic activity and mode of action. As most of the myxobacterial antibiotics, the aurachins were active against numerous Gram-positive bacteria, *e.g.* MICs against *B. subtilis* were for aurachin A: 5 µg/mL, aurachin B: 2.5 µg/mL, aurachin C: 0.15 µg/mL,

and aurachin D: 0.15 µg/mL. Against Gram-negative *E. coli* no activity of was observed at all (Kunze et al., 1987). Additionally, a weak but incomplete inhibition of fungi was found, *e.g.* MIC of aurachin A was 50 µg/mL against *Debaryomyces hansenii* and *Saccharoymyces cerevisiae*, whereby a turbidity of up to 25 % remained. In general the aurachins C and D were more active than A and B.

The effects of the aurachins on the NADH oxidation were tested on beef heart sub-mitochondrial particles, due to their structural similarity to the respiratory chain inhibitor 2-heptyl-4-hydroxyquinoline-*N*-oxide (HQNO). The required concentration to reach 50 %inhibition was about ten-times lower than for HQNO (Kunze et al., 1987). This potent inhibitory effect on the bacterial and eukaryotic respiratory chains was the focus of subsequent biochemical studies. Thus, it was found that the cytochromes *bo* and *bd*, both terminal oxidases of *E. coli*, were inhibited by aurachin C, whereas aurachin D and its analogues showed selectivity for inhibition of cytochrome *bd* (Meunier et al., 1995). Using a chemically synthesized derivative, *i.e. decyl*-aurachin D, it was shown that this molecule acts on the donor side of haem *b*-558, thereby preventing electron flow from the quinol substrate (Jünemann et al., 1997). In the following, the aurachins became useful tools for probing of the ubiquinol-binding site in cytochromes, due to their strong inhibitory effect on the respiratory chains (Mogi et al., 2006).

From early on, the aurachins were suspected to have an antimalarial activity, due to their structural similarity with antiplasmodial drugs. This was proven by a first *in vitro* screening against *Plasmodium falciparum* provided by the WHO (Geneva). Indeed, aurachins C (IC_{50} [ng/mL] 26/0.9) and E (13/0.4) showed good activity against *P. falciparum* clones W-2 and D-6, respectively. These values are comparable to those of chloroquine (35/1.2) and artemisinine (0.43/1.1) (Höfle et al., 2008). Further, it was found that the derivative aurachin E (**XXII**), in contrast to the aurachins A–D, did not show mitochondrial respiratory inhibition and had a low cytotoxicity. The IC_{50} against mouse fibroblasts L929 was 25 µg/mL for aurachin E (**XXII**), compared to values between 1.3 and 3.2 µg/mL for the derivatives A–D. The rare E variant can be obtained in a semisynthetic approach by using a one-step reaction starting with the better accessible aurachin C (Höfle et al., 2008). However, no *in vivo* activity was

observed in a murine malaria model with *Plasmodium berghei* at 100 mg/kg, whereas chloroquine showed an ED_{90} of 2.8 mg/kg (Milhous et al., 1985).

1.3.2 Thuggacins

Three thiazole-containing macrolides (**XXIII**-**XXVIII**) were isolated in 2007 from *Sorangium cellulosum* strain So ce895 (Steinmetz et al., 2007). Due to their origin they were named Soce-thuggacin A (**XXIII**), B (**XXIV**) and C (**XXV**) (sometimes, however only named thuggacins). A further compound identified in *S. cellulosum* strain So ce895 was 13-methyl-thuggacin A (**XXVI**). Special features of Soce-thuggacin A are, besides the thiazole ring a diene moiety (11*E*, 13*Z*), an α,β unsaturated lactone with an *n*-hexyl side chain attached at C-2 and, additionally a side chain at C-16 containing three hydroxyl and a diene functionality. In solution Soce-thuggacin A, a 17-membered macrolide, rearranges under acyl migration to give Soce-thuggacin B, a 18-membered macrolide, and Soce-thuggacin C, a 19-membered macrolide. For the determination of the stereochemistry of Soce-thuggacins A–C a combination of chemical methods was applied, *e.g.* chemical derivatisation, NMR studies, molecular modelling and bioinformatic analysis of the ketoreductase domains of the biosynthetic genes (TugA, TugB, TugC) (Bock et al., 2008).

Further two variants of the thuggacins, this time named Cmc-thuggacins (or alternatively thuggacin cmc), Cmc-thuggacin A (**XXVII**), Cmc-thuggacin B (structure not shown, analogous to **XXIII** and **XXIV** with a lactone bond to C-17 OH) and Cmc-thuggacin C (**XXVIII**), were isolated from *Chondromyces crocatus* strain Cm c5. Structural differences of the latter towards the Soce-thuggacins, are the replacement of the *n*-hexyl side chain by a methyl group at C-2, an introduction of a primary hydroxyl functionality at C-32, and a side chain with removed secondary hydroxyl functionality at C-20 (Steinmetz et al., 2007). It was noted, that Cmc-thuggacins A–C just as Soce-thuggacins are present in an equilibrium with each other, especially in protic solvents (Jansen et al., 2012; Steinmetz et al., 2007).

Feeding studies with labelled precursors (1-^{13}C-acetate, 1,2-$^{13}C_2$-acetate, 1-^{13}C-propionate and $^{13}CH_3$-methionine) showed that the starter of the biosynthesis of Soce-thuggacin A is acetate, which is elongated with three propionate, and subsequently five acetate units, before a fourth propionate is incorporated.

Condensation of the carboxyl moiety of this propionate unit with cysteine provides after cyclisation the thiazole ring. Additional four acetate units form the hexyl side chain. Finally, ring closure occurs to give the lactone. The only immediate product of this biosynthetic pathway in *S. cellulosum* seems to be thuggacin A. In 2010 Müller and co-workers published the comparative analysis of the Soce- and Cmc-thuggacin biosynthetic gene clusters, which are all derived from hybrid PKS/NRPS systems. All thuggacins possess a thiazole ring, which is derived classically from oxidative cyclization of cysteine. The enzymatic domain responsible for this reaction, *i.e.* a heterocyclisation domain, makes an acyl-NH–Cys peptide bond and then cyclodehydrates the product to a thiazoline (Walsh et al., 2001). This allowed the detection of the gene clusters of the Soce- and the Cmc-thuggacins by screening the respective cosmid libraries with probes based on amplified NRPS heterocyclization domains. The *S. cellulosum* thuggacin biosynthetic gene cluster (Soce-tga) occupies 56.09 kp of the *S. cellulosum* genome, whereas the Cmc-thuggacin biosynthetic gene cluster in *C. crocatus* (Cmc-tug) has a size of 58.41 kb. Both biosynthetic gene clusters consist of twelve modules: one loading module and eleven chain extension modules. Soce-tga PKS/NRPS modules are encoded by three genes (*tgaA*–*tgaC*), whereas the Cmc-tug PKS/NRPS biosynthetic machinery is in contrast located on four genes (*tugA*–*tugD*). Variations in the PKS/NRPS systems of both biosynthetic clusters are responsible for structural diversity. Module 3 of the Cmc-thuggacins cluster contains a full reductive loop (DH, KR, ER) to give the methylene group at C-20. In contrast, module 3 of the Soce-thuggacin cluster, consisting solely of a KR and a DH domain, results in a hydroxyl moiety at C-20. It is assumed that the PKS intermediate of module 2 is transferred to the ACP of module 3 without any reduction at the β-keto group. However, before chain extension takes place, the reductive domains of module 3, *i.e.* KR and DH, form the methylene moiety at C-21. Subsequently, chain elongation occurs and now only the KR is active, resulting in the C-20 hydroxyl function. The biochemical basis resulting of this “out of sequence activity” of these two domains is still unknown. The most prominent difference between Soce- and Cmc-thuggacins is the substitution at C-2. According to the methyl group at C-2 in the Cmc-thuggacins the recognition motif of the AT, encoded by module 11 (Cmc, TugD) reveals a specificity for methylmalonate as extender unit. No clear prediction could be

made for the AT encoded by module 11 (Soce, TgaC) in the Soce-thuggacin cluster, which is consistent with the idea that the Soce-acyltransferase (AT 11) accepts an uncommon building block to give finally the *n*-hexyl side chain. Possible sources for the hexyl side chain could be either 2-carboxy-octanyl-CoA or 2-carboxy-octanyl-ACP which seems to be provided by TgaD, for which the encoding gene is located downstream adjacent to the cluster. TgaD showed similarity to crotonyl-CoA carboxylase/reductase enzymes (CCR enzymes), and seemed to generate 2-carboxy-octanoyl-CoA by a reductive carboxylation of the fatty acids derived octenoyl-CoA. This mechanism was recently proven for the TgaD homologue CinF, which is catalysing this reaction in cinnabaramide A biosynthesis of *Streptomyces* sp. JS360 (Quade et al., 2011).

Post assembly line processing occurs in Soce-thuggacins as well as in Cmc-thuggacins to introduce hydroxyl functionalities at C-17, or at C-17 and C-32, respectively. In both thuggacin clusters TugE, respectively TgaE could be determined as hydroxylases, which are responsible for installation of the hydroxyl group at C-17, whereby the hydroxylation at C-32 in Cmc-thuggacin seems to be performed by a second enzyme encoded elsewhere in the genome of *C. crocatus*. In the case of the Soce-thuggacins the reason for non-hydroxylation at C-32 remains unclear (Buntin et al., 2010).

Comparison of the KSs, as most conserved domains of both gene clusters, suggested the thuggacin gene cluster to originate from streptomycetes and to be possibly acquired by myxobacteria via horizontal gene transfer.

A highly stereoselective total synthesis of the Soce-thuggacins A–C was achieved by Kirschning and co-workers (Bock et al., 2008). The stereochemical assignment for Soce-thuggacin A-C was determined to be 2*E*,7*R*,8*S*,10*S*,11*E*,13*Z*,16*S*,17*S*,18*R*,19*S*,20*S,* 21*E*,23*E* (Bock et al., 2008). Soce-thuggacin B was synthesized in 23 linear steps and an overall yield of 0.6 %. The total synthesis finally proved the reported structure of these metabolites.

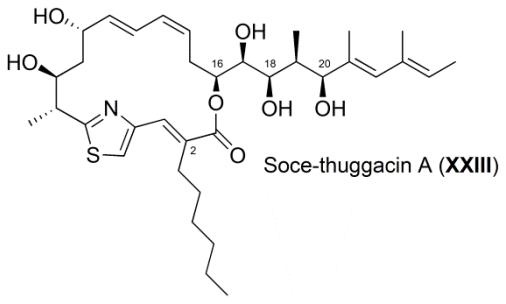

Soce-thuggacin A (**XXIII**)

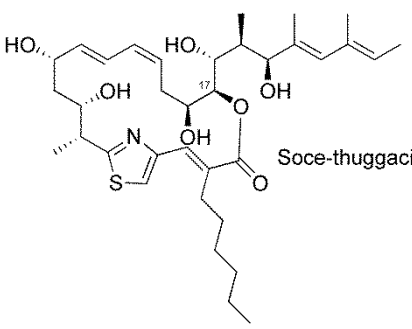

Soce-thuggacin B (**XXIV**)

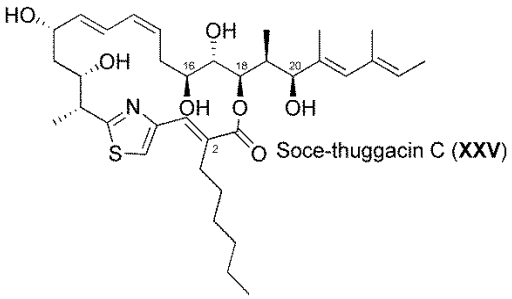

Soce-thuggacin C (**XXV**)

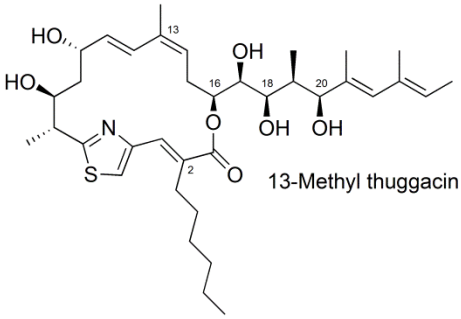

13-Methyl thuggacin A (**XXVI**)

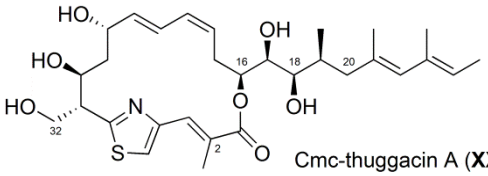

Cmc-thuggacin A (**XXVII**)

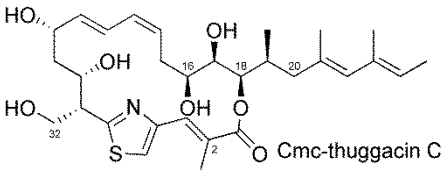

Cmc-thuggacin C (**XXVIII**)

Antibiotic activity and mode of action

Soce-thuggacin A showed inhibitory activity against Gram-positive bacteria like *Micrococcus luteus* (MIC 3 ng/mL). Of special interest is its activity toward several mycobacteria, *i.e.* MIC against *Mycobacterium phlei* was found to be 0.03 µg/mL, *M. chitae* 0.60 µg/mL and *M. tuberculosis* 8.0 µg/mL. The activities of Soce-thuggacin A and B were similar to each other, but Soce-thuggacin C was much less active (Irschik et al., 2007b). Antibacterial effects, most importantly also against Mycobacteria, was demonstrated as well for the cmc-thuggacins (Walsh et al., 2001).

Mode of action studies on Soce-thuggacin A were performed using *M. luteus*. After addition of Soce-thuggacin A to the bacterium, the first observation using radioactive precursors was the immediate stop of macromolecule synthesis like that of DNA, RNA and proteins. Further, Irschik and co-workers could show, due to the observation of the oxygen consumption of *M. luteus*, that a total inhibition of respiration was reached with 2.5 ng/mL Soce-thuggacin A (Irschik et al., 2007b). Experiments with cytoplasmatic membranes gave evidence for the inhibition of the NADH oxidase (90 % inhibition at 10 ng/mL Soce-thuggacin A). Additionally, the inhibition of the reduction of cytochromes a, b and c by NADH in membranes was detected. Summing up, Soce-thuggacin A seems to inhibit late stages of the respiratory chain which results in a disruption of the energy supply for the cells. The toxicity test against mouse fibroblast

cells L929 gave an IC_{50} of 4 µg/mL, showing a toxic effect on these eukaryotic cells (Irschik et al., 2007b).

1.4 Myxobacterial antibiotics influencing biofilm formation

Bacteria present as a biofilm show elevated resistance to antibiotics when compared with their free-living counterparts. Potential reasons for this increased resistance are that antimicrobials cannot penetrate the barrier that biofilms represent, and that many cells are metabolically inactive. It is thus of special interest to find antibiotics active against bacterial biofilms, to tackle problems associated with, *e.g.* urinary tract infections, dental health and biofilms on medical implants (Peach et al., 2013).

1.4.1 Carolacton

The macrolide carolacton (**XXIX**) was isolated in 1998 by Höfle and co-workers from *Sorangium cellulosum* strain So ce960 (Höfle, 1998). Structural characteristics are a 12-membered lactone ring with two secondary hydroxyl functions at C-17 and C-18, and a terminal carboxyl group at the side chain. The two double-bonds $\Delta^{15,16}$ and $\Delta^{7,8}$ are *trans* configured (Jansen et al., 2010). The configuration of all eight stereogenic centres was determined via chemical derivatisation, and the absolute configuration was a refined result of the X-ray single-crystal structure of **XXIX**.

Total synthesis was achieved by Schmidt and Kirschning in 2012 (Schmidt and Kirschning, 2012). The overall yield was 4.3 % for 22 linear steps, using commercially available acetoxypropionic acid as starting material.

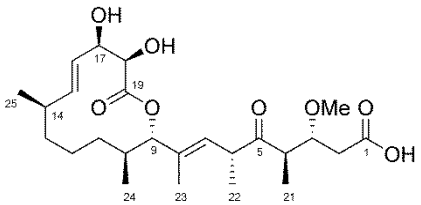

Carolacton (**XXIX**)

Activity and mode of action. Especially worthwhile mentioning is the antibiotic activity of carolacton against *E. coli* strain tolC with an MIC of 0.06 µg/mL, and its influence on biofilm formation. The main focus in further investigations was placed on the activity of carolacton against the caries and endocarditis associated bacterium

Streptococcus mutans. The latter is able to form biofilms and proved to be sensitive towards carolacton. At a concentration of 5 ng/mL, 33 % of the cells in the biofilm died, whereas a concentration of 25 ng/mL resulted in 66 % dead cells (Jansen et al., 2010). Inhibition of biofilms in nanomolar concentrations implied that carolacton addresses a primary target, present only in a few copies per cell (Reck et al., 2011). Wagner-Döbler and co-workers suggested carolacton to target quorum sensing systems of *S. mutans* (Kunze et al., 2010). With the help of LIVE/DEAD *BacLight* bacterial viability staining, they gained a dose-response-relationship curve which showed a sigmoidal shape with a low threshold of 10 nM. No substantial increase of activity above this concentration was observed, which indicated that carolacton targets a signalling pathway. Confocal laser scanning microscopic images with LIVE/DEAD stained carolacton treated *S. mutans* cells visualized changes in cell morphology. Cells were elongated, bulged, and the number of bacterial cells stringed together in one chain increased (Kunze et al., 2010). Further, the applied method indicated that carlocaton induces membrane damages, which was confirmed by the detection of cytoplasmatic proteins and external DNA in an analysis (SDS-page and quantitative PCR) of the supernatant of carolacton treated biofilms. A time related profile of the transcriptional response of *S. mutans* to carolacton treatment indicated the regulation of genes with an impact on biofilm formation, autolysis, cell shape, cell division and pyrimidine and histidine metabolism. The investigation of correlated two-component signal transduction systems (TCS) (*e.g.* VicKRX, SMU.1037c/1038c, SMU.659/660 and ComDE) revealed that carolacton mainly interacts with the serine/threonine protein kinase (STPK) PknB (Banu et al., 2010). The latter conclusion could be confirmed by the insensitivity of a *pknB* deletion mutant *S. mutans* EA 72 to carolacton treatment (Banu et al., 2010). These conclusions were further supported by the close similarity of the transcriptome of the *pknB* deletion mutant with that of the carolacton treated biofilm.

Summing up, recent insights into the mode of action of carolacton indicated that this compound interferes with the STPK PknB and hence with PknB-mediated signalling. This in turn influences pyrimidine biosynthesis, cell wall and biofilm formation, as well as the ComDE mediated bacteriocin production. The alterations in cell wall composition result in weakened cell walls, leading to loss of integrity at low pH and

leakage of cytoplasmatic proteins and DNA, and finally cause cell death (Reck et al., 2011). In 2013 the biofilm reducing activity of carolacton in comparison to chlorhexidine and triclosan was reported (Apel et al., 2013). The incorporation of **XXIX** at a concentration of 0.002 %in dental filling material gave promising results. No adverse effect on the mechanical properties of the latter, and a significant effect on biofilm-formation were observed.

Antifungal activity against *Aspergillus niger, Pythium debaryanum* and *Sclerotina sclerotiorum* in the range of 16–20 µg/mL was also reported. In 2002 the scaffold of carolacton was protected by a Japanese patent (Ishihara et al., 2002).

1.5 Myxobacterial antibiotics targeting the type II signal peptidase LspA

The novel target LspA is part of the lipoprotein processing system, which is essential in all Gram-negative bacteria, and can be conditionally essential in Gram-positives. Lipoproteins are ubiquitous in bacteria, play an important role in viability, and are also key factors in pathogenesis, since these outer membrane proteins represent virulence factors (Kovacs-Simon et al., 2011). In eukaryotic cells instead, LspA is absent, making it an attractive target for antibiotics (Hutchings et al., 2009; Tjalsma, 1999; Xiao et al., 2012). Recently, the activity of a myxobacterial compound against LspA was described (Xiao et al., 2012).

1.5.1 Myxovirescins

The myxovirescin family is represented by closely related antibiotics produced by many myxobacterial strains, whereby the first isolation and structure elucidation was performed using *Myxococcus virescens* strain Mx v48 (Gerth et al., 1982). The basic structure of the molecules is a 28-membered ring, with a lactone and a lactam functionality. Several reports on these compounds can be found in the literature, in which myxovirescin A1 (**XXX**) is also named as antibiotic TA (from strain Tel Aviv), megovalicin, or M-230B (Onishi et al., 1984; Takayama et al., 1988).

The biosynthetic gene cluster coding for the enzymes responsible for the assembly of this mixed PKS/NRPS-derived product (**XXX**) was identified in the genome-sequenced strain *Myxococcus xanthus* DK1622. The cluster has a size of approximately 83 kb and

consists of at least 21 orfs. Two PKSs might be involved in the biosynthesis of the C3-hydroxyvaleryl-ACP starter which primes the biosynthesis by condensation with the amino acid glycine. The remaining acetates required for lactone formation are subsequently incorporated by PKS modules. Further building blocks were SAM-derived methyl groups, *i.e.* C-32, C-33, C-34 and a succinate-derived ethyl side chain (C-30, C-31) (Simunovic et al., 2006). Furthermore, the incorporation of the β-methyl (C-29) and β-ethyl (C-30, C-31) groups into polyketide backbones (as mentioned before, β-branching is exemplified in many myxobacterial metabolites) was analysed by mutational studies performed within the myxovirescin gene cluster (Simunovic and Müller, 2007a; Simunovic et al., 2006). Since the identification of **XXX** in 1982, different synthetic approaches to this molecule were projected. All required a large number of steps, whereby the latest route to myxovirescin A1 (17 steps and over the longest linear sequence, 46 steps overall) resulted in an overall yield of approx. 2 % (Fürstner et al., 2007). Further, simplified derivatives were synthesized (Content et al., 2003) since it was shown that removal of some substitution on the left-hand side of the macrolactam ring, *e.g.* the oxygen bound to C-20, does not affect activity (Trowitzsch-Kienast et al., 1989).

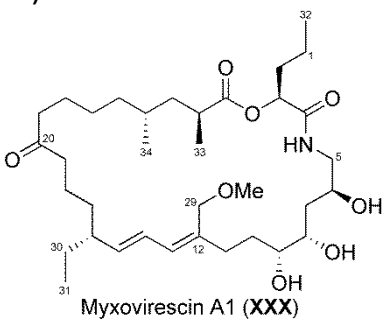

Myxovirescin A1 (**XXX**)

Antibiotic activity and mode of action. The first antimicrobial evaluation of myxovirescin A1 showed a promising MIC of 1 µg/mL against *E. coli*, while Gram-negative *P. aeruginosa*, as well as Gram-positive *S. aureus* and *B. megaterium* were affected with merely an MIC of 30 µg/mL. In an agar diffusion assay, using the aforementioned strains, only *E. coli* showed an inhibition halo (Gerth et al., 1982). In contrast, other reports stated that all *Bacillus* strains were found to be very sensitive towards the antibiotic (MIC 0.1–5 µg/mL), as well as *Pseudomonas* and *Staphylococcus* strains (MIC 5–25 µg/mL) (Rosenberg and Dworkin, 1996). A reason for these differing results may be the strong influence of the test conditions. Thus,

sensitive *E. coli* could be protected by the addition of calcium or bovine serum. In *in vivo* assays **XXX** did not protect mice infected with lethal doses of (not further specified) pathogenic bacteria (Rosenberg and Dworkin, 1996). This was due to the strong tissue binding properties of the compound (Rosenberg et al., 1984). Thus, myxovirescin A1 was not distributed in the organism as such, however retained its activity when bound to membranes or surfaces (Rosenberg and Dworkin, 1996). Due to its high adhesive properties, the compound was tested with 8 human volunteers suffering from gingivitis. They were treated with 4 applications of 0.1 mg myxovirescin A1. In this experiment the 3 indices, *i.e.* plaque, gingival and bleeding, showed a rapid decrease (Manor et al., 1989). Concerning toxicity it was reported that "relatively large doses of myxovirescin A were not toxic to rats" (Rosenberg and Dworkin, 1996). The bactericidal activity of myxovirescin A1 needs ongoing protein synthesis and thus cell metabolism, which indicated that the compound kills bacteria in a target-specific manner. Analysis of the resistance mechanism of several *E. coli* mutants led to the conclusion that the type II signal peptidase (LspA) is the target of myxovirescin A1, since overexpression of LspA, and also inactivation of *lpp* (coding for the outer membrane "Braun's" lipoprotein), both specifically conferred resistance to *E. coli*. (Xiao et al., 2012). Thus, two consequences of the LspA interaction could be responsible for the bactericidal effect: (i) a toxic build-up of Lpp inside the cell leading to lethal cross-linking of the cell wall and the inner membrane, and (ii) the inhibition of the proper localization of essential lipoproteins to the outer membrane (Xiao et al., 2012). This conclusion is also supported by the fact that the biosynthetic gene cluster of myxovirescin encodes two *lspA* paralogs that might play a role in self-resistance of the producer strain. The identification of the molecular target, *i.e.* LspA, for myxovirescin A1 opened up new opportunities for lead optimization. LspA represents a novel antibiotic target and therefore the highly active myxovirescin A1 can be seen as a promising lead structure for further studies.

1.6 Myxobacterial antibiotics with an unknown mode of action

1.6.1 Chondrochlorens

Chondromyces crocatus strain Cm c5, reported as the producer of thuggacins (see above), was also found to produce the chondrochlorens. 2003 the group of Höfle reported two chloro-hydroxy-styryl amides, the characteristic styrene moiety of which is linked by an amide bond with a 14-membered aliphatic side chain (Jansen et al., 2003). Chondrochloren A (**XXXI**) and B (**XXXII**) differ merely concerning the methoxy or ethoxy functionality at C-2, respectively.

Sequencing efforts of a cosmid library of the genome of *C. crocatus* strain Cm c5 led to the elucidation of the biosynthetic gene cluster of the chondrochlorens, which spans over a contiguous stretch of ~68 kb on the *C. crocatus* chromosome (Rachid et al., 2009). The biosynthetic mixed type PKS/NRPS gene cluster consists of 10 core genes (*cndA–cndF*) and several post PKS/NRPS processing genes (*cndI*, encoding for a SAM depended methyltransferase; *cndH*, encoding for a tyrosine halogenase; *cndG*, encoding for an oxidative decarboxylase). The genetic architecture and the scaffold of the natural products are highly colinear. The biosynthetic process uses butyrate as the starter unit, succeeded by the condensation with three methylmalonate units, and subsequently with two methoxymalonyl units. Finally, NRPS related proteins incorporate tyrosine or 3-chloro-L-tyrosine into the PKS chain, and then the molecule is released from the biosynthetic enzymes by a thioesterase. The FAD-linked oxidative carboxylase CndG is responsible for tyrosine decarboxylation from pre-chondrochlorens A and B, which yields the styryl moiety in chondrochlorens (Rachid et al., 2010).

Investigation of the chlorination reaction performed by CndH implied that this occurs before release of the intermediate from the assembly line. This was supported by the fact that a *cndH*-deficient mutant did neither produce chondrochloren A nor B, whereas the biosynthesis of chondrochlorens could be restored to a good extent (*i.e.* approx. to 50 %) by the addition of 3-chloro-L-tyrosin. Nevertheless, investigation of the corresponding A-domain (encoded by *cndF*) in an ATP-PP_i exchange assay exhibited an insignificant preference of CndF for 3-chloro-L-tyrosine as compared with L-tyrosine (Rachid et al., 2009). CndH belongs to the FAD-dependent halogenases which are closely related to the FAD-dependent aromatic hydroxylases

(Buedenbender et al., 2009). A gene encoding for an interacting flavin reductase seems to be located elsewhere in the genome (Rachid et al., 2006).

To address the origin of the ethoxy moiety of chondrochloren B, the methyltransferase CndI was analyzed. *cndI* is located directly adjacent to the halogenase gene *cndH* in the upstream region of the chondrochloren gene cluster and showed homology to the superfamily of SAM radical enzymes, which catalyse methylation of unreactive carbon centres (Marsh et al., 2004). It was supposed that the ethoxy group would be the result of the methylation of an initial methoxy function, *i.e.* to be SAM derived. Extracts of a *cndI* deficient mutant showed significant lower amounts of chondrochloren B relative to chondrochloren A when compared to the wild-type strain, which may indeed indicate an involvement of CndI in the formation of the ethoxy group (Rachid et al., 2006).

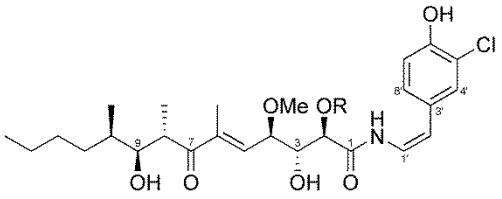

Chondrochloren A R=Me (**XXXI**)
Chondrochloren B R=Et (**XXXII**)

Antibiotic activity and mode of action

Chondrochloren A was assayed for its biological activity in agar diffusion tests using 20 µg of **XXXI** on a 6 mm paper disk. Only a weak antibiotic effect against *M. luteus* (13 mm inhibition zone) and *Schizosaccharomyces bombe* (10 mm inhibition zone) was found. *B. subtilis* and *S. aureus* were hardly affected (Jansen et al., 2003). Pre-chondrochloren with a carboxyl group at C-1' and no carbon-carbon double-bond between C-1' and C-2' (as compared to **XXXII**) showed at the 30 µg/disk agar diffusion assay no inhibition zone against *M. luteus* and *B. subtilis*. In comparison chondrochloren B (**XXXII**) produced an inhibition zone of 17 and 14 mm, respectively. Processing of the pre-chondrochlorens to chondrochlorenes via oxidative decarboxylation by CndG in biosynthesis is thus required to obtain antimicrobially active compounds (Rachid et al., 2010).

1.6.2 Indiacens A and B

From *Sandaracinus amylolyticus* strain NOSO-4T, a recently characterized new myxobacterial genus, two 3-formylindol derivatives were isolated, *i.e.* indiacen A (**XXXIII**), and indiacen B (**XXXIV**), whereby the latter represents the chlorinated derivative of **XXXIII** (Steinmetz et al., 2012). Concerning the biosynthesis of these metabolites it was assumed that the indole moiety results from tryptophan. The origin of the prenyl side chain was investigated by feeding experiments with labelled precursors, *i.e.* [1-^{13}C]acetate, [1,2-$^{13}C_2$]acetate, L-[methyl-^{13}C]methionine, [2-^{13}C]propionate, and [1,2-$^{13}C_2$]mevalonolactone. Only supplementation with mevalonolactone resulted in significant ^{13}C-enrichment at C-11. Thus, the butadienyl side chain can be expected to originate from mevalonolactone, or mevalonate, respectively (Steinmetz et al., 2012).

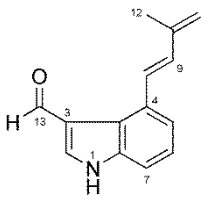

Indiacen A (**XXXIII**)

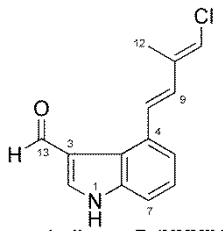

Indiacen B (**XXXIV**)

Antibiotic activity. Indiacen A and B showed antibiotic activity against some Gram-positive and Gram-negative bacteria. However, the antibiotic effects were mostly moderate. MIC against *E. coli* tolC was 16.6 µg/mL for **XXXIII**, and 33.0 µg/mL for **XXXIV**, respectively. MICs against *Arthrobacter rubellus* were 16.6 µg/mL and 0.8 µg/mL, respectively. No toxicity toward mouse fibroblast L929 cells has been noted (Steinmetz et al., 2012).

1.6.3 Maracin A and Maracen A

In 1998 maracin A (**XXXV**) and maracen A (**XXXVI**) were isolated in the group of Höfle from *Sorangium cellulosum* strain Soce 880 and Soce 1128, respectively (Herrmann et al., 1998). Characteristic for maracin A is the unusual ethynyl-*trans*-vinyl ether moiety, which is replaced in maracen A by an α-chlorovinyl group. Feeding studies with ^{13}C-labelled acetate evidenced the biosynthesis of these metabolites from nine intact acetate units, whereas the carboxy group derived from C-2 of a further acetate precursor. The oxygen of the ether linkage is discussed to have possibly the same

origin as that of divinyl ethers in the red alga *Polyneura latissima*, which results from fragmentation and Hock rearrangement of a bisallylic 6-hydroperoxide (Jiang and Gerwick, 1997).

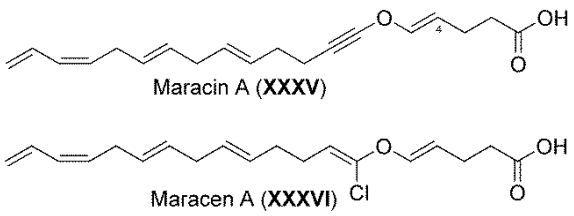

Activity and mode of action. A screening of the National Institute of Allergy and Infectious Diseases (Birmingham) aiming to find compounds against *Mycobacterium tuberculosis* showed an *in vitro* activity of maracin A and maracen A of IC_{99} < 12.5 µg/mL. So far nothing is reported concerning *in vivo* studies, also no mode of action studies were published. An *in vitro* assessment of toxicity using the mouse fibroblast line L929 showed no cytotoxic effects up to a concentration of 24 µg/mL.

1.6.4 Nannochelins

The nannochelins (**XXXVII–XXXIX**) are siderophores isolated from *Nannocystis exedens* strain Na e485 and belong structurally to the citrate-hydroxamate family (Kunze et al., 1992). In the nannochelins the carboxyl groups of the citric acid moiety are linked to an *N*-ε-cinnamoyl hydroxyl-L-lysine(-methyl ester). The three described derivatives are nannochelin A (**XXXVII**), B (**XXXVIII**), and C (**XXXIX**) and differ in the methylation state of their carboxyl groups. Thus, it could not be excluded that nannochelin A originated from nannochelin B or C by methylation during the isolation process in which methanol was used. Nannochelin B, which represents the main product, was however detected in the culture supernatant during fermentation without purification.

A total synthesis of nannochelin A was described and allows access to derivatives for future studies (Bergeron and Phanstiel, 1992; Sakamoto et al., 1996).

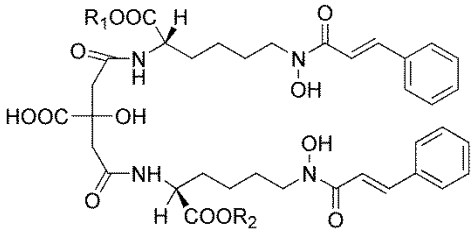

Nannochelin A R_1=R_2=Me (**XXXVII**)
Nannochelin B R_1=Me, R_2=H (**XXXVIII**)
Nannochelin C R_1=R_2=H (**XXXIX**)

Antibiotic activity. Several Gram-positive test organisms, mainly *Bacillus* species were inhibited by some of the nannochelins (40 µg of the respective nannochelin per 6 mm paper disc) in agar diffusion tests. The resulting inhibition zones were, *e.g.* 0 and 18 mm against *B. megaterium* DSM 32 and *B. subtilis* DSM 10 for **XXXVIII**, and 15 and 0 mm against the same strains for **XXXIX**. In this test inhibition of *M. luteus* GBF26 and *S. aureus* GBF 16 was incomplete. An MIC was determined for *Brevibacterium ammoniagenes* (which showed inhibition zones of 22–29 mm) and found to be 1.5 µg/mL for nannochelin A and B, and 0.39 g/mL for nannochelin C. Further, also a few fungi were inhibited, albeit to a minor extent.

Since the nannochelins are siderophores their mode of action remains even more obscure, since bacterial growth stimulation may be suggested especially for those bacteria which are able to use these siderophores for iron-uptake, *e.g.* mycobacteria (Guo et al., 2002). This mechanism could be used as a new form of drug delivery, utilizing the pathogenic organism's own iron transport system. Thus, these compounds represent interesting structures for the development of conjugates, consisting of a lethal drug covalently attached to a siderophore.

1.6.5 Roimatacene

Roimatacene (**XL**) is a polyenic carboxylic acid with the molecular formula $C_{30}H_{44}O_7$. Its isolation from *Cystobacter ferrugineus* Cb G35 was challenging due to chemical instability. The metabolite harbours an acrylic acid residue, two α-polyunsaturated alcohol groups, a tertiary alcohol, and several conjugated double bonds; all together resulting in oxygen- and light-sensitivity (Zander et al., 2011). Feeding studies with ^{13}C-labelled precursors, *i.e.* [1-^{13}C]- and [2-^{13}C]-labelled acetate, [$^{13}CH_3$]-methionine, and [1-^{13}C]-propionate, clearly showed that all methyl groups are SAM-derived. The linear chain of carbons was found to be acetate-derived with the distinctive feature

that also the "C_3 starter unit" derived from a methylated acetate building block (Zander et al., 2011).

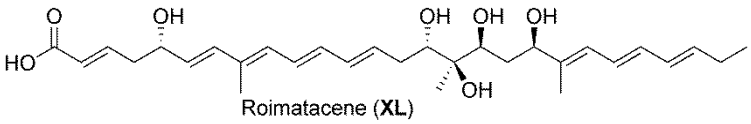

Roimatacene (**XL**)

Antibiotic activity. Unlike most other myxobacterial antibiotically active compounds, which show by their majority activity against Gram-positive bacteria, roimatacene was found active against the Gram-negative *E. coli*. Activity against *E. coli* and *Pseudomonas* species (MIC of 8.6 µg/mL *E. coli*, 4.2 µg/mL *Pseudomonas stutzeri*) was in the moderate range. Only toward *E. coli* tolC the MIC was impressive, *i.e.* 0.1 µg/mL (Zander et al., 2011). In a proliferation assay using a mouse fibroblast cell line L929 an $IC_{50} \geq 18$ µg/mL was observed. This indicated no or at the most little cell toxicity. A further evaluation of this antimicrobial metabolite, however, was not performed due to its chemical instability. Indeed, in all assays the radical scavenger 4-ethoxyphenol had to be added to avoid decomposition of the test sample. Detailed SAR- and mode of action studies may, nevertheless yield chemically more stable roimatacene derivatives. This is of special interest in the view of the selective activity against Gram-negative bacteria, a field in which new lead structures and targets are extremely desirable.

1.6.6 Sorangiadenosine

Sorangiadenosine (**XLI**) was isolated from *S. cellulosum* strain KM1003 and represents a nucleoside substituted with a sesquiterpene (Ahn et al., 2008). The molecule thus consists of three distinct units: (i) the heteroaromatic adenosine; (ii) the pentose sugar D-ribofuranose; and (iii) a bicyclic sesquiterpene of the eudesmane-type.

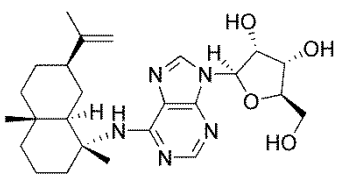

Sorangiadenosine (**XLI**)

Antibiotic activity. Determination of MIC values showed sorangiadenosine to moderately inhibit Gram-positive bacteria, *e.g.* the MIC values against *M. leuteus* IFC 12708 and *S. aureus* ATCC6538p were 6.25 and 25 µg/mL, respectively. The growth of *E. coli* cells was not inhibited.

1.6.7 Sulfangolids and Kulkenon

With the sulfangolids (**XLII–XLV**) the first sulphate ester containing secondary metabolites from myxobacteria were isolated from different *Sorangium cellulosum* strains (e.g. So ce666, So ce192, So ce1375) (Zander et al., 2012). They are macrolides with a prominent conjugated triene (**XLIV**) or tetraene (**XLII**, **XLIII**, **XLV**) moiety. Sulfangolid B (**XLIII**) carries an additional methoxy group, compared to sulfangolid A, whereas a most prominent feature of sulfangolid C (**XLIV**) is a six-membered semi-ketal ring. A ketal ring is also present in sulfangolid D (**XLV**), even though not as a hemi-ketal. Only the relative configuration of sulfangolid C (**XLIV**) was elucidated, because this molecule contains conformationally less flexible elements like the hemi-ketal ring and the dienone moiety.

For these macrolides a PKS-based biosynthesis was assumed. Thus, feeding studies with [1,2-$^{13}C_2$]-acetate, [1-^{13}C]-propionate, and [D_{10}]-leucine were performed with the producer strain of sulfangolid C (**XLIV**), So ce757, and revealed a leucine derived isovaleryl-CoA as the starter unit. The subsequent building blocks were analysed to be two methyl-malonyl and one malonyl-CoA unit. Further, the branched hemi-ketal ring and the adjacent carbons C-20 and C-33 originate from two propionate and one acetate unit. Apart from that, all other carbons in compound **XLIV** were assembled from acetate units. The sulphate residue is assumed to originate from the growth medium used. The release of the molecule from the PKS machinery goes most probably along with lactonisation, resulting in the final macrolide ring (Zander et al., 2012). The genetic basis of the biosynthesis is currently under investigation.

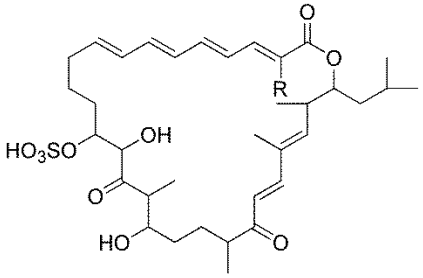

Sulfangolid A R=H (**XLII**)
Sulfangolid B R=OMe (**XLIII**)

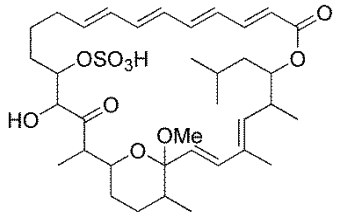

Sulfangolid D (**XLV**)

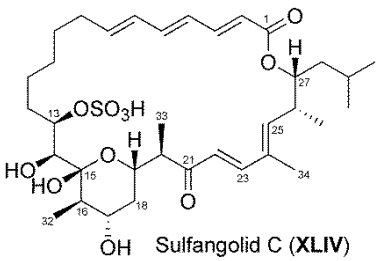

Sulfangolid C (**XLIV**)

Antibiotic activity. The antibiotic spectrum of sulfangolid C ammonium salt was analysed by agar diffusion tests. Only marginal activity against Gram-positive bacteria was observed. In the case of *S. aureus*, *B. subtilis* and *Nocardia corallina* 10 µg/disc of **XLIV** resulted in an inhibition zone of 8–10 mm, while no inhibition was observed for *E. coli* tolC. Sulfangolid C also showed activity in an anti-HIV screen (Martinez et al., 2013). Due to the conjugated double bonds the compounds are very sensitive to light, which poses a major obstacle for further investigations (Zander et al., 2012).

Kulkenon (**XLVI**) is a further metabolite produced by a *S. cellulosum* strain (So ce1426) and shows structural similarity to the sulfangolids. Compared to the latter, molecule **XLVI** carries an additional methyl group (C-30) and is devoid of a sulphate ester moiety The macrolide ring consists only of 26 carbons instead of 28 as in the case of sulfangolids (Zander et al., 2012). Any further development of sulfangolids is hindered by their instability, since these macrolides decompose during storage.

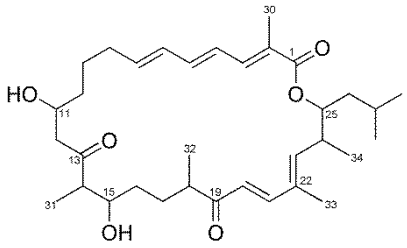

Kulkenon (**XLVI**)

1.7 Antibiotics from marine myxobacteria

The investigation of marine myxobacterial species has started only recently, due to the fact that these organisms are yet hard to cultivate and slow-growing. However, in 2013 some antibiotically active substances have been isolated from marine myxobacteria.

Salimyxin B (**XLVII**) and enhygrolide A (**XLVIII**) from *Enhygromyxa salina* strains SWB005 and SWB007, showed inhibitory activity toward the non-pathogenic

Arthrobacter cristallopoietes with MIC values of 8 and 4 µg/mL, respectively (Felder et al., 2013a). Another compound isolated by Felder et al. (Felder et al., 2013b) named salimabromide (**XLIX**) (only present in strain SWB007) possesses a new carbon skeleton, consisting of four rings including a highly brominated benzene ring, a furano lactone residue, and a cyclohexane ring, bridged by a seven-membered cyclic moiety. The antibiotic activity was moderate with an MIC against *A. cristallopoietes* of 16 µg/mL.

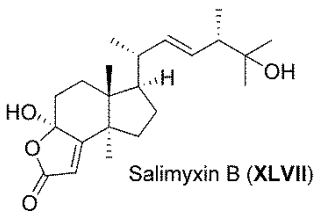

Salimyxin B (**XLVII**)

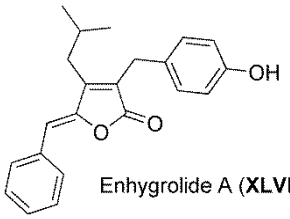

Enhygrolide A (**XLVIII**)

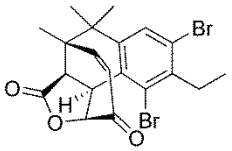

Salimabromide (**XLIX**)

2 Scope of the study

This study focuses on the biosynthesis of corallopyronin A, an antibiotically active natural product biosynthesized by the myxobacterial strain *Corallococcus coralloides* B035. In the laboratory of Prof. König this producer strain was isolated from a soil sample in 2004 and enabled the identification of the corresponding putative biosynthetic gene cluster (Erol et al., 2010). Corallopyronin A was reported as potential drug against lymphatic filariasis and River blindness (Schiefer et al., 2012) and currently undergoes preclinical evaluation (Schäberle et al., 2014b).

The aim of the present study was to obtain a deeper understanding of the biosynthesis of corallopyronin A, which is even more important in the light of its preclinical evaluation. Merely a detailed knowledge of its biosynthesis can enable a further successful development and bioengineering of this promising antibiotic.

Corallopyronin A is generated by a *trans*-acting acyltransferase (AT) mixed type polyketide synthase/non-ribosomal peptide synthetase (PKS/NRPS). Two chains are separately assembled during the biosynthetic process, one solely PKS- and the other PKS/NRPS derived. The *trans*-acting ketosynthase (KS) CorB probably mediates the interconnection of both chains by a Claisen-type reaction resulting in the pyrone ring formation. Further remarkable chemical characteristics of corallopyronin A are the methyl carbamate starter unit of the eastern chain, as well as the C-11, C-12 double-bond representing a rare β,γ pattern, the latter contradicting the co-linearity rule usually valid for classical PKS/NRPS machineries (Piel, 2010). In order to elucidate the genetic and enzymatic basis of the origin of this unusual β,γ pattern of the C-11, C-12 double-bond in corallopyronin A the most likely involved dehydratase CorJ DH* was to be investigated during this study. Analogously to the biosynthesis of rhizoxin (Kusebauch et al., 2010) we assumed a specific domain (CorJ DH*) to shift the double-bond from the α,β to the β,γ position after elongation of the nascent PKS chain.

The current study aimed to demonstrate this enzymatic reaction in an appropriate *in vitro* assay. Therefore, the chemical synthesis of a substrate of CorJ DH*, a *N*-acetylcysteamine (SNAC) activated intermediate of corallopyronin A biosynthesis was planned. Also the heterologous expression of such domains from the corallopyronin A gene cluster, which could be expected to be involved in the double-bond isomerisation (CorJ DH*, CorJ ACP) was targeted. The double-bond migration was

envisaged to be detected by applying high-resolution MS measurements using the phosphopantetheinyl (ppant) ejection assay (Meluzzi et al., 2008) and by NMR analysis. To obtain evidence for the essential amino acids involved in the double-bond migration process, mutated enzyme variants were planned to be constructed and expressed.

The *in vitro* analysis of the heterologously expressed shift domain (CorJ DH*) and its mutated variants should provide a basic understanding of carbon-carbon double-bond shift reactions in polyketide biosynthesis beyond that of corallopyronin A.

3 Material and Methods

3.1 Solvents and Reagents

Solvents and reagents were obtained from Roth (Karlsruhe, Germany), Sigma-Aldrich (Steinheim, Germany) or Fluka (Taufkirchen, Germany).

3.2 Enzymes

The enzymes used in this work were obtained from Fermentas (St. Leon Rot, Germany), Promega (Mannheim, Germany) or Roth (Karlsruhe, Germany). They were applied following the respective manufacturer´s recommendations for use. Restriction enzymes were purchased together with the appropriate reaction buffers and were applied according to the provided company´s protocols.

3.3 Molecular biological kits

Molecular biological kits were received from Quiagen (Hilden, Germany), Promega (Mannheim, Germany), Epicentre (Madison, U.S.A) or Zymo Research Europe (Freiburg, Germany). They were used accordingly to the respective provided company´s protocols.

3.4 Media, stock solutions and buffers

Media and stock solutions used to prepare media were sterilized either via steam sterilization or via membrane filtration.

Media	**Ingredients**
LB medium	10 g tryptone, 5 g yeast extract, 10 g NaCl, water ad 1000 mL, pH=7.5
LB agar	10 g tryptone, 5 g yeast extract, 5 g NaCl, 15 g agar, water ad 1000 mL, pH=7.5
VY/2 agar	50 ml yeast suspension (10 %), 1.36 g $CaCl_2$ x $2H_20$, 15 g agar, water ad 1000 mL, pH=7.2;

	after sterilization add 1 mL trace element solution I and 1 mL vitamin B_{12} solution
MD1 + G medium	3 g casitone, 0.7 g $CaCl_2$ x $2H_2O$, 2 g $MgSO_4$ x $7H_2O$, 2.2 g glucose, water ad 1000 mL, pH=7.5; after sterilization add 1 mL trace element solution I and 1 mL vitamin B_{12} solution
SOB medium	20 g tryptone, 5 g yeast extract, 0.5 g NaCl, 0.186 KCl, water ad 1000 mL, pH=7.5
SOC medium	20 g tryptone, 5 g yeast extract, 0.5 g NaCl, 0.186 KCl, water ad 1000 mL, pH=7.5, after sterilization add 1 mL of 1 M glucose solution
PMM medium (Stephan et al., 2006)	12 g glucose, 8 g Na_2HPO_4, 5 g KH_2PO_4, 3 g $(NH_4)_2SO_4$, water ad 1000 mL, after sterilization add 1 mL magnesium sulphate solution, 10 mL trace element solution II, 30 mL salt solution.

Stock solutions	**Ingredients**
Magnesium stock solution (Stephan et al., 2006)	250 mg $MgSO_4$ x $7H_2O$, water ad 1000 mL.
Salt solution (Stephan et al., 2006)	10 mg $FeSO_4$ x $7H_2O$, 10 mg $CaCl_2$ x $2H_2O$, water ad 1000 mL
Trace element solution I	20 mg $ZnCl_3$, 100 mg $MnCl_2$ x $4H_2O$, 10 mg H_3BO_3, 10 mg $CuSO_4$, 20 mg $CoCl_2$, 5 mg SnCl2 x $2H_2O$, 5 mg LiCl, 20 mg KBr, 20 mg KI, 10 mg Na_2MoO_4 x $2H_2O$, 5.2 g Na-EDTA x $2H_2O$, water ad 1000 mL
Trace element solution II (Stephan et al., 2006)	200 mg $FeCl_3$ x $6H_2O$, 200 mg $MnSO_4$ H_2O, 50 mg $ZnSO_4$ x $7H_2O$, 20 mg $CuCl_2$ x $5H_2O$, 10 mg $(NH_4)_6Mo_7O_{24}$ x $4H_2O$, water ad

	1000 mL
Vitamin B_{12} solution	0.5 mg cyanobobalamine ad 1 mL water
Ampicillin stock	100 mg ampicillin ad 1 mL water
Apramycin stock	100 mg apramycin ad 1 mL water
Carbenicillin stock	100 mg carbenicillin ad 1 mL water
Chloramphenicol stock	12 mg ampicillin ad 1 mL ethanol
Kanamycin stock	60 mg kanmycin ad 1 mL water
Streptomycin stock	100 mg streptomycin ad 1 mL water
Tetracyclin stock	10 mg tetracyclin ad 1 mL water

Buffer	**Composition**
Buffer 1	50 mM Tris- HCl (pH=8), 10 mM EDTA, 100 µg/ml RNase A
Buffer 2	200 mM NaOH, 1 %SDS
Buffer 3	3 M potassium acetate (pH=5.5)
TE-buffer	10 mM Tris- HCl (pH=8), 1 mM EDTA
10x TBE-buffer	0.89 M Tris, 0.02 M EDTA, 0.87 M H_3BO_3
Protein lysis buffer	50 mM NaH_2PO_4, 300 mM NaCl, 10 mM imidazole, pH=8
Protein wash buffer	50 mM NaH_2PO_4, 300 mM NaCl, 20 mM imidazole (alternative 40 mM), pH=8
Protein elution buffer	50 mM NaH_2PO_4, 300 mM NaCl, pH=8; for gradual elution use 100, 150, 200, 300 mM imidazole
10x glycine SDS electrophoresis buffer	250 mM Tris, 2 M glycine, 1 % SDS, pH=9
Staining solution	10 %acetic acid, 50 % ethanol, 0.005 % coomassie brilliant blue R-250, 40 % water
Destaining buffer	10 % acetic acid, 30 % methanol, 60 % water

3.5 Bacterial strains

In the main focus of this study is the producer strain of corallopyronin A *Corallococcus coralloides* B035 which harbours the biosynthetic gene cluster of corallopyronin A. The strain *Pseudomonas* putida KT2440 is envisaged to be the heterologous host for parts of the corallpoyronin A gene cluster. E*. coli* XL1 Blue was used for plasmid construction. For protein expression experiments either *E. coli* Bap-1 or *E. coli* BL21 were used. *E.coli* BW25113 was used for Lamda Red strategies in correlation with the knock-out approach of the *trans*-acyltransferase in *Corallococcus coralloides* B035.

Organism	**Genotype**	**Provider**
Corallococcus coralloides B035	wild type	own strain collection
Pseudomonas putida KT 2440	wild type	Prof. Piel lab
E. coli XL1 Blue (K12)	recA1 endA1 gyrA69 thi-1 hsdR17 supE44 relA1 lac [F´proAB $lacI_qZ\Delta M15$ Tn 10 (Tet^r]	Agilent (Böblingen, Germany)
E. coli Bap-1	n.a.; sfp from *B. subtilis*	(Pfeifer and Khosla, 2001)
E. coli BL21	F^- ompT gal dcm Ion hsdSb (r_B^- m_B^-) λ(DE3 [lac lacUV5-T7 gene1 ind 1 sam7 nin5])	Invitrogen (Karlsruhe, Germany)
E.coli BW25113	F-, Δ(araD-araB)567, ΔlacZ4787 (::rrnB-3), λ-, rph-1, Δ(rhaD-rhaB)568, hsdR514	(Gust et al., 2003)

3.6 Vectors

Vector	Resistance	Manufactuer
pcc1FOS™	chloramphenicole	Epicentre Biotechnologies (Madison, U.S.A)
pET28a(+)	kanamycin	Merck (Darmstadt, Germany)
pGEM-T	ampicillin	Promega (Mannheim, Germany)
pIJ773	apramycin	(Gust et al., 2003)
pIJ778	streptomycin	(Gust et al., 2003)
pKD46	ampicillin	(Datsenko and Wanner, 2000)
SuperCos1	ampicillin, kanamycin	Agilent (Böblingen, Germany)

3.7 DNA constructs in this study

Construct	Vector	Insert
FJ7	SuperCos1	Genomic DNA from *Corallococcus coralloides* B035 with parts of the corallopyronin Acluster
FJ7 AT::aadA	SuperCos1	*AT::aadA*
FJ7 AT::aac(3)IV	SuperCos1	*AT::* aac(3)IV
FJ7_aadA_EcoRV/SpeI	SuperCos1	*aadA*_EcoRV/SpeI
pIB861_apra	pIB861	*aac(3)IV*
FJ7_pm/xylS	SuperCos1	pm*, xylS, aac(3)IV*
pGEMT_trpE/tetA	pGEMT	*trpE, tetA*
FJ7_pm/xylS/trpE	SuperCos1	pm*, xylS, trpE, tetA, aac(3)IV*
pGEMT_CorJ DH*	pGEMT	*corJ DH**
pGEMT_CorJ ACP	pGEMT	*corJ ACP*
pGEMT_CorJ DH*ACP	pGEMT	*corJ DH*ACP*
pGEMT_CorJ DH*H47A ACP	pGEMT	*corJ DH**H47A *ACP*
pGEMT_CorJ DH*D211N ACP	pGEMT	*corJ DH**D211N *ACP*
pet28a_CorJ DH*	pet28a(+)	*corJ DH**
pet28a_CorJ ACP	pet28a(+)	*corJ ACP*
pet28a_CorJ DH*ACP	pet28a(+)	*corJ DH*ACP*

pet28a_CorJ DH*H47A ACP	pet28a(+)	*corJ DH** H47A *ACP*
pet28a_CorJ DH*D211N ACP	pet28a(+)	*corJ DH** D211N *ACP*

3.8 Primers

Primers used in this work were designed from multi sequence alignment and purchased from Eurofins MWG Operin (Ebersberg, Germany). Oligonucleotides were reconstituted in sterile water and adjusted to a concentration of 100 pmol/µL. They were stored at -20 °C for longer periods and at -4 °C for a short time. A list of the sequences of primers out of this work is given in the appendix (8.1).

3.9 Software and databases

Basis Local Alignment Search Tool; Blast [www.blast.ncbi.nlm.nih.gov] provided by the National Centre for Biotechnology Information (NCBI) is used for multiple sequence alignment for protein primary sequences and for nucleotide sequences. Blastx translates nucleotide sequences in its corresponding amino acid sequence which subsequently are compared to the amino acid database. Blastp uses a protein query for comparison with the protein database. Blastn was used to compare a nucleotide sequence with the nucleotide database of NCBI.

ClustalW [www.ebi.ac.uk/Tools/msa/clustalw2] provides by the European Bioinformatics Institute (EBI), part of the European Molecular Biology Lab (EMBL), was applied to from multiple sequence alignments of nucleotide or amino acid sequences. Given reference sequences are NCBI derived.

Clone Manager is a purchased program (Sci-Ed Software) and was used due to its set of tools for primer design and for planning of cloning experiments as well as for graphic map drawing.

NEBcutter V2 (www.tools.neb.com/NEBcutter2; New England Biolabs) was applied to carry out restriction side analysis.

Artemis Genome Browser and Annotation Tool is a freely available program provided by the Sanger Institute. It was utilized to visualize bioinformatic features and to annotate open reading frames in sequences plasmid, cosmid or genome derived as well as to analyze the GC-content of a sequence.

ProtPram is a free bioinformatic tool provide by the Swiss Institute for Bioinformatics. It was applied to calculate the molar extinction factor ε, necessary for determination of the concentration of purified heterologously expressed proteins.

3.10 General molecular biological methods

3.10.1 Sterilization

Solutions, media and all working tools used to apply on microbial organisms were sterilized by steam sterilization at 121 °C and 2 bar for 20 min in a Varioclav steam sterilizer. Heat sensitive solutions were sterilized by filtration through an 0.22 µm membrane, instead.

3.10.2 Cultivation, storage and disposal of organisms

All working-steps concerning cultivation of microorganisms were done on a lamina air flow clean bench to provide sterile conditions. Instruments, solutions, media and other working materials were beforehand sterilized via steam sterilization, membrane filtration or by the heat of a Bunsen burner flame.

Corallococcus coralloides B035 was inoculated from a Petri dish and incubated in 300 mL flasks containing 100 mL MD1+G liquid medium on a horizontal shaker at 30 °C and 160 rpm or on VY/2 agar plates in an incubator at 30 °C. The incubation time was between three and five days. *Pseudomonas putida* KT2440 was incubated either in 100 mL liquid LB medium in 300 mL flasks on a horizontal shaker at 30 °C and 160 rpm, on LB agar plates or on PMM agar plates at 30 °C in an incubator. Incubation times vary between 3 h and two days according to the experiment, respectively. Small cultures of *Escherichia coli* cells were carried out in 10 mL flasks filled with 3 mL LB liquid medium or in 2 mL tubes at 160 rpm at 30 °C or 37 °C, depending on the hosted plasmid or cosmid. For cultivation on LB agar plates 250 µL of a *Escherichia coli* suspension was spread on the agar plate. After the solvent was moved into the agar the plate was incubated at 30 °C or 37 °C in an incubator. The incubation time was 16 h, if not stated otherwise.

For long terms of storage glycerin cultures were prepared. Therefore 500 µL of a fully grown liquid culture was mixed with 500 µL of a sterile 87 % glycerin solution in a

cryogenic vial. After thoroughly merging the vial was stored at -80 °C. For short period storage glycerin cultures were frozen at -20 °C.

For waste disposal of microorganisms they were autoclaved for 20 min at 121 °C and 2 bar.

3.10.3 Antibiotic selectivity test

Corallococcus coralloides B035 (Erol et al., 2010) was tested toward natural resistance against different antibiotics. VY/2 plates were incubated with 300 µL liquid culture at 30 °C for 5. Growth on the agar plates was determined and the inhibition capacity was classified (Schmitz, PhD thesis, 2013).

3.11 Molecular biological methods concerning bacterial organisms

3.11.1 Transformation of bacteria

Preparation of competent cells for heat shock procedure. A 3 mL LB culture was inoculated with a single bacteria colony and incubated over night at 37 °C and 160 rmp. The culture was further transferred into a 300 mL flask containing 70 mL 2xYT medium and incubated at 37 °C and 180 rpm to an OD_{600}=0.3-0.4 and subsequent harvested centrifugation for 10 min at 8000 rpm at 4 °C. To achieve competence the cells were treated with 10 mL of ice cold $CaCl_2$/$MgCl_2$-solution (70 mM $CaCl_2$, 20 mM $MgCl_2$) and incubated on ice for 30 min. After harvesting the cells again by centrifugation they were suspended in 3.5 mL ice cold $CaCl_2$/$MgCl_2$-solution and 875 µL glycerol was added. The chemically competed cells were finally stored in 100 µL aliquots at -80 °C until usage.

Preparation of competed cells for electroporation procedure. Electro-competed cells were always freshly prepared in order to use on the same day. Following procedure was modified after Gust et al., 2003. During the whole procedure cells were strictly kept ice cold. 100 mL SOB medium in a 500 mL flask were inoculated with 3 mL pre-culture and incubated until OD_{600}=0.5. The culture was splitted into two 50 mL falcon tubes. After harvesting the cells via centrifugation, 6000 rpm for 5 min, the supernatant was removed and each pellet was washed with 25 mL 10 % glycerol

solution. This step was repeated and further washing steps were done with 20 mL, 10 mL and 5 mL 10 % glycerol solution. The pellets were combined, suspended in 300 µL 10 % glycerol solution and finally stored on ice in 100 µL aliquots.

Transformation of *Escherichia coli* cells by heat shock. For reasons of *in vivo* amplification of plasmids or protein expression *E. coli* cells were transformed with foreign DNA. Therefore a 100 µL aliquot of chemical competed cells were thawed on ice, mixed with 5–10 µL DNA and incubated on ice for 30 min. Afterwards, the cells were subjected to heat shock at 42 °C for 90 s and immediately replaced on ice for 2 min. For recovery purpose the cells were incubated in 1 mL LB medium at 37 °C and 1000 rpm for 1 h. 250 µL of the cell suspension were spread on agar plates containing the suitable antibiotics for selection of positive transformants and incubated over night at 30° or 37 °C. In the case of pGEM-T vector as introduced DNA the agar plates contained x-gal (4 mg/mL) as additive in order to select via blue-white screening. Positive clones were verify by whole-cell PCR (3.12.2).

Transformation of Escherichia coli cells by electroporation. Freshly prepared electro-competed cells were mixed with 4–20 µL of the DNA to be introduced and filled into a pre-chilled electroporation cuvette with a diameter of 2 mm. Following a voltage of 2.5 kV was applied in Biorad MicroPulser™. The cells were rapidly recovered with 1 mL ice cold SOC medium and incubated in a 10 mL tube at 30 °C at 160 rpm for 1–2 h. Afterwards, 600 µL of the cell suspension were spread on agar plates containing suitable antibiotics for selection and the plates were incubated at 30 °C over night.

Electroporation of Pseudomonas putida KT2440 cells. 2 mL of a pre-culture were inoculated in 100 mL LB medium and incubated until a OD_{600}=0.5 at 30 °C and 160 rpm. During the next steps it was important to keep the sample ice cold. Hence, the cells were harvested via centrifugation at 6000 rpm for 5 min at 4 °C, the supernatant was removed and the pellet was suspended in 25 mL ice cold 10 % glycerol solution. Washing steps with 20 mL, 10 mL and 5 mL 10 % glycerol solution followed. Finally the cell suspension was taken up in 300 µL 10 % glycerol solution and allocated in 100 µL samples. The electro- competed cells were mixed with 4–20 µL of

DNA to be transferred, and filled in a pre-chilled electroporation cuvette. To apply a voltage of 2.5 kV a Biorad MicroPulser™ was used. The cells were recovered immediately with 600 µL of ice cold LB medium and incubated for 2 h at 30 °C and 160 rpm. Positive transformants were selected on PMM solid agar containing suitable antibiotics and verified via whole cell PCR (3.12.2).

3.12 Molecular biological methods concerning nucleic acids

3.12.1 Isolation of DNA

Isolation of vector DNA. Plasmids, fosmids or cosmids were isolated from the host strain (usually *E. coli*). Normally 3 mL liquid media were inoculated with one single colony and incubated over night. For larger demand of vector DNA midi or maxi preparations were done. Thus means 10 mL or 100 mL medium were inoculated. Vectors were purified with Promega´s PureYield Miniprep or with Qiagen Plasmid Mini, Midi or Maxi Kit according to the manufactures instructions. Otherwise, bacterial cells of a 3 mL culture were harvested via centrifugation and suspended in 350 µL buffer 1, treated with 350 µL buffer 2 and neutralized with 400 µL ice cold buffer 3. Cell debris and proteins were pelleted by centrifugation and removed. The supernatant containing the remaining DNA was again purified with 800 µL phenol/chloroform in equal parts to remove protein remains. Solved DNA in the aqueous phase was precipitated by isopropanol and centrifugation. The obtained DNA pellet was finally washed with 70 % ethanol, dried and dissolved in 20–100 µL sterile water.

Isolation of genomic DNA. For isolation purpose of *Corallococcus coralloides* B035 and *Pseudomonas putida* KT2440 derived genomic DNA the Promega Genomic Wizard Kit was used according to the manufacturers' instructions.

3.12.2 PCR

Polymerase chain reaction. PCR is a method exerted for amplification of DNA sequences of interest inbetween two primer regions. Oligonucleotides appropriate to the DNA sequence of interest were designed with the help of the program Clone

Manager. First DNA was denaturated to single stranded DNA by heating what allows the primers to anneal to the homolog DNA region. Then a thermostable DNA polymerase elongates the DNA stand beginning at the primers 3' end. Repetitive cycles of different temperatures for denaturation, annealing and elongation make a exponential amplification of determined DNA regions possible. In this study the *Thermus aquaticus* (*Taq*) derived DNA- polymerase was used for all PCR reactions. The composition of the PCR reaction mixture, appropriate in this study, is shown as follows.

10x PCR buffer	4 µL
10x $MgCl_2$-solution (25 mM)	1 µL
DMSO	1 µL
Primer 1 (100 µM)	0.5 µL
Primer 2 (100 µM)	0.5 µL
dNTPs (10 mM)	0.4 µL
Taq polymerase (5 U/µL)	0.16 µL
DNA template	1 µL
Water	ad 20 µL

Whole cell PCR. For rapid testing on DNA introduced into bacteria, bacterial material was directly stirred into the PCR mixture. The first denaturation step of repetitive cycles of the PCR protocol was in this respect prolonged to ensure complete denaturation of the double stranded DNA.

Sequential PCR amplification. In order to exchange one amino acid in a protein it was necessary to gain an exchange of nucleotides in the protein encoding DNA sequence. To achieve that side specific mutation a chimeric DNA molecule was created by sequential PCR amplification. In the first round amplifications two PCR products were gained containing a region of overlapping homology to each other. Both PCR products were purified away from the primers, mixed in one reaction tube and annealed by denaturation a renaturation. *Taq* DNA-polymerase was added and gained one PCR fragment with the length to the sum of the two fragments. In the second round

amplification complementary outside set primers were added to the mixture in order to amplify the heteroduplex DNA species. Hereafter the applied PCR program is shown.

1. Initial enaturation	95 °C	3.0 min
2. Denaturation	95 °C	30 s
3. Annealing	65 °C	30 s
4. Elongation	72 °C	1.0 min
5. Final elingation	72 °C	5.0 min
6. Cooling	4 °C	hold

Steps 2–4 were repeated 10 times, without primers. In the following outside set primers were added and the PCR program was run again. Then steps 2–4 were repeated 20 times.

3.12.3 Restriction digestion

DNA restriction endonucleases belongs originally to bacterial defence mechanism against foreign DNA. Their restriction sides are marked as palindromic DNA sequence of 4–8 nucleotides. After cleavage of the phosphodiester-bonds within the DNA backbone blunt or sticky ends remain corresponding to the restriction enzyme used, respectively. The effectiveness of each restriction enzyme depends on temperature, reaction medium and methylation pattern of the DNA to be restricted. Purchased restriction enzymes in this work were applied according to the manufacturers' instructions. Restriction digestion was performed to prepare PCR- fragments, vectors and other DNA molecules for cloning purpose. Usually DNA was restricted by two different restriction enzymes, e.g. for clear orientation of incorporated DNA fragments in vectors. In the case of a digestion reaction with only one enzyme the linearised vector was subsequently dephosphorylated to prevent self-ligation.

3.12.4 Dephosphorylation of linear DNA

Vectors cut with only one restriction enzyme had to be dephosphoylized to avoid self-ligation when foreign linear DNA should be introduced. To prevent self-ligation the

vector's open ends were dephosphorylated by calf intestine alkaline phophatase (CIAP) or by shrimp alkaline phosphatise (SAP) according to the manufacturers' instructions. To remove the phophatase, which potentially disturb subsequent ligation reactions, the DNA mixture was purified away from the enzyme using a Qiagen MiniPrep Kit.

3.12.5 Agarose gel electrophoresis and DNA recovery

Mixtures of DNA fragments of different size were separated by gel electrophoresis, *e.g.* restricted vectors, PCR fragments or genomic DNA. The areas of interests were cut out of the gel and the DNA was purified with the help of a Qiagen gel extraction kit following manufacturers' instructions. Isolated DNA was dissolved in ultrapure, sterile water.

3.12.6 Ligation of DNA into a vector

To introduce DNA fragments into a vector, both had to be subjected to a restriction digestion (3.12.3). Subsequent ligation of the resulting linear DNA molecules were performed by a T4 DNA- ligase, which is able to link the 5'-phopshodiester moiety and the 3'-hydroxyl functionality of linear DNA molecules with each other. Thus, DNA molecules with blunt or with compatible sticky ends could be stitched together. The result was a circular double stranded DNA molecule consisting of a selected DNA fragment and the vector scaffold. T4 DNA-ligase was used analogously to a standard protocol and to the manufacturers' instructions. For *in vivo* amplification of the obtained vector construct and for save storage it was transferred into a bacterial host like *Escherichia coli* XL1 blue (3.5 and 3.11.1).

3.12.7 Sequencing of DNA constructs and PCR fragments

To determine the sequence of PCR fragments and to exclude mutations in plasmids their DNA sequence had to be analyzed. Sequencing was performed by GATC Biotech AG (Konstanz, Germany) on an ABI3730xl after the Sanger dideoxy method (Sanger et al., 1977). For sequencing reaction either specific primer pairs complementary to the

PCR fragment, or general primer pairs complementary to the vector were used. The obtained sequence information were processed with Clone Manager.

3.13 Molecular biological methods concerning proteins

3.13.1 Heterologous expression of the proteins

For the *in vitro* investigations of proteins a sufficient amount of the desired protein is required. In order to obtain that usually over expression of the respective protein in a heterologous host is applied. Therefore the DNA sequence of the target protein was cloned into an expression vector (*i.e*. pET28a(+)). The pET28a(+) vector contains an isopropyl-β-D-thiogalactopyranosid (IPTG) inducible promoter as well as an affinity tag like the 6-his tag to facilitate the purification of the protein via affinity chromatography.

In the first step the DNA sequence of the protein was amplified and the resulting PCR fragment was ligated into the pGEMT vector. To exclude mutations in between the amplified DNA sequence the construct was submitted to sequencing at GATC (3.12.7). Second the DNA encoding for the protein was cut out of the pGEMT construct and cloned into the multiple cloning side of the expression vector (pET28a(+) so that the DNA sequence of the protein is in-frame with the 6-his tag within the vector. Finally *E. coli* Bap-1 or BL21 cells were transformed with the generated plasmid, and positive transformants were determined by whole-cell PCR (3.12.2).

A 3 mL pre-culture of the pET28a(+) construct was used to inoculate the main culture of 1 L LB medium, containing kanamycin. The culture was grown at 37 °C to an OD_{600} of ~0.5 and then chilled to 16 °C. To induce protein expression IPTG was added to the medium in a final concentration of 0.5 or 1 mM and the culture was further incubated overnight at 16 °C.

3.13.2 Cell lysis by sonication

Cells used for protein expression were harvested by centrifugation at 4000 rpm for 30 min at 4 °C. Afterwards the pellet was resuspended in 2 mL lysis buffer and placed on ice. Cells were lysed with the help of the Branson Sonifier 250, set to output level 4, 50 % duty cycle. The samples were sonified five times with ten pulses each. Cell

debris and insoluble parts were pelleted by centrifugation at 8000 rpm for 15 min at 4 °C. The supernatant containing the soluble protein was collected for further purification via affinity chromatography.

3.13.3 Purification of the recombinant protein by Ni-NTA affinity chromatography

Proteins containing a 6-his tag can easily be purified by affinity chromatography on a Ni-NTA matrix. The twice positive charged Ni^{2+} ions interact with the histidine residues of the 6-his tag and bind the protein to the matrix while other proteins elute. With increasing concentrations of imidazole unspecific linked proteins can be eluted due to the competition of imidazole with hisitine for the binding to Ni^{2+}. The 6-his tag ensure that the target protein elutes only at high imidazole concentrations.

The Ni-NTA gravity flow column consists of a Ni-NTA agarose matrix which is equilibrated with lysis buffer. The sample, also dissolved in lysis buffer, was added to the column and is allowed to pass the matrix. The resulting flow through was added once again to the matrix to ensure a nearly complete binding of the protein to the Ni-NTA matrix. Then the column was washed twice with 4 mL washing buffer. Subsequent elution of the protein occurred in five elution steps with each 0.5 mL elution buffer with increasing imidazole concentrations (100, 150, 200, 300, 300 mM imidazole). All fractions, flow through fraction to last elution fraction, were collected and stored on ice to avoid protein degradation.

3.13.4 SDS-Polyacrylamind gel electrophoresis (SDS-PAGE) and Coomassie staining

All collected fractions of the protein purification were subjected to SDS-PAGE to record the purity and the average quantity of the target protein in each fraction. First the fractions were boiled and treated with mercapto ethanol to reduce all di-sulfide bonds to gain unfolded proteins. During electrophoresis in a SDS milieu the proteins are charged completely negative and are able to be strictly separated due to their molecule weight. The separating gel is gained by the polymerization of bis-acrylamid to polyacrylamide which gives a molecular sieve. Depending on the molecular weight of the proteins to be separated the concentration of polyacrylamide can be adapted. To achieve focussed protein bands, discontinuous gels were used where the

separating gel is covered with a stacking gel with a lower acrylamid concentration. In a first step the separating gel was prepared, which was pipetted between two plastic plates with a spacer distance of 1.5 mm directly after initiating the polymerisation by APS (ammoniumperoxosulfate). To form a smooth surface the separating gel was covered with isopropanol, which was removed before addition of the stacking gel. The reaction mixture of both components of the discontinuous gels is as follows:

SDS stacking gel

Tris/HCl pH 6.8 (1 M)	375 µL
SDS (10 %)	30 µL
Bis-acrylamide (30 %)	510 µL
Water	2040 µL
APS (10 %)	30 µL
TEMED	3 µL

SDS separating gel

Tris/Hcl pH 6.8 (1 M)	2500 µL
SDS (10 %)	100 µL
Bis-acrylamide (30 %)	4000 µL
Water	3300 µL
APS (10 %)	100 µL
TEMED	4 µL

For each run the reservoir of the electrophoresis assembly were filled with fresh SDS electrophoresis buffer. The protein samples were mixed with denaturing loading buffer and boiled for 5 min at 90 °C, before loading them on the gel. Electrophoresis was performed in a XCell SureLock® Mini-Cell. The voltage was 100 V until the samples reached the separating gel, then it was increased to 130 V. As a reference a molecule size marker was loaded on the gel as well.

Following directly after the electrophoresis the proteins were visualized by a coomassie-staining. The gel was immersed in the staining solution and shortly heated in a microwave and subsequent incubated several minutes on a horizontal shaker.

Destaining of the background colour was performed by shaking with destaining buffer for several hours at room temperature. Gels were documented with the INTAS illuminator.

3.13.5 Concentration of the proteins and buffer exchange

Samples containing purified heterologously expressed proteins were concentrate using spin filter column (Millipore, 10 kDa exclusion size). This method was also used to remove imidazole from the elution buffer, which could disturb subsequent assays. The elution buffer was replaced in several centrifugation steps with 50 mM Tris/HCl (pH 8) to achieve a final volume of 250 to 500 µL protein solution. Proteins scheduled for the MS based ejection assay (3.17.1) were buffered in 50 mM deuterated Tris/HCl (pH 8), which was prepared beforehand: 50 mM aqueous Tris/HCl solution (1 mL each sample) were dried in a SpeedVac completely, and were resolved in the same volume of D_2O.

3.13.6 Determination of the protein concentration

Proteins containing tyrosine and tryptophan residues and disulphide bonds will absorb in the UV range of 280 nm making the correlation between absorbance and protein-concentration for purified proteins possible. The calculation is based on the Lambert-Beer equation (**formula 3-1**). It requires the knowledge of the molar extinction factor (ε) which was calculated for a given protein sequence with the program ProtPram provided by the Swiss Institute for Bioinformatics.

Formula 3-1: $$concentraion = \left[\frac{mol}{L} \right] = \frac{OD \times d}{\varepsilon}$$

OD_{280}=optical density at λ=280 nm

d=dilution factor

ε=molar extinction factor [$M^{-1}cm^{-1}$]

3.14 Chromatography

Affinity chromatography. See Molecular biological methods concerning proteins (3.13.3).

Thin layer chromatography. For reaction control during synthesis of compounds **1**, **5–8**, **10–13** thin layer chromatography was performed on Merck aluminum sheets, silica gel 60 F_{254}. After detection under UV light (254 nm) development took place using a solution of ninhydrin in ethanol (0.2 % (m/V). As purification method column chromatography was carried out on Merck silica gel 60 (70–230 mesh). As eluent a mixture of ethyl acetate/petroleum ether or a mixture of dichloromethane/methanol was used.

High performance liquid chromatography (HPLC). HPLC was performed on either a Merck-Hitachi system equipped with an L-6200A pump, an L-4500A photodiode array detector, a D-6000A interface with D-7000 HSM software and a Rheodyne 7725i injection system, or a Waters system, controlled by a Waters millennium software, consisting of a 717 puls autosampler, 600 pump with in-line degasser and a 996 photodiode array detector. Either a Waters Atlantis C18 column (5 µm, 4.6×250 mm), or a Waters Symmetry 300 C4 column (5 µm, 4.6 mm×250 mm) were used for preparative HPLC purification of synthesis products of enzyme assay reaction products.

3.15 NMR spectroscopy

^{1}H-NMR and ^{13}C-NMR spectra were recorded on a Bruker Avance 300 DPX operating at 300 MHz (^{1}H) or 75 MHz (^{13}C), on a Bruker Avance 500 DRX operating at 500 MHz (^{1}H) or 125 MHz (^{13}C) or on a Brucker Avance 600 operating at 600 MHz (^{1}H) or 300 MHz (^{13}C) respectively. Processing of the NMR spectra was done using Bruker 1D WIN-NMR, 2D WINNMR or XWIN-NMR Version 2.6 or 3.1. Chemical shifts were given in ppm relating to the center of the solvent peak at reference: [D4]MeOH 3.35/49.3 ppm, [D6]DMSO 2.49/39.7 ppm. Multiplicity of carbon atoms was deduced by DEPT experiments. Structural assignment were based on spectra resulting from

one or more of the following NMR experiments: ^{1}H, ^{13}C, DEPT 135, ^{1}H-^{1}H COSY, ^{1}H-^{13}C HSQC (direct correlation) and ^{1}H-^{13}C HMBC (long range correlation).

3.16 Mass spectrometry

HPLC-MS (ESI) measurements were performed by Frau M. Schneider (Pharmaceutical Institute of the University of Bonn) or by Frau. E. Eguereva (Institute for Pharmaceutical Biology of the University of Bonn) employing an Agilent 1100 Series HPLC including DAD, with a RP 18 column (Macherey-Nagel Nucleodur 100, 125 mmx2 mm, 5 µm) coupled with an API 2000, Triple Quadrupole, LC/MS/MS, applied Biosystems/MDS Sciex and ESI source. A gradient elution of (from 90 % H_2O to 100 % MeOH in 10 min, then 100 % MeOH to 20 min, with added NH_4Ac, 2 nM, DAD 220.0–400.0 nm) was chosen for compound characterization and purity determination. Mass spectrometric analysis of proteins was done by M. Sylvester (Institute for Biochemistry and Microbiology of the University of Bonn) using a Thermo LTQ Orbitrap Velo coupled with an Advion TriVersaNanoMate enabling a continues electron spray.

3.17 In vitro assays to prove the functional role of the DH*

3.17.1 Phosphopantethein (Ppant) ejection assay

The activity of the heterologously expressed shift domain CorJ DH* was determined in a MS based *in* vitro assay: the ppant ejection assay, which enables the analysis of carrier bound intermediates (Meluzzi et al., 2008). In the first reaction step the SNAC-activated substrate should bind to the ppant arm of the *holo*-ACP protein. The second reaction step should be the shift of the double-bond, performed by the “shift domain§ CorJ DH*. Therefore the substrate **1** was loaded onto the phosphopantethein arm of the CorJ ACP unit of the heterologously expressed didomain CorJ DH*-ACP by co-incubation at room temperature. The shift reaction started directly at this time (substrate addition was set as time point zero). The assay volume was 100 µL containing 2 % DMSO: 10 µL protein solution, 2 µL substrate **1** (equal to 0.2 mM), 38 µL buffer (deuterated Tris 50 mM, pH 8.0). The reaction mixture was incubated at room temperature for 1 h, 3 h and 20 h. To stop the

reaction it was directly injected into the HPLC column (Waters Symmetry 300 C4; solvent: linear gradient from 70 % water to 65 % acetonitrile over 30 min, flow: 1.0 mL/min) to obtain a desalted sample, which was immediately lyophilized with liquid nitrogen.

The respective samples were dissolved in an adequate volume of electro spray solution (49.5 % H_2O, 49.5 % methanol, 1% formic acid). 10 µL samples were loaded onto the 96 well plate of the NanoMate spray robot coupled to the LTQ Orbitrap Velos. A spray chip with 5 µm nozzle diameter was used at a spray voltage of 1.6 kV and 0.3 psi pressure setting. An environmental polysiloxane ion with *m/z* 445.12003 was used as lock mass for internal calibration. Typical mass deviation was <2 ppm. Isolation and fragmentation were performed in the linear ion trap, detection of the final product spectrum was done with the Orbitrap analyzer.

The same procedure and assay conditions were applied for investigating of CorJ *holo*-ACP, CorJ DH*H47A *holo*-ACP and CorJ DH*D211N *holo*-ACP.

3.17.2 NMR based assay

The double bond shift mediated by the “shift domain” CorJ DH* was additionally monitored using a NMR based *in vitro* assay. To perform this assay the didomain CorJ DH*-ACP was heterologously expressed in *E. coli* BL21, as an *apo*-enzyme, without a ppant arm. The purified protein CorJ DH* *apo*-ACP (re-buffered in non-deuterated Tris-buffer) was incubated with substrate **1** for 16 h. The assay volume was 500 µL containing 1 % DMSO: 250 µL protein solution, 5 µL substrate **1** (equal to 0.5 mM), 245 µL buffer (Tris 50 mM, pH 8.0). The assay was stopped by adding an equal volume of methanol. The protein was pelleted by centrifugation. The supernatant was transferred to a new vial and dried *in vacuo*. Subsequently, the sample was prepared for adjacent NMR experiments by dissolving it in deuterated methanol.

3.18 Chemical syntheses of compounds 1, 5–8, 10–13

Syntheses of compounds **1**, **5**–**8**, **10**–**13** were carried out in cooperation with Dr. Maxim Frizler of the research group of Prof. Dr. M. Gütschow (Institute for Pharmaceutical Chemistry I of the University of Bonn).

3.18.1 (E)-4-Methoxycarbonylaminobut 2-enoic acid (6)

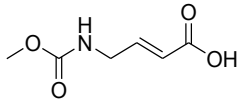

For the first step, crotonic acid (**3**) (8.60 g, 100 mmol) was dissolved in CCl_4 (200 mL). Subsequently, *N*-bromosuccinimide (21.4 g, 120 mmol) and AIBN (500 mg, 3.05 mmol) were added and heated under reflux to 95–100 °C for 2 h. After the mixture was cooled down to rt, the solvent was removed and the resulting solid was recrystallized from ethyl acetate/petroleum ether to give (E)-4-bromobut-2-enoic acid (**4**) (7.10 g, 43 %). Analytical data of **4** were in agreement with those reported in the literature (Höfling et al., 2008). Secondly, compound **4** (3.20 g, 19.4 mmol) was treated dropwise with 25 % aq. NH_3 (15 mL) and the reaction mixture was stirred for 20 h at rt. The solvent and excess ammonia were removed under reduced pressure to obtain a brown solid which was subsequent dissolved in water and passed through a column of acidic resin (Dowex 50W-X8). The column was washed with water and compound **5** was eluted with 5 % NH_3. The solution was concentrated and poured into ethanol. The resulting precipitate was filtered off and dried to yield 15 (0.25 g, 11 %). Finally, compound **5** (210 mg, 1.78 mmol) was dissolved in water containing $NaHCO_3$ (0.30 g, 3.57 mmol) to convert it into the corresponding free acid **6**. Thereafter the solvent and remaining NH3 were evaporated. The residue was dissolved in a dioxane/H_2O mixture (2:1) and treated with methyl chloroformate (0.17 g, 1.8 mmol). After evaporation of the solvent the residue was suspended in H_2O and the aqueous suspension was adjusted with 10 % $KHSO_4$ to pH ~2 and extracted with ethyl acetate (3 × 30 mL). The combined organic layers were concentrated *in vacuo*, the resulting residue was adjusted to pH ~9 using $NaHCO_3$ and again extracted with ethyl acetate (3 × 30 mL) to remove by-products. The aqueous phase was acidified under vigorous stirring with 37 % HCl and extracted with ethyl acetate (3 x 30 mL). The combined

organic layers were washed with brine. The solvent was removed to obtain compound **6** (200 mg, 71 %). ^{1}H NMR (500 MHz, [D6]DMSO) δ 3.54 (s, 3H, CH_3OCONH), 3.75–3.78 (m, 2H, $NHCH_2CH=CH$), 5.77 (dt, 3J=15.8 Hz, 4J=1.9 Hz, 1H, $NHCH_2CH=CH$), 6.73 (dt, 3J=15.8 Hz, 3J=4.7 Hz, 1H, $NHCH_2CH=CH$), 7.41 (bs, 1H, $NHCH_2CH=CH$), 12.24 (bs, 1H, COOH); ^{13}C NMR (125 MHz, [D6]DMSO) δ 41.15 ($NHCH_2CH=CH$), 51.62 (CH_3OCONH), 121.34 ($NHCH_2CH=CH$), 145.56 ($NHCH_2CH=CH$), 156.85 (OCONH), 166.97 (COOH).

3.18.2 (E)-S-2-Acetamidoethyl 4-(methoxycarbonylamino)but-3-enethioate (7)

(**7**) (**8**)

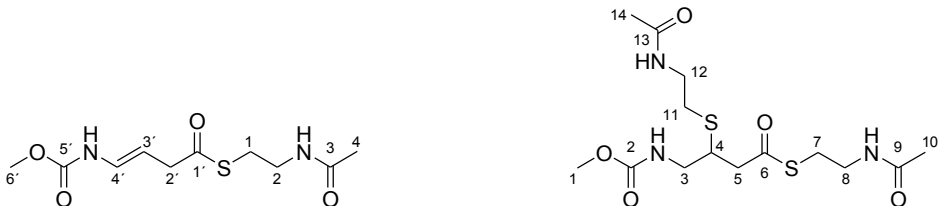

Compound **6** (210 mg, 1.32 mmol) was dissolved in DCM (15 mL) and subsequently treated with DMAP (16 mg, 0.13 mmol) and EDC (230 mg, 1.45 mmol). *N*-acetylcysteamine (160 mg, 1.34 mmol) was dissolved in DCM and added dropwise under ice cooling to the reaction mixture. It was allowed to warm up to rt and stirred over 2 h. After evaporation of the solvent the residue was suspended in H_2O and extracted with ethyl acetate (3 × 30 mL). The combined organic layers were washed with 10 % $KHSO_4$ (10 mL), H_2O (10 mL), sat. $NaHCO_3$ (10 mL), H_2O (10 mL), and brine. The solvent was dried ($NaSO_4$) and removed in vacuo. The oily residue was purified by column chromatography on silica gel using ethyl acetate as eluent to obtain **7** (6 mg, 1.7 %). Compound **8** was the main product when two equivalents of N-acetylcysteamine (315 mg, 2.64 mmol) were added to the reaction mixture. ^{1}H NMR of **7** (300 MHz, [D4]MeOH) δ 1.95 (s, 3H, $NHCOCH_3$), 3.03 (t, ^{3}J=6.6 Hz, 2H, SCH_2CH_2NH), 3.27 (d, ^{3}J=7.3 Hz, 2H, $NHCH=CHCH_2$), 3.35 (t, ^{3}J=6.6 Hz, 2H, SCH_2CH_2NH), 3.73 (s, 1H, CH_3OCONH), 5.17 (dt, ^{3}J=14.3 Hz, ^{3}J=7.3 Hz, 1H, $NHCH=CHCH_2$), 6.62 (d, 3J=14.3 Hz, 1H, $NHCH=CHCH_2$). ^{1}H NMR of **8** (300 MHz, [D4]MeOH) δ 1.96 (s, 3H, $NHCOCH_3$), 1.98 (s, 3H, $NHCOCH_3$), 2.29 (dd, 1H, ^{3}J=4.8 Hz, ^{2}J=15.7 Hz, $COCH_2$), 2.74 (t, ^{3}J=6.6 Hz, 2H, SCH_2CH_2NH), 2.78 (dd, 1H, ^{3}J=8.0 Hz, ^{2}J=15.7 Hz, $COCH_2$), 3.07 (t, ^{3}J=6.6 Hz, 2H, SCH_2CH_2NH), 3.27 (m, 1H, $NHCH_2CH$), 3.28 (m, 1H, SCH), 3.36 (m, 1H, $NHCH_2CH$), 3.38 (m, 2H, SCH_2CH_2NH), 3.39 (m, 2H, SCH_2CH_2NH), 3.68 (s, 3H, CH_3OCONH) 8.13 (bs, 1H), 8.25 (bs, 1H) ; ^{13}C NMR of **8** (125 MHz, [D4]MeOH) δ 22.6 (2 x $COCH_3$), 29.38 ($CH(S)CH_2CH_2$), 31.42 (SCH_2CH_2), 40.1, 40.5 (SCH_2CH_2), 43.2 ($CH(S)CH_2CH_2$), 45.9 ($CH(S)CH_2CH_2$), 47.9 (CH_2CO), 52.6 ($COOCH_3$), 159.6 ($COOCH_3$), 173.4, 173.5 ($COCH_3$), 198.3 (COS).

3.18.3 *S*-2-Acetamidoethyl 2-bromoethanethioate (10)

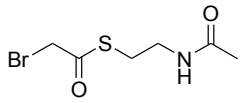

Bromo-acetylbromide (**9**) (5, 1.69 g, 8.37 mmol) was dissolved in THF (20 mL), treated with triethylamine (1.02 g, 10.1 mmol), and *N*-acetylcysteamine (1.00 g, 8.39 mmol) was added dropwise. The resulting reaction mixture was stirred for 1.5 h at room temperature. The solvent was removed and the oily residue was suspended in H_2O. The aqueous suspension was extracted with ethyl acetate (3 × 30 mL), washed with 10 % $KHSO_4$ (30 mL), H_2O (30 mL), sat. $NaHCO_3$ (30 mL), and sat. NaCl (30 mL), and dried over Na_2SO4. The crude product was purified by column chromatography using ethyl acetate as eluent to obtain **10** as a white solid (0.45 g, 22 %). NMR data are in accordance with those from literature (Roblot et al., 1993). ^{1}H NMR (500 MHz, [D6]DMSO) δ 1.78 (s, 3H, $NHCOCH_3$), 2.97 (t, ^{3}J=6.8 Hz, 2H, SCH_2CH_2NH), 3.19 (app. q, 2H, SCH_2CH_2NH), 4.43 (s, 2H, $BrCH_2CO$), 8.02 (bs, 1H, SCH_2CH_2NH); ^{13}C NMR (125 MHz, [D6]DMSO) δ 22.62 ($NHCOCH_3$), 29.36, (SCH_2CH_2NH), 34.82 (SCH_2CH_2NH), 37.95 ($BrCH_2CO$), 169.43 ($NHCOCH_3$), 192.75 ($BrCH_2CO$).

3.18.4 S-2-Acetamidoethyl 2-(diethoxyphosphoryl)ethanethioate (11)

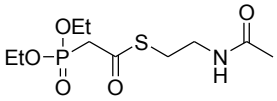

Compound **10** (0.43 g, 1.79 mmol) was solved in THF, treated with triethyl phosphite (0.30 g, 1.81 mmol) and stirred at 130 °C in a sealed tube for 3.5 h. The reaction mixture was dissolved in ethyl acetate (60 mL), washed with sat. $NaHCO_3$ (2 × 30 mL) and brine (30 mL) and dried over Na_2SO_4. The crude oily product was purified on column chromatography using ethyl acetate (10 fractions, the volume of each fraction was 50 mL) and additionally ethyl acetate/MeOH (7:3) as eluents to obtain **11** as an oily product (0.16 g, 30 %). NMR spectroscopic observations are in agreement with those reported in literature (Zhou et al., 2010). ^{1}H NMR (500 MHz, [D6]DMSO) δ 1.23 (t, ^{3}J=7.1 Hz, 6H, 2 × OCH_2CH_3), 1.78 (s, 3H, $NHCOCH_3$), 2.92 (t, ^{3}J=6.9 Hz, 2H, SCH_2CH_2NH), 3.14–3.18 (m, 2H, SCH_2CH_2NH), 3.45 (d, ^{2}JPH=21.1 Hz, 2H, PCH_2CO), 4.00–4.05 (m, 4H, 2 × OCH2CH3), 7.99 (t, ^{3}J=5.1 Hz, 1H, $NHCOCH_3$); ^{13}C NMR (125 MHz, [D6]DMSO) δ 16.21, 16.26 (2 × OCH_2CH_3), 22.62 ($NHCOCH_3$), 28.81 (SCH_2CH_2NH), 38.17 (SCH_2CH_2NH), 42.23 (d, $^{1}J_{PC}$=127 Hz, PCH_2CO), 62.17, 62.22 (2 × OCH_2CH_3) 169.38 ($NHCOCH_3$), 190.31 (d, $^{2}J_{PC}$ = 6.7 Hz, PCH_2CO).

3.18.5 (E)-S-2-Acetamidoethyl 4-(tert-butyloxycarbonylamino)but-2-enethioate (12)

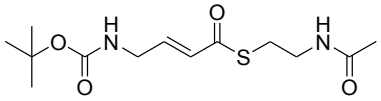

Compound **11** (0.13 g, 0.44 mmol) was dissolved in THF (20 mL). Sodium hydride (18 mg (60 % in mineral oil), 0.45 mmol) was added, and the resulting reaction mixture was stirred at -10 °C for 30 min. *N*-(tert-Butyloxycarbonyl)glycinal (70 mg, 0.44 mmol) was added, and it was stirred for 1 h at -10 °C. TLC was used for reaction control. THF was removed, and the resulting residue was extracted with ethyl acetate (3 × 30 mL). The combined organic layers were washed with brine (30 mL) and concentrated in vacuo. The precipitated white solid was filtered off. The crude oily product was purified by column chromatography using ethyl acetate as eluent to obtain **12** as an oily product (40.0 mg, 30 %). ^{1}H NMR (500 MHz, [D6]DMSO) δ 1.38 (s, 9H, $C(CH_3)_3$), 1.78 (s, 3H, $NHCOCH_3$), 2.96 (t, ^{3}J=6.8 Hz, 2H, SCH_2CH_2NH), 3.18 (app. q, ^{3}J=6.0 Hz 2H, SCH_2CH_2NH) 3.74 (bs, 2H, $NHCH_2CH=CH$), 6.17 (dt, ^{3}J=15.7 Hz, ^{4}J=1.8 Hz, 1H, $NHCH_2CH=CH$), 6.77 (dt, ^{3}J=15.7 Hz, ^{3}J=4.6 Hz, 1H, $NHCH_2CH=CH$), 7.16 (bs, 1H, $NHCH_2CH=CH$), 8.02 (t, ^{3}J=5.4 Hz, 1H, SCH_2CH_2NH); ^{13}C NMR (125 MHz, [D6]DMSO) δ 22.61 ($NHCOCH_3$), 28.12 (SCH_2CH_2NH), 28.29 ($C(CH_3)_3$), 38.27 (SCH_2CH_2NH), 40.81 ($NHCH_2CH=CH$), 78.22 ($C(CH_3)_3$), 127.10 ($NHCH_2CH=CH$), 143.40 ($NHCH_2CH=CH$), 155.63 (OCONH), 169.36 ($NHCOCH_3$), 188.69 (CHCOS).

3.18.6 (E)-*S*-2-Acetamidoethyl 4-(methoxycarbonylamino)but-2-enethioate (1)

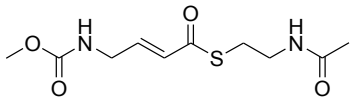

Compound **12** (30 mg, 0.099 mmol) was dissolved in CH_2Cl_2 (30 mL), treated with TFA (5.0 mL) and stirred 30 min at 0 °C. The solvent was evaporated under reduced pressure and the oily residue (compound **13**) was dissolved in 20 mL dry THF. TEA (40 mg, 0.40 mmol) and methyl chloroformate (37 mg, 0.39 mmol) were added, and it was stirred for 2 h at 0 °C. THF was removed. The oily residue was treated with H_2O and extracted with ethyl acetate (3 × 30 mL). The combined organic layers were washed with brine (30 mL) and concentrated in vacuo. The crude oily product was purified by column chromatography using ethyl acetate as eluent to obtain **1** as an oily product (15 mg, 58 % from **12**). 1H NMR (500 MHz, [D4]MeOH) δ 1.96 (s, 3H, NHCOCH_3), 3.11 (t, ^{3}J=6.6 Hz, 2H, SCH_2CH$_2$NH), 3.38 (t, ^{3}J=6.6 Hz, 2H, SCH$_2$CH_2NH), 3.70 (s, 3H, CH_3OCONH), 3.92–3.93 (m, 2H, NHCH_2CH=CH), 6.27 (dt, ^{3}J=15.5 Hz, ^{4}J=1.6 Hz, 1H, NHCH$_2$CH=C*H*), 6.90 (dt, ^{3}J=15.5 Hz, ^{3}J=4.7 Hz, 1H, NHCH$_2$C*H*=CH); 13C NMR (75.4 MHz, [D4]MeOH) δ 22.46 (NHCO*C*H$_3$), 29.03 (S*C*H$_2$CH$_2$NH) 40.12 (SCH$_2$*C*H$_2$NH), 42.32 (NH*C*H$_2$CH=CH), 52.71 (*C*H$_3$OCONH), 128.61 (NHCH$_2$CH=*C*H), 143.13 (NHCH$_2$*C*H=CH), 159.44 (OCONH), 173.46 (NH*C*OCH$_3$), 190.60 (CH*C*OS). LC-MS(ESI) (90 % H_2O to 100 % MeOH in 10 min, then 100 % MeOH to 20 min, DAD 220.0–400.0 nm) tr=6.52, 97 % purity, m/z=261.34 ([M + H]$^+$).

4 Results

4.1 Corallopyronin A and its biosynthesis: An overview

Corallopyronin A (**scheme 4-1**) is a myxobacterial compound which was isolated in the lab of Prof. Dr. König from the strain *Corallococcus coralloides* B035. Its potent antibacterial activity, *e.g.* against *Staphylococcus aureus*, including methicillin-resistant strains was shown by MIC values of 0.25 µg/mL (Irschik et al., 1985; Jansen et al., 1985). Recently, it was shown that it possesses also superior *in vivo* antimicrobial activity against *Wolbachia* (Schäberle et al., 2014b; Schiefer et al., 2012). Corallopyronin A is currently in the focus of a translational project, attempting to establish this molecule as a new antibiotic drug.

Feeding experiments with ^{13}C-labeled precursors resulted in the deduction of its biosynthetic building blocks and led to the conclusion that corallopyronin A originates from two separate chains. The western chain is solely PKS- and the eastern chain is PKS/NRPS derived. Both are interconnected by Claisen condensation and subsequent lactonisation, resulting in the characteristic pyrone ring (Erol et al., 2010; Kohl et al., 1984) (**scheme 4-1**). The western side chain contains beside several double-bonds two acetate derived methyl groups (C-26 and C-21), one SAM derived methyl group (C-17), and one hydroxyl function. The biosynthetic origin of the latter is not proven, yet. Possibly, it is a result of a post-PKS modification with involvement of the putative cytochrome P450 acting protein CorO. Responsible for the incorporation of the methyl groups (C-26 and C-21) in the western chain is a β-branching cassette encoded in the gene cluster. Characteristics of the eastern chain are beside the SAM originated methyl group, the unusual vinyl carbamate functionality. Feeding studies with ^{13}C labeled sodium bicarbonate gave the assumption that carbonic acid and SAM are constituent parts of that moiety (Erol et al., 2010). Further studies in our lab could prove hydrogen carbonate to be the starter unit in corallopyronin A biosynthesis. *In vitro* experiments with the heterologously expressed *O*-methyltransferase (CorH) showed that a hydrogen carbonate precursor was methylated SAM dependent. Further, this methylated hydrogen carbonate could be attached to the heterologously expressed first carrier protein CorI ACP1 of the loading module (Schäberle et al.,

2013) (**figure 4-1**). Completion of the vinyl carbamate moiety takes place by the A-domain mediated incorporation of the amino acid glycine.

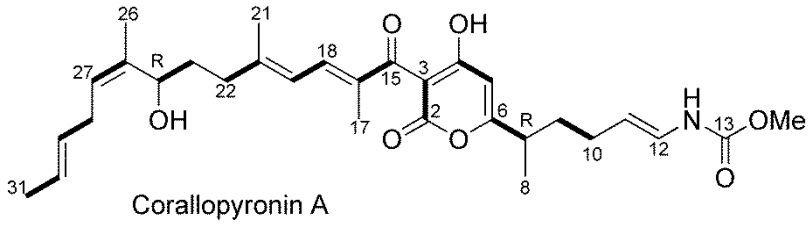

Scheme 4-1. Corallopyronin A. A myxobacterial compound derived from a PKS/NRPS machinery. Bold carbon bonds represent acetate units incorporated by feeding ^{13}C-labeled acetate. C-16 and C-21 were also acetate derived, since labelling occurred when 1,2-^{13}C-acetate was fed. Feeding of methyl-^{13}C-methionine resulted in the ^{13}C marked methyl groups C-8, C-14 and C-17, indicating a SAM depended methylation. Feeding of 1-^{13}C-glycine resulted in a labelled carbon C-11, whereas feeding of 2-^{13}C, ^{15}N-glycine labelled C-12 and the adjacent amino group.

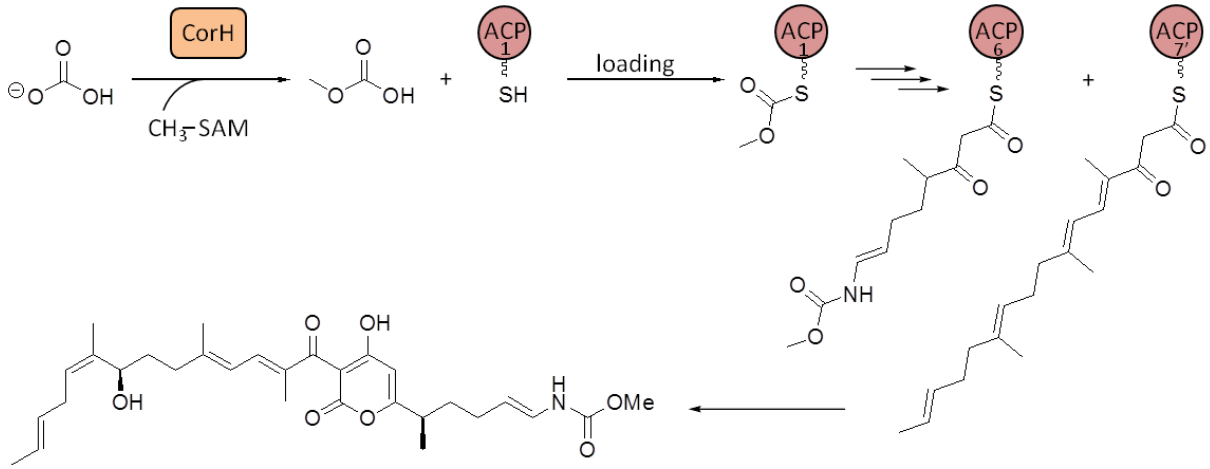

Figure 4-1. Highlighted step in the biosynthesis of corallopyronin A. The *O*-methyltransferase CorH catalysed the methylation of carbonate by SAM resulting methylated carbonate. Methylcarbonate acts as starter molecule in corallopyronin A biosynthesis and was loaded onto CorI ACP1 of the loading module of the *trans*-PKS/NRPS assembly line (Schäberle et al., 2013).

Findings concerning the biosynthesis of corallopyronin A from feeding studies could be confirmed by *in silico* elucidation of the biosynthetic gene cluster. The latter also allowed to understand the biosynthetic process in more detail (Erol et al., 2010). The putative biosynthetic gene cluster is 65 kbp large and consists of the 16 open reading frames *corA–corO*, whereas one open reading frame (*orf1*) could not be attributed to a specific step in the biosynthesis.

The cluster starts with *corA* encoding for a *trans*-acyltransferase (*trans*-AT) and a *trans*-enoylreductase (ER). The stand-alone domain *trans*-AT serves malonyl-CoA extender units to the ketosynthases (KS) of every module. Whereas the *trans*-ER stand-alone domain is responsible for the reduction of carbon-carbon double-bonds to single-bonds. C*is*-acting ER domains are totally missing in this cluster. Another "stand-alone" protein is CorB, which has ketosynthase (KS) properties and seems to be involved in the final chain connection between the eastern and the western chain by a Claisen-type condensation. Further investigations in CorB are currently ongoing in our lab. The proteins encoded by the genes *corCDEFG* appear to form a functional unit containing an acyl-carrier protein (ACP), a KS, a HMG-CoA-synthase (HCS) and a decarboxylase (ECH) and an isomerase (ECH). That unit is named "β-branching cassette" because it mediates an aldol addition of an acetyl group onto a β-keto moiety of a growing PKS chain with subsequent dehydration and decarboxylation to give the methyl branches C-21 and C-26. Further downstream, *corH* encodes for the *O*-methyltransferase (*O*-MT) CorH, which was already mentioned in connection with the methylation of hydrogen bicarbonate to give the starter unit of the eastern chain of corallopyronin A (s.a.). Constitutive domains for the assembly of the eastern and the western chain are organized on six and seven modules, respectively, which are encoded by the genes *corI*, *corJ* and *cork*, *corL.* Finally CorM, CorN and CorO process the two chains in post-PKS modifications to gain corallopyronin A. CorM with its thioesterase activity likely acts in cooperation with CorB to form pre-corallopyonin A. CorN belongs to the crotonyl/enoyl CoA hydratase superfamily, which is also known to contain isomerases and may be involved in the double-bond shift from $\Delta^{24,25}$ to $\Delta^{25,27}$. CorO shows similarities to cytochrome P450 enzymes and may catalyze the final hydroxylation at C-24 and therewith complete the biosynthesis of corallopyronin A (**figure 4-2**) (Erol et al., 2010).

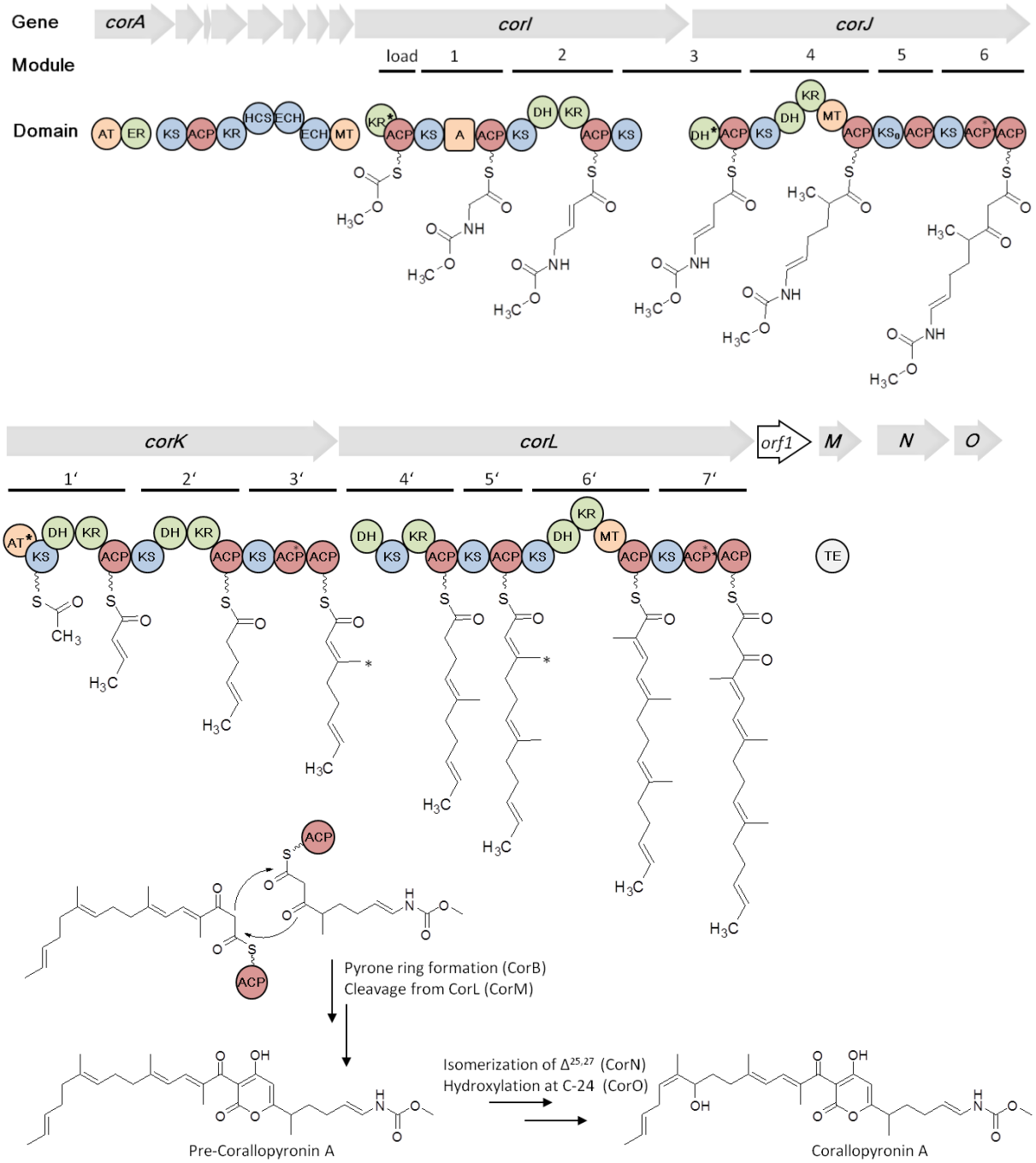

Figure 4-2. Complete corallopyronin A gene cluster and the hypothetical biosynthetic pathway. A: adenylation domain; ACP: acyl-carrier protein; AT: acyltransferase; DH: dehydratase domain; KR: ketoreductase domain; KS: ketosynthase domain; MT: methyltransferase domain. KS_0: inactive KS; AT^*, ACP^* and KR^* are presumably inactive due to mutations. DH^*: putative "shift domain". Methyl groups introduced by the β-branching cassette are marked with an asterisk. Figure is modified after Erol et al. 2010.

4.2 Attemps to prove the putative biosynthetic gene cluster of coralloyronin A

In the beginning of this thesis in 2009 it was envisaged to prove the still putative biosynthetic gene cluster of corallopyronin A. To do this, two approaches were planned to be exploited: first, a knock-out or disruption of a gene related to the respective biosynthesis in the producer strain *Corallococcus coralloides* B035 and second, expression of parts of the gene cluster (*corA*–*corJ*) in the heterologous host *Pseudomonas putida* KT2440. The basis of these molecular biological strategies was a cosmid library of the genome of *C. coralloides* B035, which was established by Erol et al. during their investigation relating to the early work on the biosynthetic cluster of corallopyronin A. During the latter study they found cosmid FJ7 to contain 39 kbp sequence information putatively related to the biosynthesis of corallopyronin A, namely the genes *corA*–*corJ* (Erol et al., 2010).

The first experiments aimed to disrupt the *trans*-acyltransferase (AT) coding sequences within the gene *corA* in the host strain *C. coralloides* B035. Therefore the gene sequence of the *trans*-AT was replaced by a streptomycin resistance cassette (*aadA*) in cosmid FJ7 using the lambda-red recombineering technique (**figure 4-3 A, B**) (Gust et al., 2003). Analogously the recombinant cosmid FJ7 AT::aac(3)IV containing an apramycin resistance cassette was prepared with the same purpose. Subsequently the producer strain *C. coralloides* B035 was transformed with the generated construct *e.g.* FJ7 AT::aadA with was inteneted to recombine homologously with the corallopyronin A gene cluster in the host strain (**figure 4-3 B, C**). A disruption of the *trans*-AT locus in *corA* in *C. coralloides* B035 would result in a mutated strain which could not produce corallopyronin A anymore. A lack of corallopyronin A production might have been detected via LCMS of the extracts of the bacterial cells. All efforts to gain a knock-out mutant of the producer strain, however, failed so far. The crucial point seemed to be the transformation of *C. coralloides* cells by electroporation, which has been described in literature as a successful method for transformation of myxobacteria (Magrini et al., 1998; Simunovic and Müller, 2007b). In the meantime, in 2013, Sucipto *et al.* published the evidence of the putative biosynthetic gene cluster of the antibiotic myxopyronin A, closely related to corallopyonin A, by gene deletion experiments in the producer strain *Myxococcus fulvus* Mx f50 (Sucipto et al., 2013).

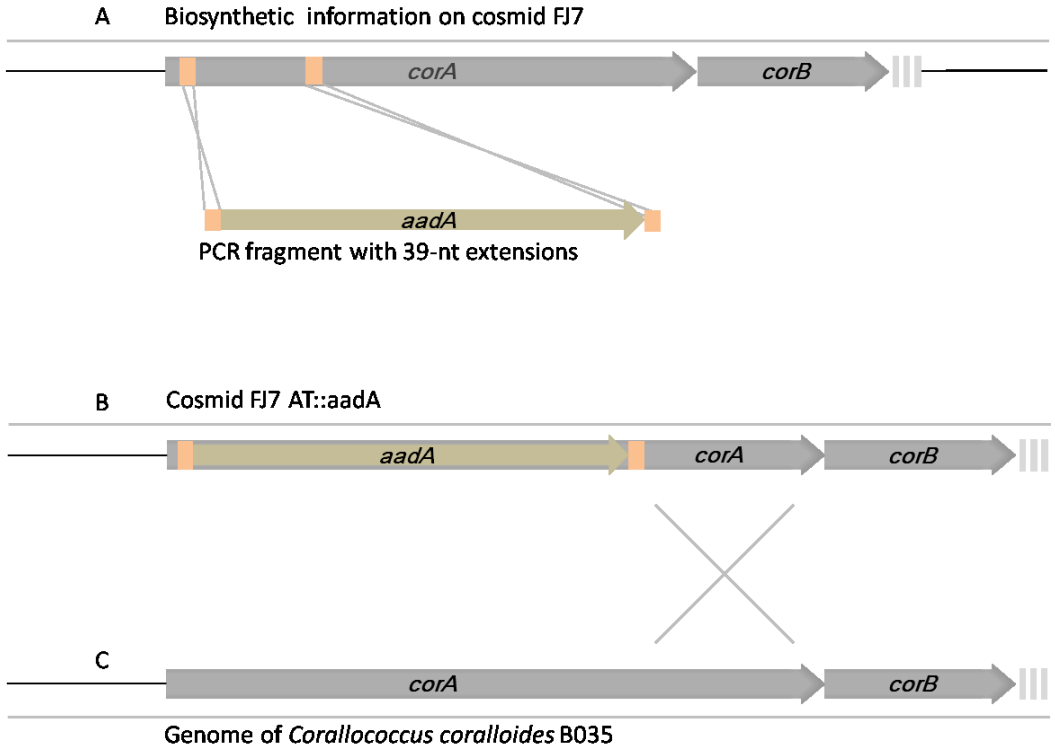

Figure 4-3. Strategy for the disruption of the *trans*-AT domain encoding sequence in *corA* in *Corallococcus coralloides* B038. A) A gene replacement cassette containing the streptomycin resistance gene *aadA* was amplified by PCR with primers containing 39-nt 5' homology extensions (marked orange) matching the sequence of the *trans*-AT sequence inside the target gene *corA*. The PCR fragment was used to transform *E.coli* BW25113/pIJ790 harbouring the cosmid FJ7. B) Streptomycin resistant transformants were selected and the recombinant cosmid FJ7 AT::aadA was identified via PCR and restriction analysis. C) *C. coralloides* B038 was transformed with cosmid FJ7 AT::aadA by electroporation. Homologous recombination should occur between cosmid and genomic DNA. Positive transformants would have been selected due to their streptomycin resistance. Primer sequences are depicted in the appendix (**table 8-1**).

As a second strategy it was envisaged to express the assembly line (*corA-corJ*) of the eastern chain of corallopyronin A in the heterologous host *Pseudomonas putida* KT2440. Therefore a construct based on the cosmid FJ7 was created. This construct was modified by insertion of a pm/*xylS* expression promoter system, a tetracycline-resistance gene for selection of positive transformants of *P. putida* KT2440 and a DNA fragment derived from the chromosome of *P. putida* KT2440 to enable the integration of the whole cosmid construct into the heterologous genome by homologous recombination (Wenzel et al, 2005). Efforts to introduce the construct FJ7 pm/xylS/trpE (54 kb) via electroporation into the heterologous host have failed up to now (**figure 4-4**).

Figure 4-4. Cosmid construct FJ7 pm/xylS/trpE for heterologous expression of the eastern chain of corallopyronin A in the host *P. putida* KT2440. The biosynthetic genes of the corallopyronin A cluster are coloured in gray. The genes introduced into the cosmid backbone to prepare the cosmid for expression in the heterologous host are coloured in olive. Primer sequences are showm in the appendix (**table 8-2**).

4.3 Double-bond migration in corallopyronin A biosynthesis: investigation of the protein CorJ DH*[2]

As already mentioned (4.1) corallopyronin A is a compound with an unusual biosynthetic pathway (**figure 4-2**). The focus of this study is on the biosynthetic origin of the carbon-carbon double-bond Δ^{11} which represents a rare β,γ pattern and does not match the classical co-linearity rule of PKS/NRPS assembling (Piel, 2010).

In module two of the biosynthetic gene cluster of corallopyronin A glycine is incorporated whose carbonyl functionality is reduced to the corresponding D-hydroxy intermediate by the ketoreductase CorI KR. Subsequent dehydration of the D-hydroxy moiety occurs mediated by CorI DH and the localization of the resulting *trans* double-bond is expected to be in α,β position (Δ^{10}) according to usual PKS/NRPS machinery (Alhamadsheh et al., 2007; Wu et al., 2005) (**figure 4-5**). However, the respective double-bond Δ^{11} in corallopyronin A led to the assumption that the α,β double-bond (Δ^{10}) was isomerised to the β,γ position (Δ^{11}) (**figure 4-5** and **figure 4-6**). CorJ DH* was supposed to mediate double-bond migration in corallopyronin A assembling and was thus termed “shift domain”.

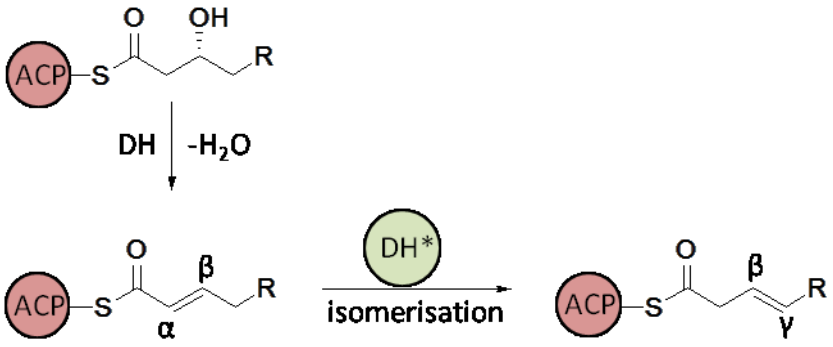

Figure 4-5. *Trans* double-bond formation in PKS biosynthesis and DH* mediated double-bond isomerisation from the α,β to the β,γ position. DH: dehydratase; DH*: shift domain, *e.g.* CorJ DH* in corallopyronin A biosynthesis. Reduction of D-hydroxy intermediates results in a *trans* double-bond (Wu et al., 2005).

[2] Results are published in Lohr et al., 2013; alpha, beta –> beta, gamma, bouble-bond migration in corallopyronin A biosynthesis.

To get more insights into the origin of the β,γ double-bond of corallopyronin A we investigated in the genetic and enzymatic background of the α,β (Δ^{10}) to β,γ (Δ^{11}) double-bond shift. Similar cases of shifted double-bonds are known from only a few other polyketides, *e.g.* ansamitocin (Taft et al., 2009), bacillaene (Moldenhauer et al., 2007, 2010), and rhizoxin (Kusebauch et al., 2010) (**scheme 4-2**).

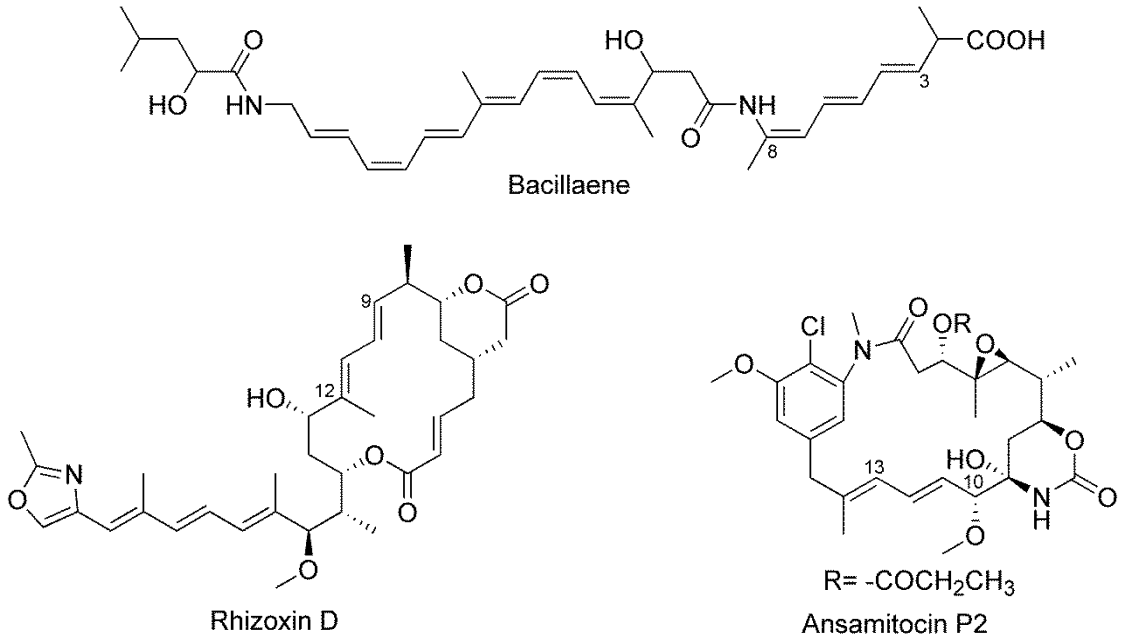

Scheme 4-2. PKS derived compounds bearing α,β to β,γ shifted double-bonds: *e.g.* ansamitocin ($\Delta^{10,12}$ to $\Delta^{11,13}$), bacillaene ($\Delta^{2,4,6}$ to $\Delta^{3,5,7}$), and rhizoxin ($\Delta^{8,10}$ to $\Delta^{9,11}$).

Concerning the polyketide ansamitocin an unusual but functional DH domain was assumed to place the conjugated double-bonds Δ^{10} and Δ^{11} in β,γ position (Δ^{11} and Δ^{12}, respectively) (Kubota et al., 2006; Spiteller et al., 2003). Feeding the producer strain *Actinosynnema pretiosum* with SNAC esters, representing analogous of the respective PKS intermediates, led to conclude that the diene system in β,γ pattern is generated during processing of the polyketide chain. It was likewise proposed that the β,γ diene moiety occurs during the dehydration step DH mediated on module 3 by a vinylogous *syn*-elimination reaction (Taft et al., 2009).

Moldenhauer et al. was able to gain the thioesterase (TE) deletion mutant JM1 (Moldenhauer et al., 2007) of the bacillaene producer strain *Bacillus amyloliquefaciens* CH12 and could thereby analyze late-pathway intermediates of

bacillaene. It could be shown that the β,γ double-bond installation of the double-bonds Δ^3 and Δ^5 was performed on the same modules that performed the elongation of the PKS chain (module 14 and 15, respectively). However, the origin of the third double-bond $\Delta^7$of the triene system, introduced on module 16, could not be figured out clearly. In that respect the authors consider a α,β to β,γ isomerisation by module 16, including the shift domain BaeR DH*, as alternative to β,γ desaturation as demonstrated for module 14 and 15 (Moldenhauer et al., 2010).

In the biosynthesis of the PKS/NRPS derived compound rhizoxin both mechanisms could be evidenced to give the β,γ diene moieties Δ^{11} and Δ^9. The first unsaturation Δ^{11} is introduced simultaneously to the double-bond shift in module 7 of the biosynthetic gene cluster which corresponds to a formal β,γ dehydration. Regarding double-bond Δ^9 it was shown that first elongation of the nascent polyketide chain takes place and second a distinct "shift module" (module 9) downstream mediates the double-bond migration resulting in a β,γ double-bond (Δ^9). The corresponding shift domain appeared to be the protein RhiE DH* (Kusebauch et al., 2010).

For the β,γ double-bond Δ^{11} in corallopyronin A we proposed a similar process as shown for double-bond Δ^9 in the rhizoxin pathway. We proposed a distinct domain in the assembly line performing the double-bond shift. Therefore, this study mainly focuses on module 3 of the biosynthetic gene cluster of corallopyronin A which consists of a ketosynthase (CorI KS), an unusual dehydratase (CorJ DH*) and an acyl-carrier protein (CorJ ACP) (**figure 4-6**). A peculiarity of module 3 is that it is encoded on two genes, subdividing the domains of one module from each other, and is therefore named "split module" (Silakowski et al., 2001). So that the KS domain is localized on the protein CorI and the domains DH* and ACP are part of the protein CorJ (**figure 4-6**). The ketosynthase CorI KS is assumed to be inactive, despite of the presence of a catalytic triad (Erol et al., 2010), that means no elongation occurs of the nascent PKS chain in module 3. The further investigations ignore the role of CorI KS and focus on the functional role of CorJ DH* and the corresponding carrier protein CorJ ACP.

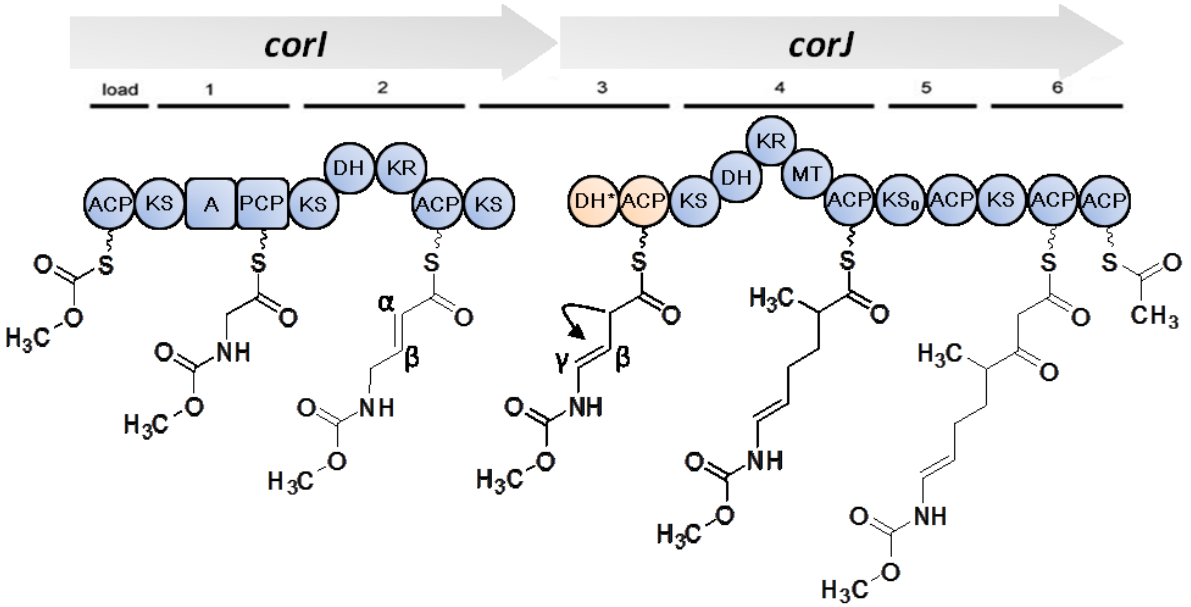

Figure 4-6. Part of the corallopyronin A biosynthetic gene cluster with the focus on the double-bond shift performed by the "shift module" (marked in orange). Module 3 consist of a ketosynthase (KS), a putative shift domain (DH*) and an acyl-carrier protein (ACP) encoded by the genes *corI* and *corJ*, respectively.

Comparison of CorJ DH* to other shift domains (DH*) and to a dehydratase domain (DH). To classify the putative corallopyronin A shift domain (CorJ DH*) its protein sequence was compared with a classical dehydratase domain (EryAII DH) and with two known shift domains (RhiE DH*, BaeR-DH*) and with one suspected shift domain (DifK DH*). For bioinformatic analysis multiple sequence alignment using ClustalW was performed with the amino acid sequences of CorJ DH* (Erol et al., 2010), RhiE DH* (Kusebauch et al., 2010), BaeR-DH* (Moldenhauer et al., 2010) and DifK DH* (Chen et al., 2006). The isomerisation activity of RhiE DH* and BaeR DH* had been proven indirectly by knock-out experiments of the respective gene locus and subsequent analysis of the PKS intermediates of rhizoxin D and bacillaene, respectively (as described above) (Kusebauch et al., 2010; Moldenhauer et al., 2007). DifK DH* is suspected to be a similar shift domain but detailed insight referring its function as double-bond mediating enzyme have not been published, yet (Piel, 2010). To depict the differences between shift domains and a classical dehydratase domain (EryAII DH), the primary sequence of EryAII DH, derived from the erythromycin biosynthesis gene cluster, was included into the alignment (**figure 4-7**). The amino acid sequences compared in the alignment were extracted from the complete

proteins CorJ, RhiE, BaeR, DifK and EryAII, respectively (accession numbers see legend of **figure 4-7**).

For classical DH domains two consensus sequences are reported, the first Hx_3Gx_4P and the second approximately 165 amino acids downstream DxxxQ/H (Akey et al., 2010). Our alignment clearly showed the deviations of the shift domains RhiE DH*, BaeR DH*, DifK DH* and CorJ DH* from the classical DH domain EryAII DH and classified CorJ DH* as a putative shift domain. In all of the aligned amino acid sequences of the shift domains the second motif DxxxQ/H is missing, which is in agreement with the literature (Kusebauch et al., 2010). Additionally, in the case of CorJ DH*, the first conserved motif is mutated to Hx_3Gx_4L, *i.e*. an exchange of prolin (P) by leucin (L) occurred in position 56 compared to the corresponding motif in EryAII DH. In CorJ DH* the amino acid aspartat (D211) of the second motif DxxxQ/H is, deviating from the other shift domains, present but the whole motif is mutated to Dx_3V, representing an exchange of histidine (H) or glycine (G) by valine (V215) compared to EryAII DH (**figure 4-7**).

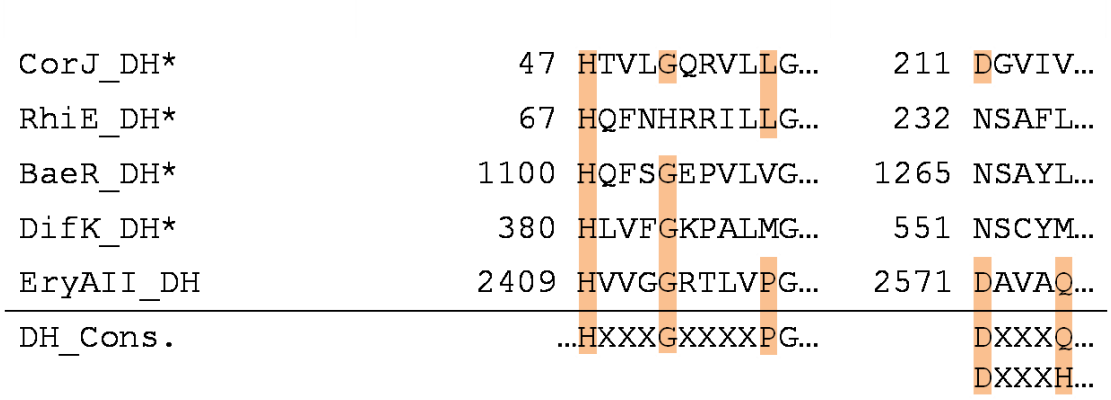

Figure 4-7. Multiple sequence alignment of the amino acid sequences of a dehydratase domain (DH) and of shift domains (DH*). The conserved catalytic residues for DH domains are highlighted in orange. The corresponding accession numbers are ADI59532.1 (CorJ), YP_003748161.1 (RhiE), ABS74065.1 (BaeR), CAJ57411.1 (DifK), AAV51821.1 (EryAII). Cons.=consensus sequence. The numbering is according to CorJ, RhiE, BaeR, DifK and EryAII.

4.4 *In vitro* assays envisaged to investigate the functional role of CorJ DH*

To prove the functionality of CorJ DH* as a double-bond migration catalyzing protein, two enzyme assays were planned to be established by which the isomerisation of the respective carbon-carbon double-bond could be traced. The first assay (4.7.1) was to base on a mass spectrometric tracing of the CorJ DH* mediated double-bond shift of an ACP-bound substrate (**2**). The second assay (4.7.2) was to rely on a comparison between the NMR spectra of (i) the educt (substrate of CorJ DH*, **1**), (ii) the reference compound **7** containing a double-bond in β,γ pattern and (iii) of the reaction product of the assay with CorJ DH* and **1.** Both assays require the heterologously expressed proteins involved in the $\Delta^{10,11} \rightarrow \Delta^{11,12}$ double-bond shift in corallopyronin A biosynthesis: the suspected shift domain CorJ DH* and its corresponding carrier protein CorJ ACP. CorJ DH* and CorJ ACP were planned to be expressed as individual domains, as well as a didomain CorJ DH*-ACP which closely resembled the natural arrangement. The didomain CorJ DH*-ACP was envisaged to be expressed as well in its *holo* form (CorJ DH* *holo*-ACP) using *E. coli* Bap-1 cells as in its *apo* form (CorJ DH* *apo*-ACP) feasible due to expression in the standard expression host *E. coli* BL21. CorJ DH**holo*-ACP should be applied in the first *in vitro* assay with subsequent mass spectroscopic analysis, whereas CorJ DH**apo*-ACP thought to be used in the second *in vitro* assay followed by an NMR based analysis.

Furthermore, there was the need of a suitable substrate for CorJ DH*. On the one hand it should be an analogue of the respective intermediate of corallopyronin A biosynthesis, and on the other hand it should be able to be transferrable to the phosphopantetheine residue of the CorJ *holo*-ACP domain. In order to fulfil the latter requirement a *N*-acetylcysteamine (SNAC) thioester analogue of the respective biosynthetic intermediate of corallopyronin A was synthesised (**1**; **figure 4-14** and **scheme 4-5**).

4.5 Heterologous expression of CorJ DH*-ACP, CorJ DH* and CorJ ACP

The DNA of cosmid FJ7 was used for amplification of the respective primary sequence of the proteins. The generation of the cosmid library of *C. coralloides* B035 is described in Erol *et al*., 2010. In order to obtain the expression construct for the CorJ DH*-ACP didomain a segment harbouring the start of corJ was amplified with the primer pair (8.1, **table 8-3**) CorJ_start/ corJ_end_ACP yielding a fragment of 1227 bp. The corresponding coding sequence of the CorJ ACP and of the single shift domain CorJ DH* were amplified as well. Here the primer pairs ACP_1_upstream/ corJ_end_ACP and corJ_start/ DH_shift_neu were used to obtain a fragment of 309 bp and 736 bp, respectively. Each fragment was ligated into the cloning vector pGEM-T (Promega) and checked for identity by sequencing with standard primers (SP6 and T7). From this plasmid the desired fragment was cut out using the restriction sites *Eco*RI/*Hin*dIII, which were introduced beforehand by the primers used. The fragment was ligated in the likewise restricted expression vector pET28a which links the protein to an N-terminal 6x His-tag upon expression. After ligation *E. coli* XL1 Blue cells were transformed with the ligation mixture and plated on LB supplemented with kanamycin for selection. After identifying positive clones by plasmid isolation and test restriction the corresponding plasmid was isolated and transferred into the respective expression host. Cloning and transformation procedures were applied according to described methods (3.11.1) (**figure 4-8**). Respective protein sequences are depicted in the appendix 8.2.

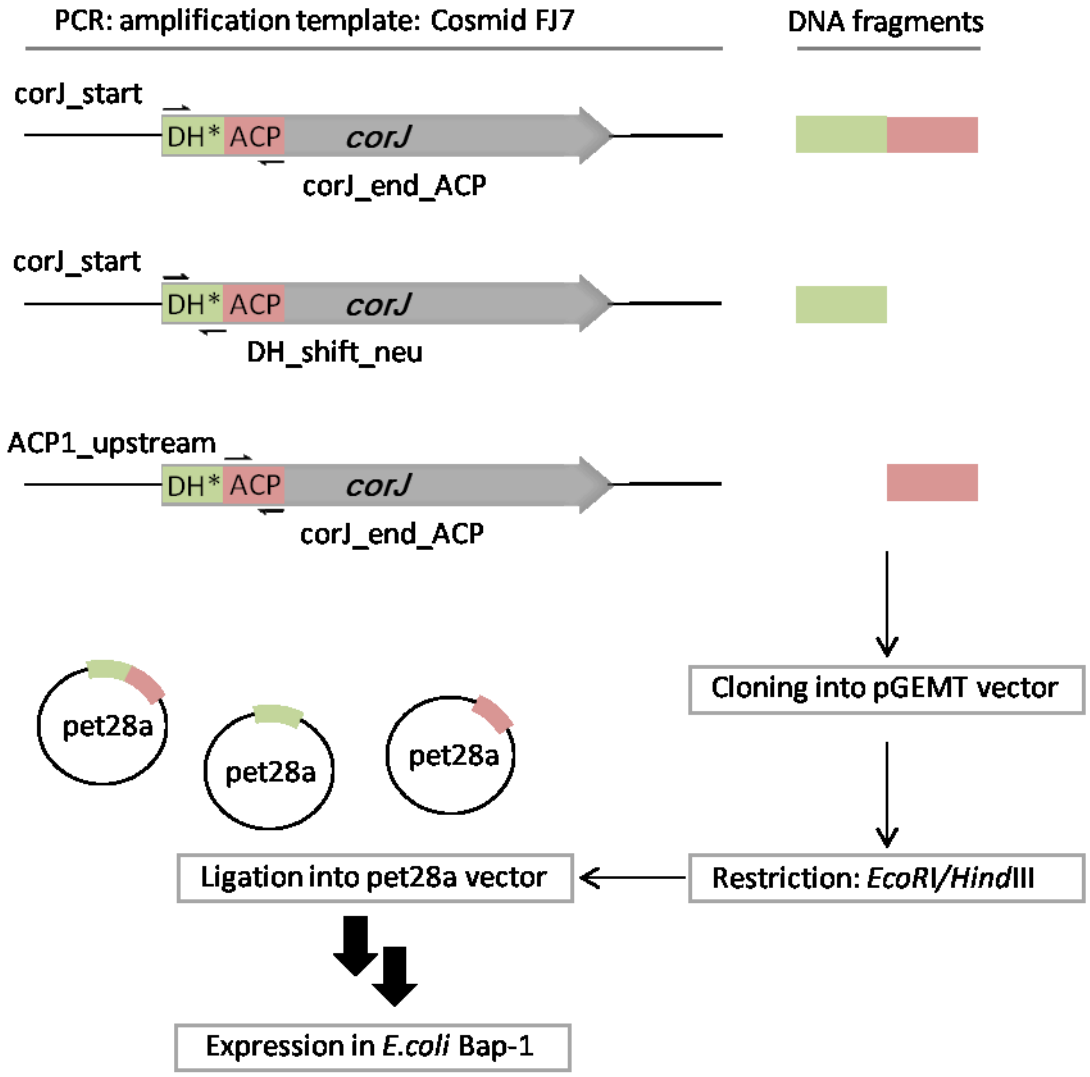

Figure 4-8. Preparation of *corJ DH*-ACP*, *corJ DH** and *corJ ACP* for heterologous expression in *E. coli* Bap-1. Comsid FJ7 served as template for amplification of respective DNA fragments which were ligated into pGEMT vector. Following restriction with *Eco*RI and *Hind*III allowed ligation into the pet28a vector. *E. coli* Bap-1 cells were transformed with the pet28a constructs, respectively, for heterologous expression of the proteins CorJ DH*-ACP, CorJ DH* and CorJ ACP.

The heterologous host. As heterologous host *E. coli* strains Bap-1 and BL21 were applied. Using the pre-engineered *E. coli* strain Bap-1 enabled the heterologous expression of the proteins CorJ (DH*-) ACP as *holo*-enzymes, since this strain carries a genomic copy of the *Bacillus subtilis* gene *sfp*, coding for a promiscuous phosphopantetheinyl transferase (**figure 4-9**) (Quadri et al., 1998). For the expression

of the single shift domain CorJ DH* and of the didomain CorJ DH*-ACP, predetermined for the NMR based assay, the standard expression strain *E. coli* BL21 was chosen as heterologous host.

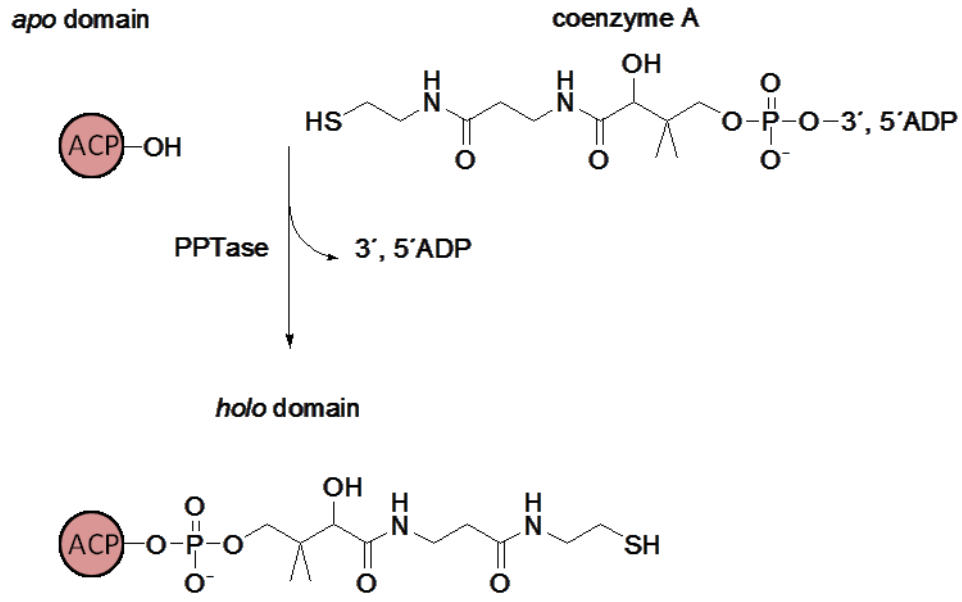

Figure 4-9. Schematic representation of the phosphopantetheinylation of an acyl-carrier protein (ACP) by the phosphopantetheine transferase (PPTase) Sfp. Modified after Quadri et al., 1998.

Protein purification. The individual proteins CorJ DH*, CorJ ACP and the didomain CorJ DH*-ACP were purified based on their attached his-tags via affinity chromatography on Ni-NTA columns according to the described protocol (3.13.3). For elution of the protein from the Ni-NTA columns five elution steps with increasing imidazole concentrations were used. **Figure 4-10** exemplary shows a SDS-page picture of the purified fractions of the heterolgously expressed CorJ DH*-ACP protein. Elution fractions 1–5 were pooled, concentrated, re-buffered in Tris buffer (pH8) and used for subsequent assays. **Figure 4-11** presents the purified proteins CorJ ACP, CorJ DH*, and CorJ DH*-ACP on a SDS-page. The protein concentration was determined by UV spectroscopy in a nanodop spectrophotometer and gave the following concentrations: CorJ DH*: 4.35 µg/µL, CorJ ACP: 3.04 µg/µL, CorJ DH**holo*-ACP: 19.09 µg/µL and CorJ DH**apo*-ACP: 19.73 µg/µL.

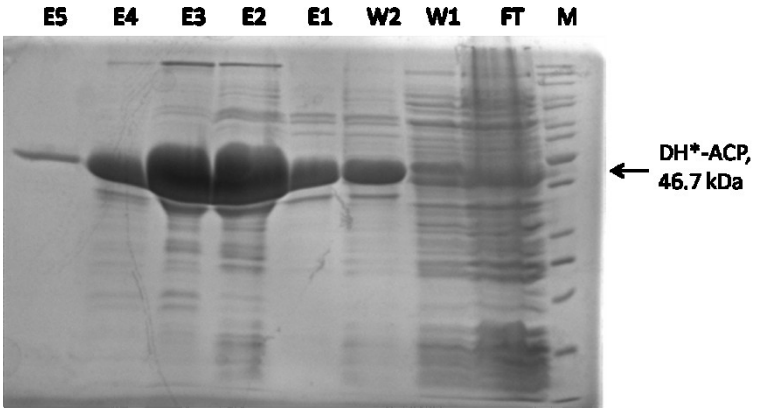

Figure 4-10. Purification of CorJ DH**holo*-ACP (46.7 kDa) by affinity chromatography on Ni-NTA column. SDS gel shows the fractions of the purification steps: FT (flow through; W1 (wash 1, 20 mM imidazole); W2 (wash 2, 40 mM imidazole); E1–5 (elution 1–5, 100–300 mM imidazole); M (size marker).

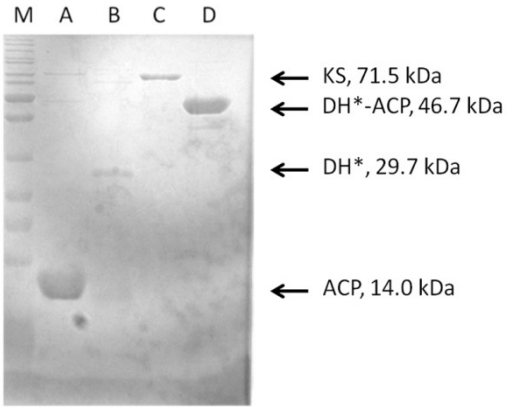

Figure 4-11. SDS-page of the proteins A) CorJ ACP; B) CorJ DH*; C) CorI KS (not further mentioned in this study) and D) CorJ DH**holo*-ACP; M (size marker).

4.5.1 Single amino acid exchange in the shift domain CorJ DH*

An alignment of the primary sequence of shift domains CorJ DH*, RhiE DH*, Bae DH* and DifK DH* with the ordinary dehydratase domain EryAII DH (**figure 4-7**) showed that the histidine residue of the motife Hx_3Gx_4L is highly conserved within DH and DH* and seems to be part of the active site residue of these enzymes. The alignment revealed as well that the aspartic acid D211 of CorJ DH* of the motife Dx_3Q/H is likely to be involved in the double-bond shift in corallopyronin A biosynthesis. Its potential role could be the accepting of the proton released from the γ-position. The respective motives in the protein sequence of the compared shift domains RhiE, BaeR and DifK showed the amino acid asparagine (N) instead of aspartic acid (D), which deviates from the motife Dx_3Q/H found in the shift domain CorJ DH*. To prove the involvement of the conserved histidine residue (His47) in CorJ DH* a mutational exchange to alanine (CorJ DH*H47A) was performed. Likewise, to investigate the functional role of aspartic acid (D) and asparagine (N), a point mutational exchange of aspartic acid to asparagine was approached (CorJ DH*D211N). Both point mutants were expressed in *E. coli* Bap-1 cells as a didiomain containing the adjacent ACP in *holo* form.

Heterologous expression of the active site mutants CorJ DH*H47A holo-ACP and CorJ DH*D211N holo-ACP. To achieve the envisaged amino acid exchanges in the active site of CorJ DH*, to give the active side mutants CorJ DH*H47A and CorJ DH*D211N, respective point mutations were introduced into the primary sequence coding for CorJ DH* by two-step sequential PCR (3.12.2). For each amino acid exchange (H47A and D211N) two primers were designed carrying the point mutation translated into its DNA code. In a first round the point mutation was introduced into the two amplified fragments using (i) the forward primer CorJ_start and the reverse primer carrying the sequence coding for the amino acid exchange (H47A_rev and D211N_rev, respectively), and (ii) the forward primer carrying the sequence coding for the amino acid exchange (H47A_for and D211N_for, respectively) and the reverse primer corJ_end_ACP (**figure 4-12 A**). The two fragments obtained by the first round of PCRs (160 bp and 1089 bp) served as templates for the second PCR (**figure 4-12 B**). First 10 cycles were performed without primers in the sample, then the primers

CorJ_start and corJ_end_ACP were added, and 20 further cycles were performed (**figure 4-12 C**). Primers used for the D211N exchange were D211N_for and D211N_rev, respectively; primers used for the H47A exchange were H47A_for and H47A_rev, respectively. The fragments (1227 bp) obtained by the second round of PCR were ligated into pGEMT vector, and the succesfull cloning was proven by sequencing. Restriction and ligation into the expression vector pET28a was performed as described above for the wild type protein (4.5).

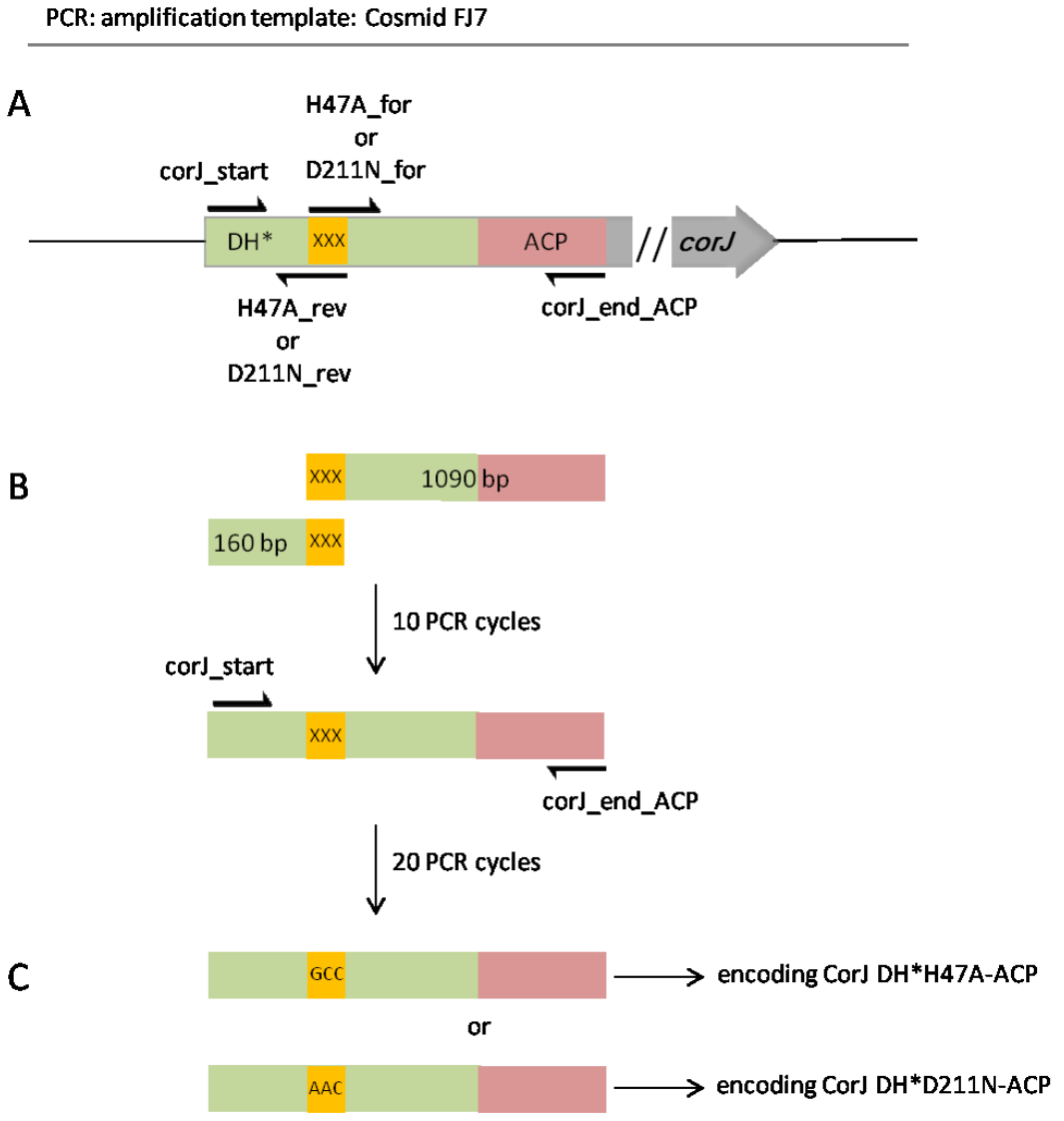

Figure 4-12. Principle of a sequential PCR procedure. A) two separate PCR reaction were performed with the primer pairs corJ_start/ H47A_rev and H47A_for/ corJ_end_ACP (analogously performed with primers D211N_rev and D211N_for). B) The resulted PCR fragments were purified, mixed and subjected to 10 PCR cycles

before the primer pair corJ_start/ corJ_end_ACP was added to the PCR reaction. Subsequent 20 PCR cylces yielded DNA fragments shown in C. Depending on which primer pair (H47A_rev/ H47A_for or D211N_rev/ D211N_for) was used in the first PCR either a point mutation encoding for the amino acid alanine (A) or asparagines (N) was introduced into the DNA fragment. Highlighted in yellow: site of point mutational modification.

Likewise, *E. coli* Bap-1 was chosen as heterologous host for over-expression of the mutated didomains CorJ DH*H47A *holo*-ACP and CorJ DH*D211N *holo*-ACP. Conditions and purification procedures stayed the same as for the wild type proteins, decribed above. **Figure 4-13** presents a picture of the SDS gel with the purified fractions of DH*H47A-ACP and CorJ DH*D211N-ACP. Elution fractions 1–5 were pooled, re-buffered into Tris (pH8) and assays were performed directly afterwards to avoid loss of activity. The protein concentration was determined using a nanodrop spectrophotometer and gave the following concentration: CorJ DH*H47A *holo*-ACP: 8.42 µg/µL, CorJ DH*D211N *holo*-ACP: 8.73 µg/µL.

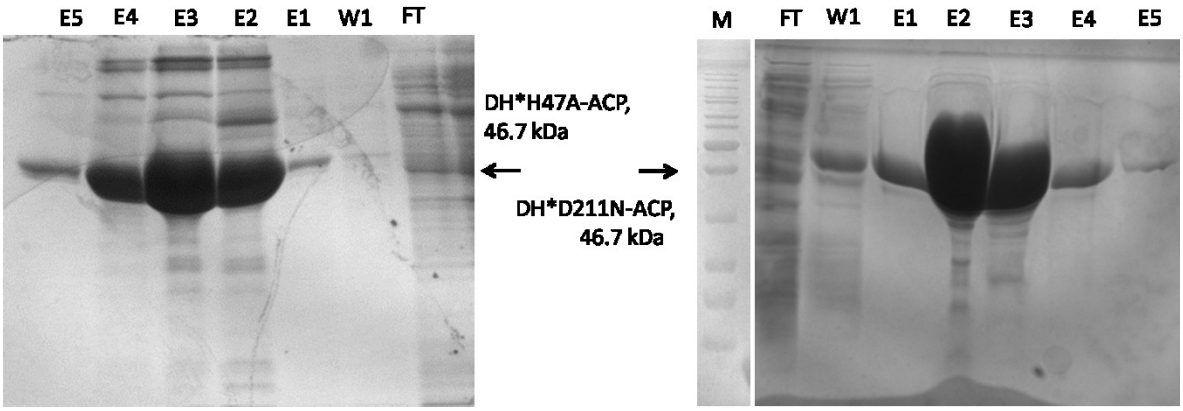

Figure 4-13. Purification of CorJ DH*H47A *holo*-ACP and CorJ DH*D211N *holo*-ACP (46.7 kDa) by affinity chromatography on Ni-NTA column. SDS Gel shows fraction of purification steps: FT (flow through); W1 (wash 1, 20 mM imidazole); E1–5 (elution 1–5, 100–300 mM imidazole); M (size marker).

4.6 Syntheses of the *N*-acetylcysteamine (SNAC) activated substrate for the shift domain CorJ DH*

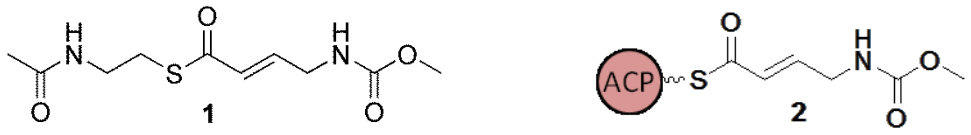

Figure 4-14. *N*-acetylcysteamine activated substrate **1** for the shift domain (CorJ DH*) and ACP-bound intermediate **2** of the corallopyronin A biosynthetic pathway.

The substrate suitable for assaying the shift domain CorJ DH* should be an analogue to the corresponding molecule in the assembly line of corallopyronin A (**figure 4-14**). As well, the substrate was planned to be synthesized as an activated acyl-thioester to facilitate loading onto the phosphopantetheine (ppant) arm of the acyl-carrier protein (ACP).

Polyketide synthases (PKS) normally utilize acyl-coenzmye A (CoA) precursors (Hertweck, 2009), but here we chose to use a shorter sulfhydryl substance such as *N*-acetylcysteamine (SNAC), analogue to the acceptor terminal portion of CoASH (Arora et al., 2005). Acyl-SNAC substrates have been used successfully in several enzyme assays with the aim to elucidate dehydratase reactions, e.g. dehydratase domains of the ansamitocin, the borrelidin and the nachangmycin biosynthesis cluster (Guo et al., 2010; Taft et al., 2009; Vergnolle et al., 2011).

4.6.1 Synthesis of compound 7

The first approach to obtain **1** yielded in compound **7**, which represents the isomer of **1** with the double-bond in β,γ position (**scheme 4-3**).

In the first reaction step crotonic acid **3** was converted into the corresponding 4-bromocrotonic acid **4** via a radical mechanism using the radical forming agent azobisisobutyronitrile (AIBN) and *N*-bromosuccinimide (NBS). After recrystallisation from a mixture of petroleum ether and ethylacetate compound **4** was obtained (43 %). In the following step the bromine residue was replaced by an amino moiety using aqueous ammonia to yield 10 % of 4-aminocrotonic acid (**5**) after purification using a cation exchange resin. The conversion of the amino functionality to a carbamate moiety was performed under basic conditions using methyl chloroformate to give 4-methoxycarbonylaminobut 2-enoic acid (**6**) in yields of about 74 %. The analytical data of the compounds **4** and **5** were in accordance with data from literature (Höfling et al., 2008). It has to be mentioned that compounds **3**–**6** are commercial available, however due to the need of greater amounts it was preferred to synthesise them by ourselves. Finally, a coupling of **6** with *N*-acetylcysteamine (SNAC) via 1-Ethyl-3-(3-dimethylaminopropyl)carbodiimide (EDC)/4-Dimethylaminopyridine (DMAP) standard procedure (Neises and Steglich, 1978) should have resulted in the desired substrate **1**. However, a mixture of different products was obtained from which compound **7** was isolated.

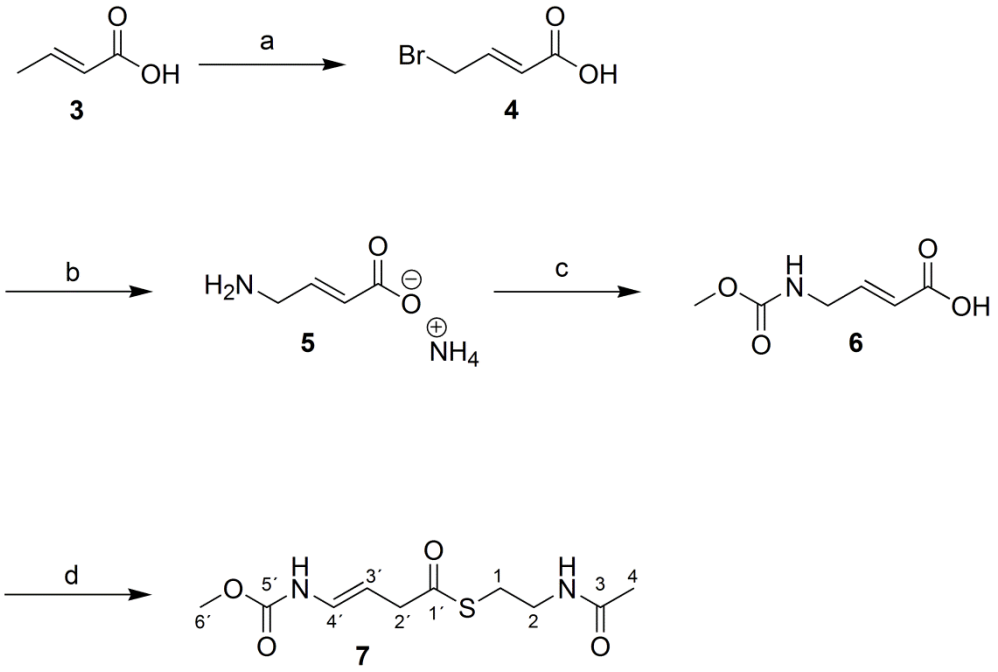

Scheme 4-3. Synthesis of **7**. *Reagents and conditions:* a) NBS, AIBN, CCl_4, 95 °C; b) 25 % aq. NH_3, rt; c) $ClCO_2Me$, dioxane/H_2O, $NaHCO_3$, rt; d) EDC, DMAP, 1 eq. *N*-acetylcysteamine, DCM, rt.

Isolation and identification of compound 7. The reaction mixture was purified by column chromatography on silica gel using ethyl acetate as eluent to obtain **7** (6 mg, 1.7 %). A subsequent recorded LC-MS chromatogram showed two separated peaks with a retention time of 10.4 and 10.7 min and a mass to charge ratio of 261 (M+H) (LC-MS chromatogram and MS traces in appendix **figure 8-6**). According to that finding it was supposed to obtain compound **1** and **7** after separation on a HPLC column under analogous conditions. However, separation merely yielded compound **7** (>1 mg) (column: Waters RP C18 Atlantis; solvent: linear gradient from 95 % water to 100 % ACN in 45 min, flow: 1 mL/min).

1D and 2D NMR experiments were performed to elucidate the structure of the isolated compound. Characteristic resonances for a methoxy group at δ 3.73 ppm (C-6') and an acetyl methyl group at δ 1.95 ppm (C-4) could be detected in the ^{1}H NMR. Also two proton resonances were found at δ 5.17 ppm (C-3') and δ 6.62 ppm (C-4'), for which a coupling constant of 14.3 Hz suggested a *trans* configuration. ^{1}H-^{1}H COSY correlations between both H-4' (δ=2.29) and H-3'(δ=5.17) with H-2' (δ=3.27) confirmed the structure of the western part the molecule, whereas cross-coupling

between H-1 (δ=3.03) and H-2 (δ=3.35) verified the eastern part of the molecule, shown in **scheme 4-3** compound **7** (**table 4-1**). Spectra shown in appendix **figure 8-4** and **8-5**.

Table 4-1. 1D and 2D NMR spectroscopic data of compound **7**. [a] $[D_4]$MeOH, 300 MHz

Position	δ_H[a] (*J* in Hz)	COSY[a]
1	3.03 (2H, t, 6.6)	2
2	3.35 (2H, t, 6.6)	1
4	1.95 (3H, s)	
2’	3.35 (2H, d, 7.3)	3´, 4´
3’	5.17 (1H, dt, 14.3, 7.3)	4´, 2´
4’	6.62 (1H, d, 14.3)	3´, 2´
6’	3.73 (3H, s)	

4.6.2 Synthesis of compound 8

In order to obtain compound **1** the same approach as described in 4.6.1 was applied using the double amount of SNAC. Thin layer chromatography was performed and again revealed a mixture of reaction products. Subsequent separation of the mixture was performed by HPLC (column: Waters C18 Atlantis; solvent: isocratic MeOH/H_2O (80/20), flow: 1 mL/min, 60 min) and gave compound **8** (3 mg, 1.5 %). Other compounds could not be isolated and determined out of that mixture (**scheme 4-4**).

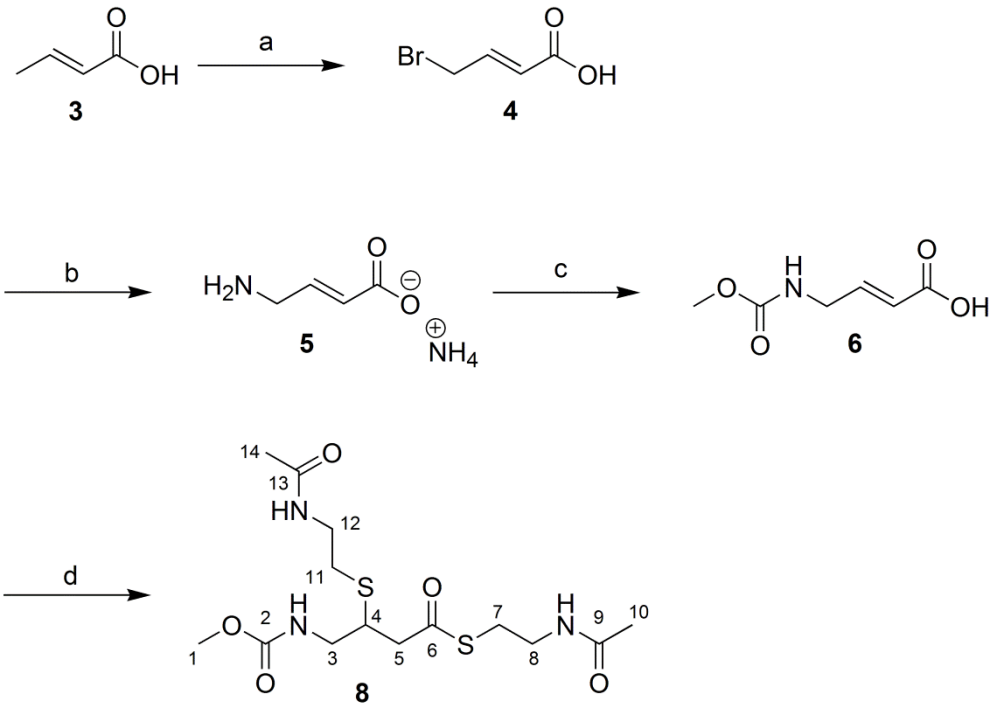

Scheme 4-4. Synthesis of **8**. *Reagents and conditions:* a) NBS, AIBN, CCl_4, 95 °C; b) 25 % aq. NH_3, rt; c) $ClCO_2Me$, dioxane/H_2O, $NaHCO_3$, rt; d) EDC, DMAP, 2 eq. *N*-acetylcysteamine, DCM, rt.

Analytical characterization was done by LC-MS/ESI experiments (column: Phenomenex Luna® 3 µm C18(2); linear gradient from 90 % H_2O to 100 % MeOH in 10 min, then 100 % MeOH to 20 min, DAD 220.0–400.0 nm). In the positive mode a signal with the *m/z* 380 could be detected, which vanished in the negative mode where two signals with *m/z* 118 and *m/z* 259 occurred instead. The first signal matches with the mass of a SNAC ion and the latter to a fragment with the same mass to charge ratio as compound **1** or **7**. Hence, the assumption came up that the isolated compound was the corresponding Michael adduct to the envisaged substrate **1** (**figure 4-15**).

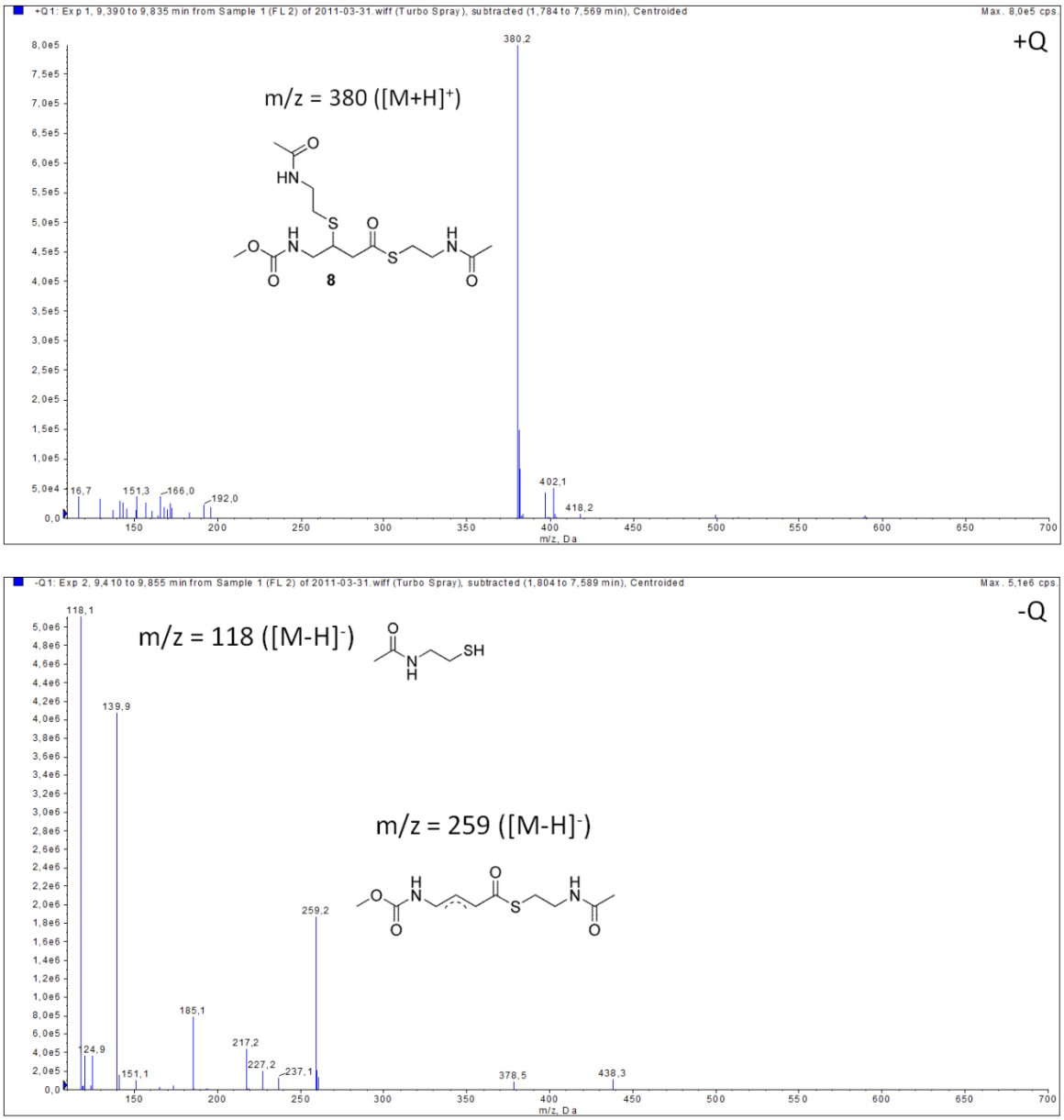

Figure 4-15. ESI-MS experiment of isolated compound **8**. Positive mode (+Q): *m/z* 380.2 ($[M+H]^+$) representing the Michael adduct **8**; Negative mode (-Q): *m/z* 118.1 ($[M-H]^-$) and *m/z* 259.2 ($[M-H]^-$) correlating with the fragmentation of **8** to *N*-acetylsteamine (SNAC) and an ion with the same *m/z* value as compound **1** or **7.**

Further characterization of the obtained product was performed via 1D and 2D NMR experiments (**table 4-2,** spectra shown in appendix **figure 8-7, 8-8, 8-9, 8-10, 8-11**). The ^{1}H NMR spectrum showed characteristic resonances for a methoxy group at δ 3.68 ppm (C-1,) and two sharp signals at δ 1.96 and 1.98 ppm for two acetylic methyl groups (C-10 and C-14), the latter indicating a double addition of SNAC to the precursor molecule **6**. In the ^{13}C NMR spectrum resonances for 14 carbon were

present, which can be grouped into three methyl groups, six methylene groups, one methine and four quaternary carbons, as was deduced from distortionless enhancement by polarization transfer (DEPT) measurement. Two of the four quaternary carbons were attributed to be involved in carbonyl functional groups (C-9, δ=173.5 and C-13, δ=173.4). ^{13}C NMR resonances for the other two quaternary carbons C-2 (δ=159.6) and C-6 (δ=198.3) indicated them to be involved in a carbamate functional group and in a thioester, respectively. Assignment of all protons to their directly bonded carbon atoms was done by ^{1}H-^{13}C HSQC data. The long range HMBC correlations between H-11 (δ=2.74) and C-4 (δ=43.2) and between H4 (δ=3.28), H-5a/b (δ=2.29, δ=2.78) and H-7 (δ=3.07) and C-6 (δ=198.3) confirmed the already suspected addition of two SNAC residues to the double-bond of **6** to form **8**. These findings were confirmed by ^{1}H-^{1}H COSY correlations between H-4 (δ=3.28) and H-5a/b (δ=2.29, δ=2.78), H-7 (δ=3.04) and H-8 (δ=3.38) and between H-11(δ=2.74) and H-12 (δ=3.39).

Table 4-2. 1D and 2D NMR spectroscopic data of compound **8**. [a] [D$_4$]MeOH, 300 MHz.

Position	δ_C[a] (mult.)	δ_H[a] (*J* in Hz)	COSY[a]	HMBC[a]
1	52.6, (CH_3)	3.68 (3H, s)		2
2	159.6, (C)			
3	45.7, (CH_2)	a: 3.36 (1H, m) b: 3.27 (1H, m)		2
4	43.2, (CH)	3.28 (1H, m)	5	2, 6
5	47.9, (CH_2)	a: 2.29 (1H, dd, 4.8, 15.7) b: 2.78 (1H, dd, 8.0, 15.7)	4	6, 7
6	198.3, (C)			
7	29.1, (CH_2)	3.07 (2H, t, 6.6)	8	6
8	40.1, (CH_2)	3.38 (2H, m)	7	9
9	173.5, (C)			
10	22.6, (CH_3)	1.96 (3H, s)		9
11	31.1, (CH_2)	2.74 (2H, t, 6.6)	12	4, 12
12	40.5, (CH_2)	3.39 (2H, m)	11	13
13	173.4, (C)			
14	22.6, (CH_3)	1.98 (3H, s)		13
NH		8.13, 8.25 (2H, bs)		

4.6.3 Abruzov and Horner-Wittig-Emmons reaction resulted in compound 1

The synthesis approaches depicted in the chapter 4.6.1 and 4.6.2 were not successful in order to obtain the envisaged compound **1**. The crucial point seemed to be the reactive double-bond in α,β position to the carbonyl moiety, acting as a Michael acceptor. Hence, it was planned to introduce the double-bond in the final reaction step. Therefore a synthetic route *via* Arbuzov and Horner-Wittig-Emmons (HWE) reactions was performed. 2-Bromoacetic acid **9** was converted into the SNAC thioester **10** and then treated with triethyl phosphite to form the corresponding Arbuzov product **11**, which reacted under strong basic conditions in the presence of *N*-Boc-2-aminoacetaldehyde to form the HWE product **12** (**scheme 4-5**). Finally, the *tert*-butyloxycarbonyl protecting group was exchanged by a methoxycarbonyl moiety to receive the desired SNAC-activated substrate **1**. Analytical data of compounds **10–12** are presented in the appendix in figure **8-12**, **8-13**, **8-14**.

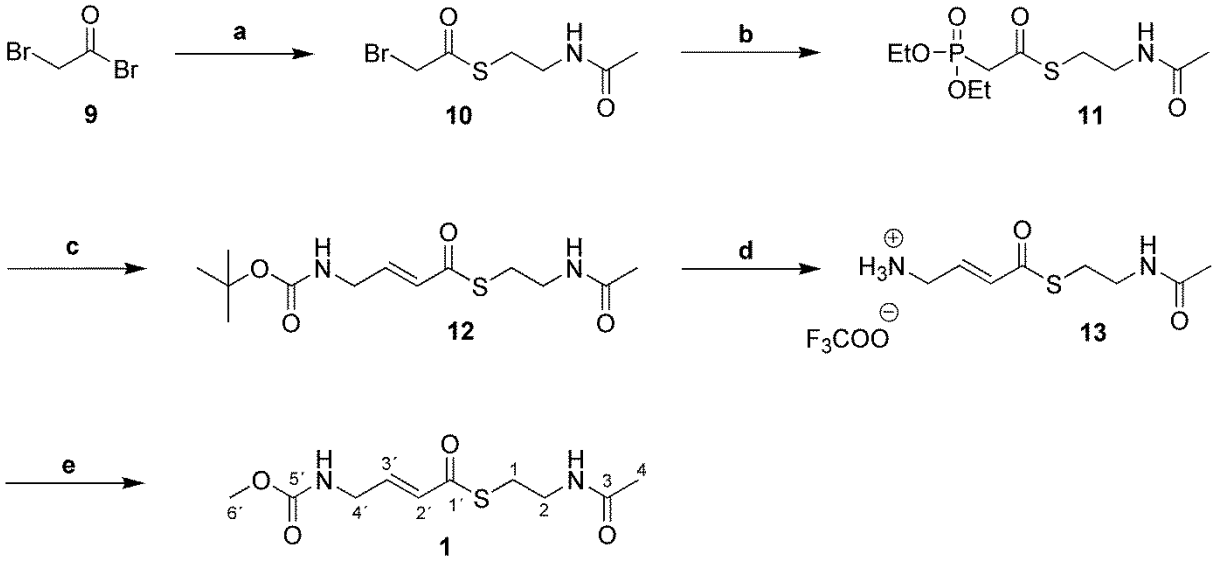

Scheme 4-5. Synthesis of compound **1** *via* Arbuzov and Horner-Wittig-Emmons reactions. *Reagents and conditions:* a) Et_3N, *N*-acetylcysteamine, THF, rt; b) triethyl phosphite, THF, 130 °C, sealed tube; c) NaH, Boc-Gly-H, THF, -10 °C; d) TFA, CH_2Cl_2, 0 °C; e) Et_3N, $ClCO_2Me$, THF, 0 °C.

Isolation and identification of compound 1. The reaction process described above was monitored by TLC chromatography and showed the formation of a main product which could be isolated via silica column chromatography using ethylacetat as eluent

to give the oily compound **1** (15 mg, 0.68 % overall). LC-MS ESI experiments and 1D NMR spectroscopy (**table 4-3**, depicted in appendix **figure 8-1** and **8-2**) confirmed the molecular structure presented in **scheme 4-5**.

The ^{1}H NMR showed resonance signals for 14 protons which correlates with the molecular structure. The exchangeable protons attached to both nitrogen atoms were not detected. The spectrum exhibit a characteristic resonance for a methoxy group at δ 3.70 ppm (C-6') and one sharp signal for the acetylic methyl group δ 1.96 ppm (C-4). Two resonance signals at δ 6.90 ppm (C-2') and δ 6.27 ppm (C-3') with a coupling constant of 15.5 Hz were detected in the ^{1}H NMR spectrum, which indicated a *trans* double-bond in the molecule. Further, two resonance signals were found with a chemical shift of δ 3.11 ppm (C-1) and δ 3.38 ppm (C-2) and a coupling constant of 6.6 Hz which allowed to be attributed to the two methylene moieties of the SNAC part of the molecule. The ^{13}C NMR spectrum displayed 10 carbon resonances, which could be distinguished into three quaternary carbons, two methine, three methylene and two methyl groups. The quaternary carbons could be attributed according to their chemical shifts first to the carbonyl atom C-5'of the urethane group (δ=159.4), second to the acetyl carbonyl-carbon C-3 (δ=173.56) and third to the carbonyl C-1' which is part of the thioester (δ=190.6). Due to their characteristics ^{13}C NMR chemical shifts both sp^{2} hybridized C atoms C-2' (δ=143.1) and C-3' (δ=128.6) were identified as associated with the single olefinic partial structure of the molecule **1** (**table 4-3**).

Table 4-3. 1D NMR spectroscopic data of compound **1**. ^{a} [D_4]MeOH, 300 MHz

Position	$\delta_C{}^{a}$ (mult.)	$\delta_H{}^{a}$ (*J* in Hz)
1	29.0, (CH_2)	3.11 (2H, t, 6.6)
2	40.1, (CH_2)	3.38 (2H, t, 6.6)
3	173.5, (C)	
4	22.5, (CH_3)	1.96 (3H, s)
1'	190.6, (C)	
2'	143.1, (CH)	6.90 (1H, d, 15.5)
3'	128.6, (CH)	6.27 (1H, dt, 15.5)
4'	42.3, (CH_2)	3.93 (2H, m)
5'	159.4, (C)	
6'	52.7, (CH_3)	3.70 (3H, s)

4.7 In vitro assays to prove the functional role of CorJ DH*

4.7.1 Phosphopantetheine (ppant) ejection assays

General procedure of the ppant ejection assay and expected outcome. The intramolecular isomerisation of a double-bond does not result in a mass difference. To still enable the functional analysis of the putative shift domain CorJ DH* using mass spectral analysis the assay was performed in deuterated buffer. Immediately after heterologous expression of the didomain CorJ DH**holo*-ACP the protein was incubated with the substrate **1** in deuterated assay buffer at room temperature (3.17.1). Substrate **1** was expected in the first reaction step to bind to the phosphopantetheine (ppant) residue of the *holo*-ACP moiety of the didomain CorJ DH**holo*-ACP to give **2** (**figure 4-16**). To prove the successful linkage a separate experiment with the sole substrate loaded CorJ *holo*-ACP domain was planned to be performed (4.7.1.1). The second reaction step should be the isomerisation of the double-bond, performed by the shift domain CorJ DH*, whereby an incorporation of two deuterium atoms should occur, one in α-position and the other in γ-position (**figure 4-17**). After an incubation time of 1 h, 3 h and 20 h the reaction was envisaged to be stopped by injection onto an HPLC column and the purified and lyophilized protein sample would be prepared for mass spectroscopic experiments (3.17.1). The exchange of protons by deuterium atoms was envisaged to be traced *via* an increase in mass of the protein-bound substrate by a tandem mass analysis approach called phosphopantetheine (ppant) ejection assay.

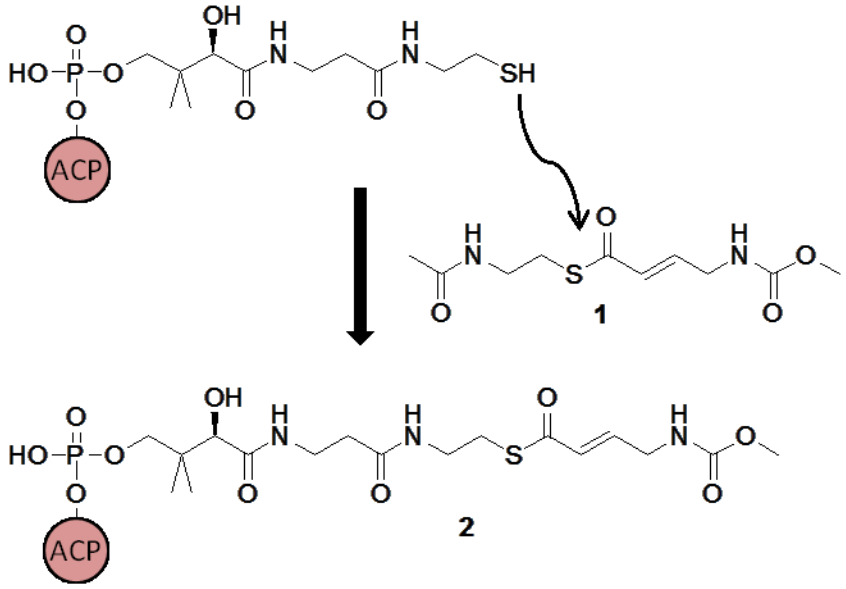

Figure 4-16. Reaction of compound **1** with the phosphopantetheine residue of CorJ *holo*-ACP domain resulted in **2**.

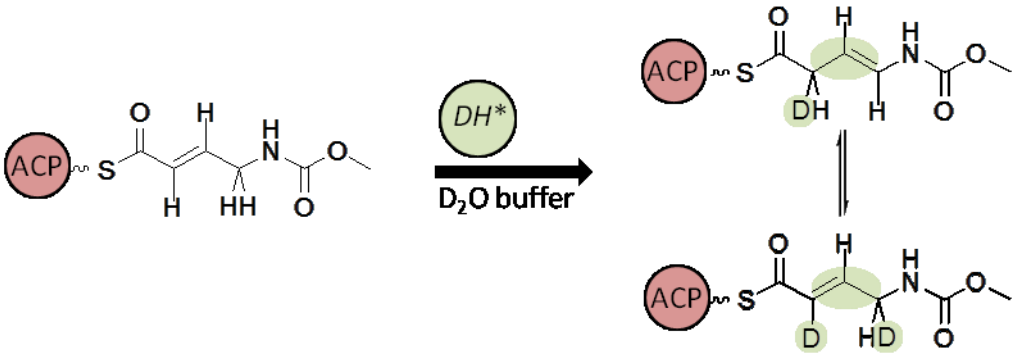

Figure 4-17. Incorporation of two deuterium atoms due to CorJ DH* mediated double-bond migration.

The "ppant ejection assay" is a "top-down" MS^n spectrometric characterization of intermediates bound to thiotemplate carrier domains (like CorJ *holo*-ACP), utilizing a typical elimination reaction of the phosphopantetheine residue (ppant) of the carrier protein during the fragmentation process yielding in the ejection ion (pant) *m/z* 261.126, depicted in **figure 4-18 A**. PKS or NRPS biosynthetic intermediates are normally bound to the sulphur of the phosphopantetheine residue of a carrier protein and form a thioester linkage. The linked intermediate increases thereby the mass of the whole carrier protein, which can be detected by a tandem mass spectrometric analysis of the whole carrier protein. N. L. Kelleher established the "ppant ejection

assay" for characterization of carrier bound intermediates without precedent trypsin digestion of the carrier protein (Kelleher et al., 1999). The "top down" approach was refined by P. C. Dorrestein and co-workers, who published twelve signature MS^3 ions of the phosphopantetheine residue which were used as reference ions for the experiments in this study (Dorrestein et al., 2006; Meluzzi et al., 2008) (**figure 4-18 B**).

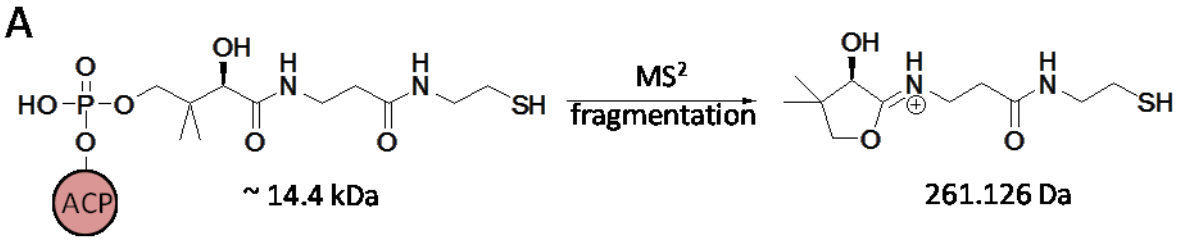

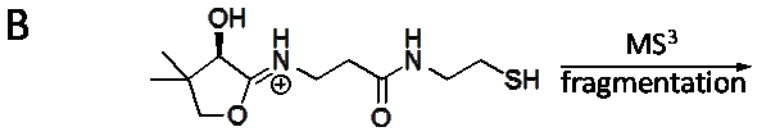

formula	m/z
$H_{10}C_5NOS^+$	132.048
$H_{12}C_7NO_2^+$	**142.086**
$H_{13}C_5N_2OS^+$	149.074
$H_{11}C_6N_2OS^+$	159.059
$H_{12}C_9NO_2^+$	**166.086**
$H_{11}C_6N_2O_2S^+$	175.054
$H_{14}C_9NO_3^+$	**184.097**
$H_{13}C_7N_2O_3S^+$	205.064
$H_{19}C_{10}N_2OS^+$	215.121
$H_{17}C_{11}N_2OS^+$	225.106
$H_{19}C_{10}N_2O_2S^+$	231.116
$H_{19}C_{11}N_2O_2S^+$	243.116

Figure 4-18. Principle of the ppant ejection assay. Elimination reaction of the phosphopantetheine residue of a *holo*-ACP. A) MS^2 experiment on an *holo*-ACP domain releases a pantetheine (pant) ejection ion with the mass of 261.126 Da. B) MS^3 experiment on the isolated pantetheine (pant) ejection ion gives 12 signature ions useful for characterization of thiotemplate bound intermediates. Masses of bold printed ions are independent of thiotemplate bound intermediates. Modified after Meluzzi et al., 2008.

4.7.1.1 Proof of the successful linkage of substrate 1 to the phosphopantethein (ppant) arm of CorJ *holo*-ACP

Substrate **1** was incubated with the heterologously expressed protein CorJ *holo*-ACP under assay conditions to examine whether a successful linkage to the ppant moiety occurred under formation of **2** (**figure 4-16**). Electro spray ionisation of this protein sample with a mass of 14.5 kDa resulted in multiply charged ions of the substrate loaded protein CorJ *holo*-ACP **figure 4-20 A**. Calculations of the charge state of the ions were done with the help of **formula 4-1**.

Formula 4-1: $z_x = \frac{y+1}{x-y}$

z_x = (charge of ion x)

x = (ion with m/z smaller than ion y), marked in **figure 4-20 A**

y = (ion with m/z larger than ion x), marked in **figure 4-20 A**

For the isolated charge state +17 (m/z 855.03, isolation width 7 m/z) ejection ions were obtained by applying normalized collision energy of 30–35 % in the linear ion trap, to result in MS^2 ejection fragments, which are recorded in spectrogram B of **figure 4-20**. The ejection ion m/z 303.137 represented a pantetheine (pant) arm with an attached acetyl unit and was not further referred to in this study (**figure 4-20**). The corresponding ejection ion of **2** is compound **2a** with a m/z of 402.169. The presence of this ion confirmed the successful binding of **10** to the phosphopantetheine residue of CorJ *holo*-ACP (**figure 4-19**). The fragment **2a** (**figure 4-19 and 4-20 C**) was further fragmented and released the MS^3 signature ions m/z 142. 050 (**2b**) and m/z 261.126 (**2c**) (**figure 4-19 and 4-20 D**). The first ion (*i.e.* **2b**, m/z 142. 050) was associated with a fragment of the substrate **1**, without SNAC. The second ion (*i.e.* **2c**, m/z 261.126) represented the unloaded pant ejection arm as shown in **figure 4-18 A** and **4-19**.

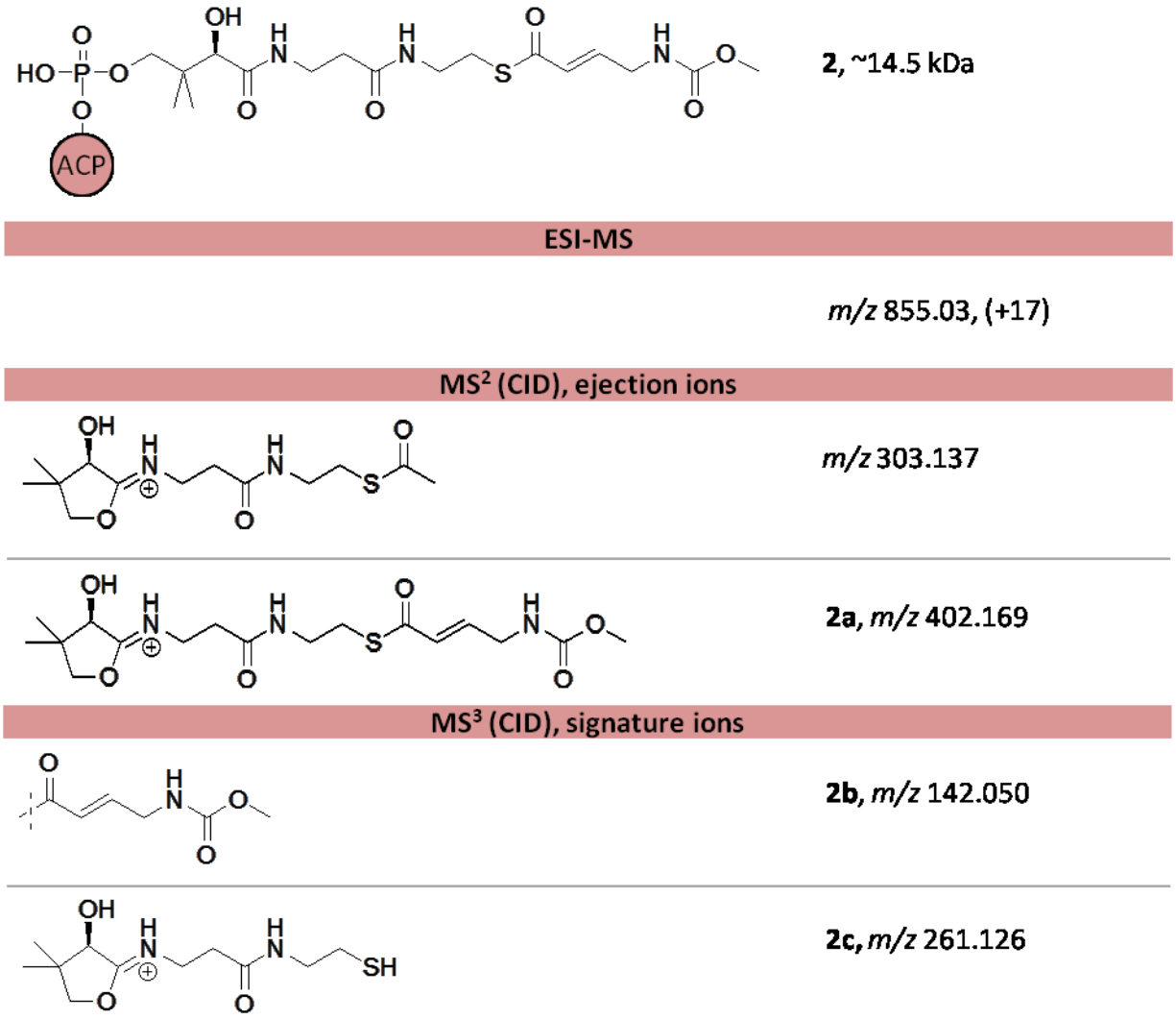

Figure 4-19. Ions observed by MS^n analysis (ppant ejection assay) of the substrate-loaded CorJ *holo*-ACP domain **2**. ESI (electrospray ionization), CID (collision-induced dissociation).

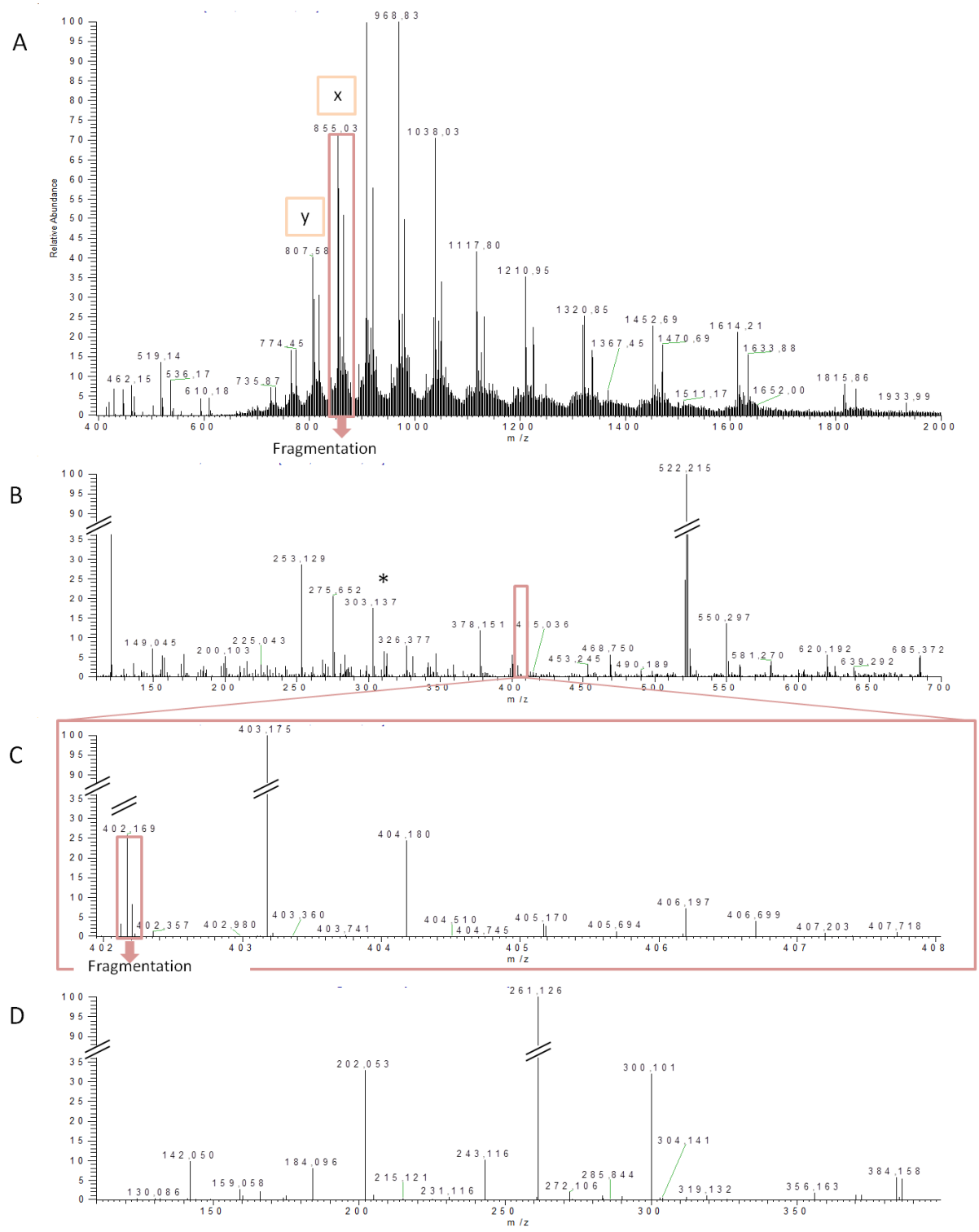

Figure 4-20. Overview for a ppant ejection experiment with the substrate-loaded CorJ *holo*-ACP. A) ESI spectrum of the substrate-loaded protein CorJ *holo*-ACP (**2**). State charges marked with x and y refer to **formula 4-1**. Charge state 17+ (highlighted in red) was isolated and fragmented. This resulted in spectrum B showing the ejection ions. The asterisk in B marks the ejection ion *m/z* 303.137 representing the phosphopantetheine arm plus an attached acetyl rest. The region of the MS^2 ejection

ions of the substrate-loaded pant residues (here: from *m/z* 400–410) is magnified in C. Exemplarily, a single ejection ion was isolated (here **2a**, *m/z* 402.169, highlighted in red) and subjected to a further round of fragmentation, yielding the respective MS^3 signature ions (Meluzzi et al., 2008) depicted in D. Fragmentation of the MS^3 ion *m/z* 402.169 resulted in the peak *m/z* 261.126 representing the sole pant moiety **2c** and in peak *m/z* 142.050 representing the substrate part **2b**.

4.7.1.2 Investigation of potential unspecific hydrogen/deuterium exchanges under assay conditions

As outlined above the functional role of the shift domain CorJ DH* was planned to be proven by a hydrogen/deuterium (H/D) exchange due to the enzymatically catalyzed double-bond migration in a deuterated buffer system. To distinguish between enzymatically mediated and unspecific H/D exchange, the sole CorJ *holo*-ACP protein was loaded with substrate **1** under assay conditions for 20 h. Possible H/D exchanges in **2** were thought to be the acidic positively charged imine group, the amid functions and the hydroxyl moiety (**scheme 4-6**). MS^n analysis of the substrate loaded protein in a ppant ejection experiment resulted in the MS^2 ejection ions *m/z* 402.169, 403.175, 404.180 and 405.187 which represented fragment **2a** and the corresponding isotopes with maximum three incorporated deuterium atoms (**scheme 4-6**, **table 4-4**). Fragmentation of each ejection ion led to the MS^3 signature ions *m/z* 261.126, 262.132, 263.138 and 264.144, respectively, which correlate with the pant arm **2c** (*m/z* 261.126) and its deuterated isotopes, respectively. In the same MS^3 fragmentation rounds signature ions occurred representing **2b** (*m/z* 142.050) and the corresponding isotope containing one deuterium atom (*m/z* 143.056) (**scheme 4-6**, **table 4-4**).

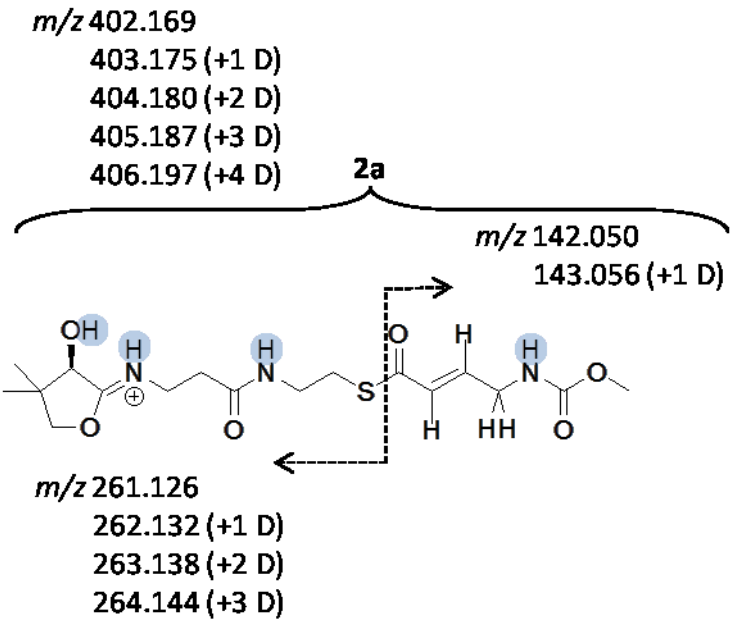

Scheme 4-6. Potential unspecific H/D exchanges in **2a** (highlighted in blue) and respective signature ions in a MS^3 experiment.

Table 4-4. MS^2 and MS^3 ions detected during tandem mass spectral analysis of **2a**. MS^2 ejections ions were isolated and subjected to a further round of fragmentation to result in MS^3 signature ions (highlighted in blue). n.i. (not investigated)

MS^2 *m/z*	MS^3 *m/z*			
402.169	261.126 and 142.050			
403.175	261.126 and 143.056	262.132 and 142.050		
404.180		262.132 and 143.056	263. 138 and 142.050	
405.187			263. 138 and 143.056	264.144 and 142.050
406.197				n.i.

4.7.1.3 Proof of the β,γ double-bond migration using the ppant ejection assay

To prove the double-bond shift activity of CorJ DH*, the didomain CorJ DH**holo*-ACP was loaded with substrate **1** and incubated in deuterated buffer at room temperature for 1 h, 3 h and 20 h. Due to a CorJ DH* mediated double-bond isomerisation an specific exchange of two hydrogen atoms by two deuterium atoms was expected. Electro spray ionization of the 47.2 kDa large substrate-loaded protein CorJ DH**holo*-ACP did not result in single charge states of the protein. Thus, MS^2 ejection ions were obtained by in-source fragmentation, applying 50–65 V fragmentation energy. The mass of the non-deuterated form of ejection ion **2a** (*m/*z 402.169) increased to 403.175, 404.182, and surprisingly to 405.188, indicating the number of incorporated deuterium atoms (**figure 4-21**, **table 4-5**). MS^3 fragmentation of each of these ejection ions yielded clear pant (*i.e.* **2c**, *m/z* 261.126), pant+substrate (*i.e. m/z* 300.102, 301.10, 302.114, 303.114) and substrate signature peaks (*i.e*. *m/z* 142.050, 143.056, 144.062, 145.068), presenting a mass increase up to +3, respectively (**figure 4-21**). The substrate derived signature ions (*i.e m/z* 142.050, 143.056, 144.062, 145.068) were each subjected to a further round of fragmentation yielding in the corresponding MS^4 fragments *m/z* 110.024, 111.030, 112.037, 113.043, respectively, as depicted in **figure 4-21**. The importance of the MS^4 fragments is that all of their protons or deuterium atoms are bound to carbon atoms. Hence, observed mass increase due to deuterium incorporation can be correlated directly to the double-bond shifting activity of CorJ DH* and a mass increase associated with an unspecific H/D exchange at the amide function, as depicted in **scheme 4-6** can be excluded.

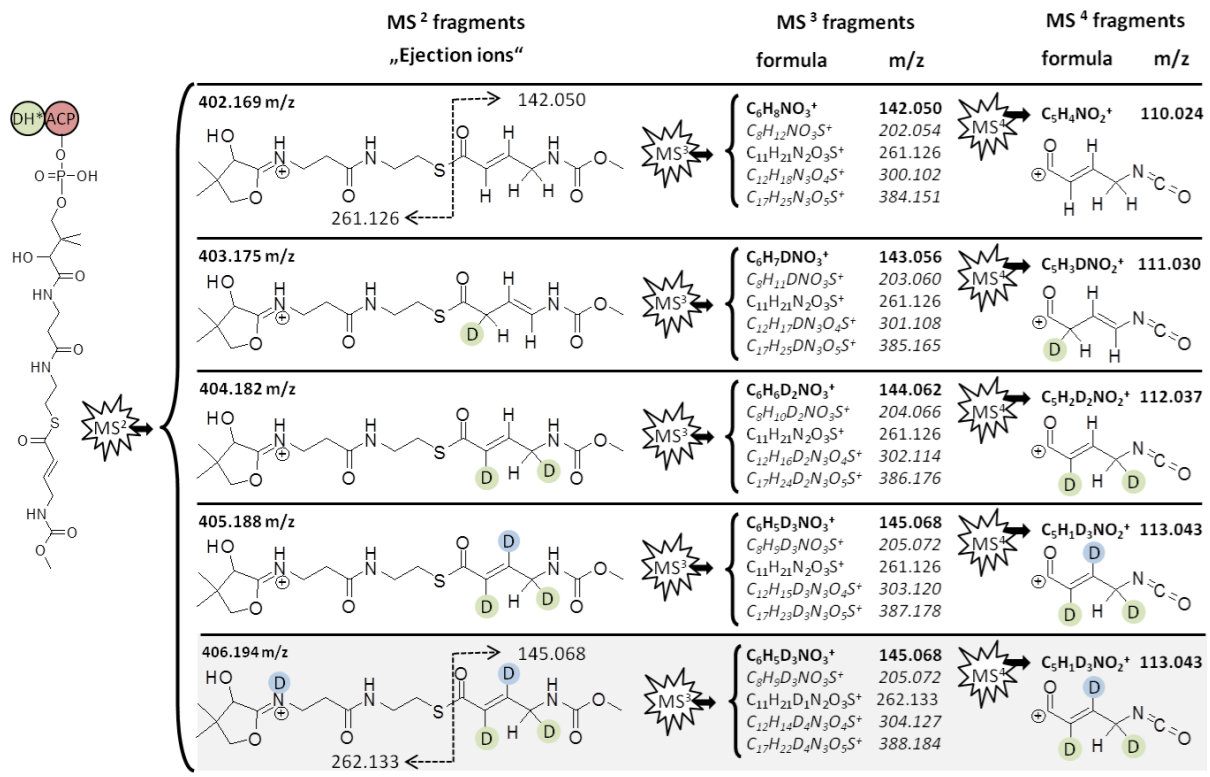

Figure 4-21. Representative pantetheine (pant) ejection ions and their fragmentations by MS^n. The ejection ion *m/z* 402.169 (**2a**) arose from the substrate loaded *holo*-enzyme CorJ DH*-ACP. The green colored deuterium atoms were supposed to be exchanged by the isomerisation activity of CorJ DH*, whereas the blue colored deuterium atoms resulted from non-enzymatic exchange. MS^3 experiments resulted in signature ions of the pant arm (**2c**, *m/z* 261.126), of the pant arm with bound substrate (*in italic*), and of the substrate-derived fragment alone (**in bold**). MS^4 of the substrate fragments yielded another series of corresponding signature ions (*m/z* 110.024 to 113.043) proving the presence of up to three deuterium atoms. The dashed arrow shows the fragmentation site of the ejection ion into a pant arm and a substrate part. The ejection ion *m/z* 406.194 (shaded in grey) represents an unspecific hydrogen/deuterium exchange at the pant arm, resulting in a mass increase to *m/z* 262.133 for the pant arm. The most likely structures of the MS^4 fragments are shown here with all hydrogens/deuterium atoms attached to carbon atoms.

Table 4-5. MS^2 and MS^3 ions detected during tandem mass analysis of the substrate loaded CorJ DH**holo*-ACP. MS^2 ejections ions were isolated and subjected to a further round of fragmentation to result in MS^3 signature ions. Highlighted in blue: *m/z* ratios related to an unspecific H/D exchange (check against **table 4-4**). Highlighted in green: masses correlating with a CorJ DH* mediated H/D exchange. n.d. (not detected)

MS^2 *m/z*	MS^3 *m/z*			
402.169	261.126 and 142.050			
403.175	261.126 and 143.056	262.132 and 142.050		
404.182	261.126 and 144.062	262.132 and 143.056	n.d.	
405.188	261.126 and 145.068	262.132 and 144.062	n.d.	n.d.
406.193		262.132 and 145.068		n.d.

Assuming CorJ DH* catalyzed the incorporation of two deuteriums (**figure 4-17**), one at the α position and the other at the γ position, the appearance of the third incorporated deuterium can just be explained by considering the structure of the substrate. Thus, when the carbon-carbon double-bond in α,β position was shifted by CorJ DH* to the β,γ position, enamine-imine tautomerism arises. This chemically feasible, but non-enzymatically caused double-bond shift resulted in the third H/D exchange at the carbon in β position, and indirectly proves the function of CorJ DH* (**scheme 4-7**).

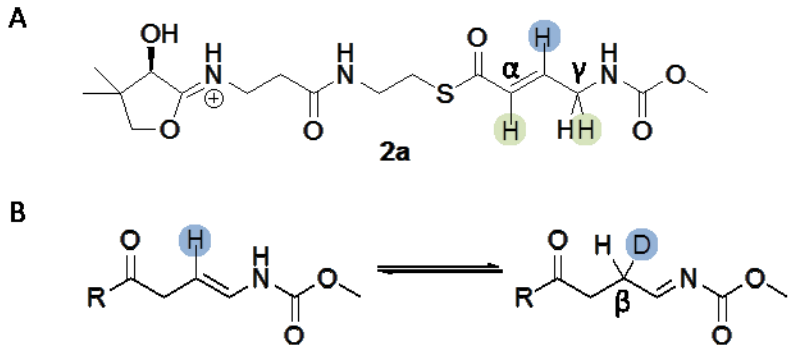

Scheme 4-7. H/D exchange in the presence of CorJ DH*. A) Highlighted in green: exchange of protons in α and γ position correlates directly with the CorJ DH* shifting activity; Highlighted in blue: H/D exchange in β position is the result of an enamine-imine tautomerism shown in B.

Time-dependency of the H/D exchange. In a time-course experiment the H/D exchange of CorJ *holo*-ACP with bound substrate was compared to that of CorJ DH* *holo*-ACP with bound substrate (**figure 4-22**). This revealed after prolonged incubation (20 h) for the merely ACP-bound substrate sample (CorJ *holo*-ACP-substrate) non-enzymatic deuteration, yielding a *m/z* value of 403.176, corresponding to a single H/D exchange. This had to derive from a non-enzymatic exchange as already shown in **scheme 4-6**. Contrary to this the heavier ions *i.e.* 405.188 and 406.194 accumulated after prolonged (3-20 h) incubation of the substrate **1** with the CorJ DH**holo*-ACP didomain. The latter is due to the incorporated deuterium atoms by the action of the shift domain CorJ DH* (**figure 4-22**).

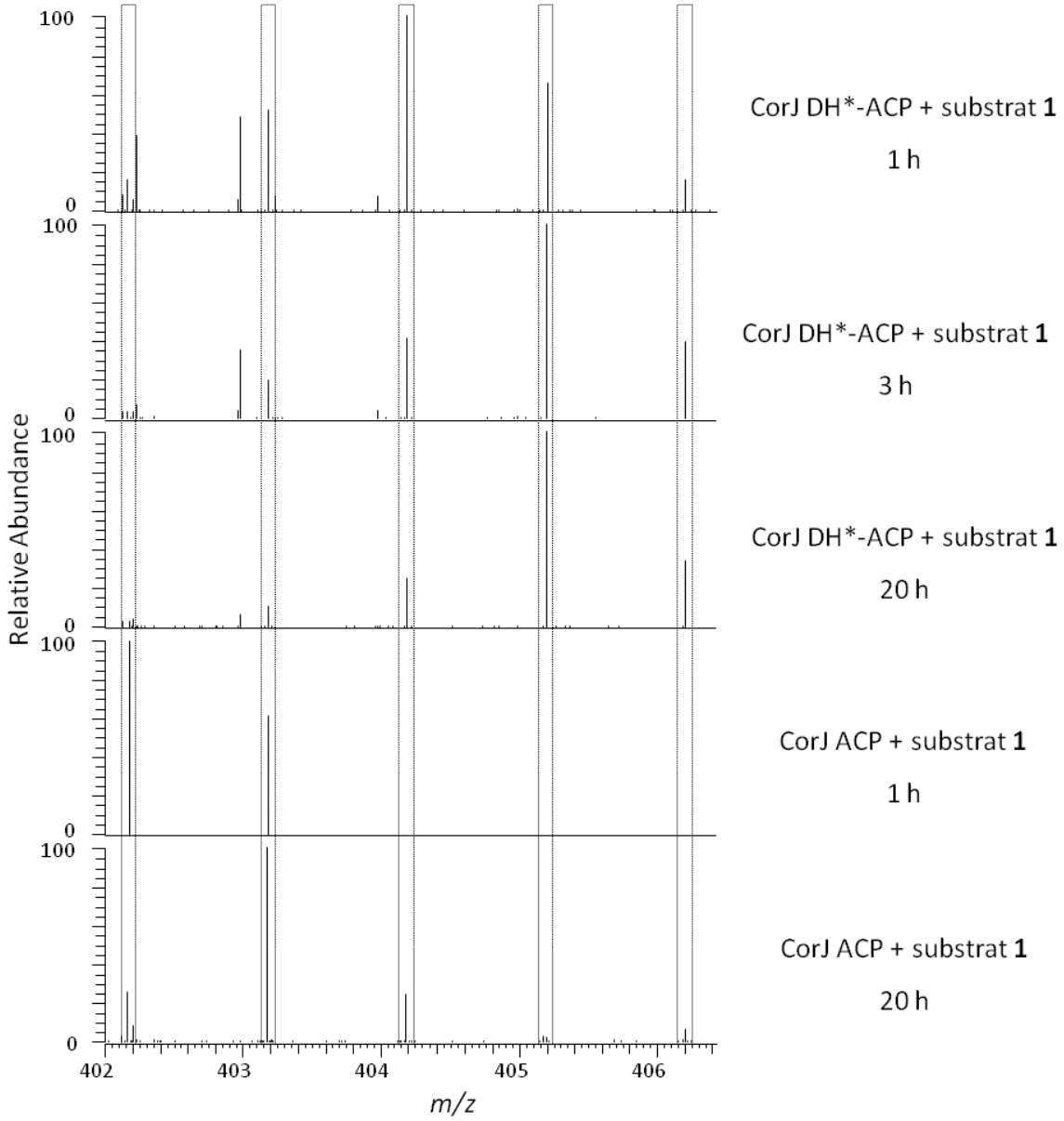

Figure 4-22. Pant ejection ions (MS^2) of the substrate bound to the single CorJ *holo*-ACP domain or to the CorJ DH**holo*-ACP didomain. The proteins with the bound substrate were incubated in deuterated buffer for 1, 3, and 20 hours (h). A time dependent increase of the heavier ions (with more incorporated deuterium atoms) was visible.

4.7.1.4 PPant ejection assay with the substrate-loaded active site mutant CorJ DH*H47A *holo*-ACP

CorJ DH*H47A *holo*-ACP was likewise heterologously expressed and assayed as CorJ DH**holo*-ACP (3.13.1). In MS^n analysis the ejection ions *m/z* 402.172 (**2a**), 403.178 and 404.183 could be recorded which represent the substrate loaded pant arm (**2a**) and its two heavier variants containing up to two incorporated deuterium atoms. Further fragmentation of each ejection ion gave the MS^3 signature ions shown in **table 4-6**. Fragmentation of the ion *m/z* 402.172 resulted in the signature ions *m/z* 261.126 and *m/z* 142.050, presenting the pant arm (**2c**) and the substrate derived fragments **2b**. Dissociation of the ejection ions *m/z* 403.178 and 404.183 gave the signature ion pairs *m/z* 261.126 and *m/z* 143.056 and *m/z* 262.132 and *m/z* 143.056, respectively. These data compared to the negative control reaction of the substrate loaded *holo*-ACP (**table 4-4**) and to the positive reaction with CorJ DH**holo*-ACP (**table 4-5**) led to the suggestion that just unspecific H/D exchange occurred and CorJ DH*H47A lost its catalytic activity regarding double-bond isomerisation.

Table 4-6. MS^2 and MS^3 ions detected during tandem mass analysis of the substrate loaded CorJ DH*H47A *holo*-ACP. Highlighted in blue: masses connected with an unspecific H/D exchange (check against **table 4-5**). n.d. (not detected)

MS^2 *m/z*	MS^3 *m/z*				
402.172	261.128 and 142.050				
403.178	261.128 and 143.056	n.d.			
404.183		262.132 and 143.056	n.d.		
405 **n.d.**					
406 **n.d.**					

4.7.1.5 PPant ejection assay with the substrate-loaded active site mutant CorJ DH*D211N *holo*-ACP

The mutant CorJ DH*D211N *holo*-ACP was expressed and assayed as described in the general procedure in 3.13.1. In MS^n measurements of the substrate loaded mutant, pant ejection ions from *m/z* 402.169 to 405.187 representing the substrate loaded pant arm **2a** and its deuterated variants were detected. Further fragmentation of each ejection ion resulted in the signature ions depicted in **table 4-7**. Signature ions indicating an unspecific H/D exchange (**table 4-7**, highlighted in blue) could be observed as well as ions which correlate with an enzymatically mediated deuterium incorporation (**table 4-7,** highlighted in green). These results led to the assumption, that CorJ DH*D211N *holo*-ACP retained its shifting activity.

Table 4-7. Observed *m/z* occurring through MS^2 and MS^3 fragmentation of the substrate loaded protein CorJ DH**holo*-ACP. Highlighted in blue: potential unspecific H/D exchange (check against **table 4-4** and **4-5**). Highlighted in green: ejection ions which were only observed due to a CorJ DH* dependent deuterium incorporation, except *m/z* 262.132. n.d. (not detected)

MS^2 *m/z*	MS^3 *m/z*			
402.169	261.127 and 142.050			
403.174	261.126 and 143.056	262.132 and 142.050		
404.181	261.126 and 144.062	262.132 and 143.056	n.d.	
405.187	261.126 and 145.069	262.132 and 144.062	n.d.	n.d.
406 n.d.				

4.7.2 Investigating CorJ DH* in an NMR based assay

The ppant ejection assay (4.7.1.3) gave evidence for the CorJ DH* mediated double-bond shift by mass spectroscopic observation of incorporation of deuterium atoms which was related to a double-bond isomerisation. Since non-enzymatic H/D exchange could not be excluded completely as reason of mass increase, it was envisaged to obtain a definitive proof of the double-bond migration mediated by CorJ DH*. Therefore, the reaction of CorJ DH* and its substrate **1** was monitored using NMR spectroscopy. For this purpose NMR spectra of the compounds **1** and **7** were used as reference spectra (see appendix **figure 8-1**, **8-4**, **8-5**) for evaluation of the outcome of the enzymatic reaction (**figure 4-23**). Compound **7** represented the aspired product with a double-bond localized in β,γ position, and **1** corresponded to the educt containing the double-bond in α,β position.

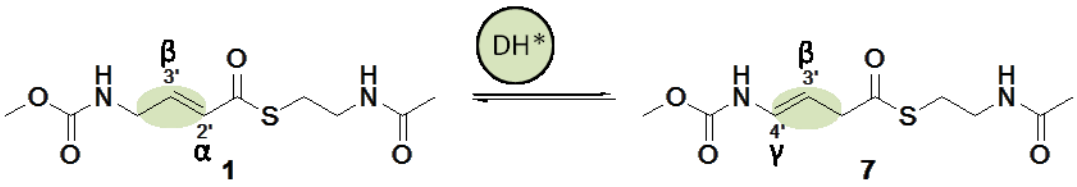

Figure 4-23. CorJ DH* mediated double-bond isomerisation in compound **1** yielded compound **7**.

General procedure. The approach required the shift domain CorJ DH*, which was heterologously expressed as the didomain CorJ DH*-ACP in its *apo* form (4.5). The absence of the phosphopantetheine residue of the *apo*-ACP moiety prevented the linkage of substrate **1** to the carrier protein and led to a freely dissolved substrate **1** in the assay buffer. The ability of CorJ DH* acting on a non-carrier bound substrate was assumed due to analogous experiments published by (Vergnolle et al., 2011). The freshly purified protein CorJ DH*-ACP was incubated with compound **1** under assay conditions as reported in 3.17.2, for 20 h at room temperature. The enzyme reaction was stopped by addition of methanol. Subsequently, the mixture was purified by HPLC and prepared for NMR experiments by dissolving it in deuterated methanol.

Evidence gained by NMR experiments for the double-bond isomerisation activity of CorJ DH*. The results of the ^{1}H NMR and the ^{1}H/^{1}H COSY 2D-NMR measurement of the reaction product (of CorJ DH* *apo*-ACP and substrate **1**) were compared with the corresponding spectra obtained for compound **1** (*i.e.* the educt) and **7** (*i.e.* the expected product). The ^{1}H NMR spectrum of the reaction product revealed a resonance signal at δ_H 6.62 corresponding to H-4´ of the β,γ shifted double-bond (as seen for compound **7**) and lacked resonance signals at δ_H 6.27 and 6.90 , corresponding to H-2´ and H-3´ of a α,β double-bond as seen for compound **1**. These results evidenced a shift of the α,β double-bond to the β,γ position due to the activity of the shift domain CorJ DH* (**figure 4-24**).

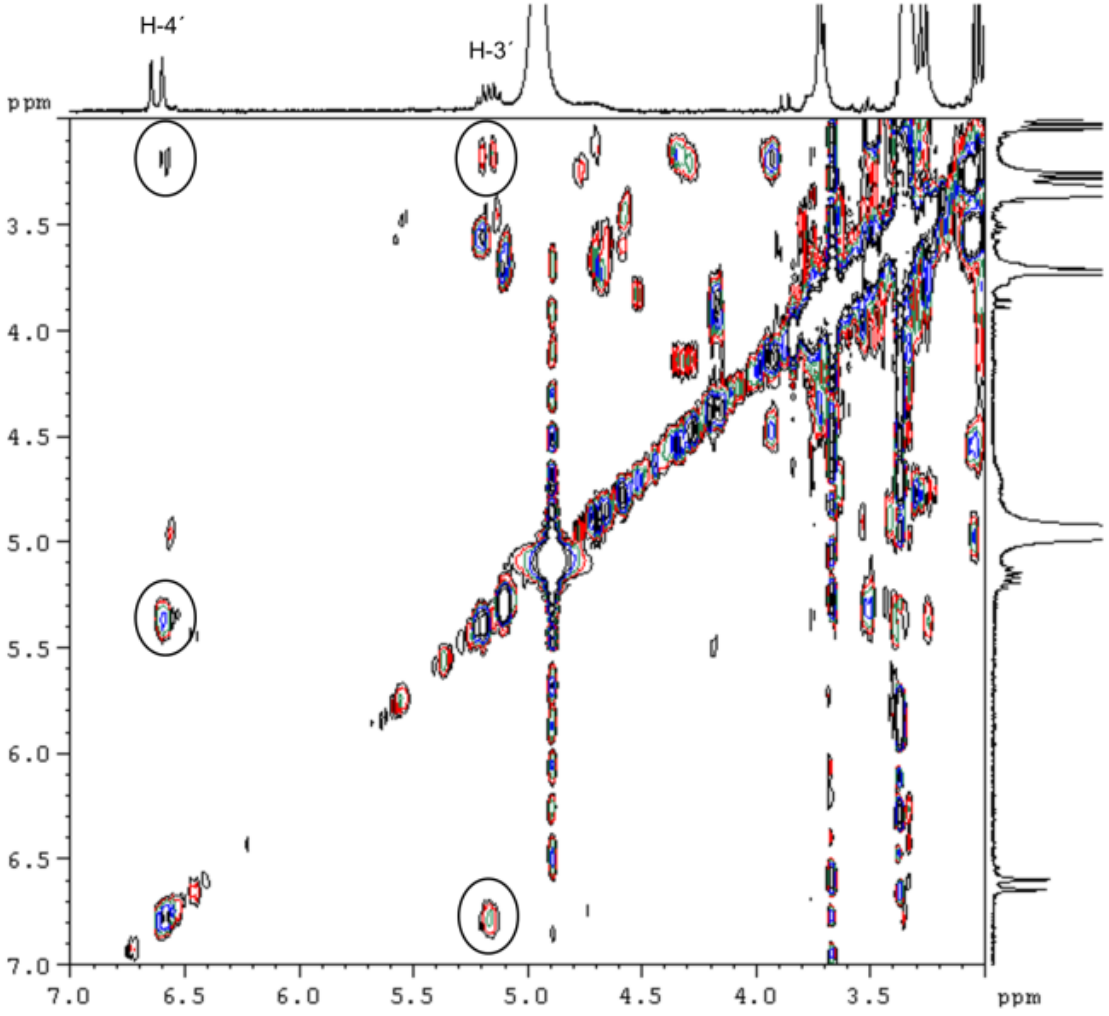

Figure 4-24. ^{1}H/^{1}H COSY 2D-NMR (600 MHz, [D_4]MeOH) spectrum of enzyme reaction product of CorJ DH* *apo*-ACP and substrate **1**. On the F1 and F2 axis, the ^{1}H NMR spectrum (300 MHz, [D_4]MeOH) of reference compound **7** is shown. Cross-peaks (highlighted in circles) prove the ^{1}H/^{1}H coupling between H-4´, H-3´ and H-2´ of the reaction product.

5 Conclusion

5.1 Drug discovery from natural products

Many of our most valuable drugs today derive from natural products, e.g. cyclosporine, lovastatine. Above all, antibiotic drug discovery is dependent on natural product research. This is even more true since the increasing emergence of bacteria resistant to antibiotics is a serious threat to modern medicine (Schäberle and Hack, 2014). Already in the 1990s it became obvious that resistances of bacteria towards established antibiotic therapies were developing much faster than new antibiotics could be discovered. Thus, pharmaceutical industry altered its discovery approaches and used "high-tech" methods like genomics, combinatorial chemistry and high throughput screening (HTS) to identify new antibacterial compounds and targets unfortunately with little success, yet (Lewis, 2013). By now 14 antibiotic classes are known (Lewis, 2013) but the number of new antibiotically active drugs introduced into therapy is dramatically dwindling (Schäberle et al., 2014b). In the light of urgently needed new antibacterial lead structures a revival of natural product drug discovery is currently taking place, and the whole cell (i.e. agar diffusion assay) screening approach introduced by S. Waksman in the 1940s does appear modern again (Lewis, 2013). There is, however, the need for innovative assays, e.g. using transgenic test organisms, and the discovery of novel natural product producer strains (Donadio et al., 2007).

Traditional antibiotic producer strains are often members of the actinobacteria or bacilli. In the last two decades δ-proteobacteria, especially myxobacteria got into the focus as alternative providers of antimicrobial natural products. Myxobacteria have been shown to produce a wide range of secondary metabolites with unique structural features and rare or novel modes of action, which make them attractive for pharmaceutical research (Weissman and Müller, 2009). A broad overview of antibacterially active myxobacterial compounds is given in a recent review (Schäberle et al., 2014c) (see also introduction of this thesis).

The observation of antimicrobially active compounds produced by myxobacteria started already in 1947 (Oxford, 1947). The compound, 1-hydroxy-6-methoxyphenazine-N5,N10-dioxide (myxin) was reported as one of the first

antibiotically active compounds from a *Sorangium* species (Peterson et al., 1966), but proved to be toxic (Chowdhury et al., 2012). In 1962 Norén and Raper published that several myxobacteria secreted natural products able to inhibit the growth of Gram-positive bacteria whereas none of the Gram-negative test organisms were found to be sensitive (Norén and Raper, 1962). This is still true today, even though very few myxobacterial metabolites being able to inhibit Gram-negatives were described.

Corallopyronin A, the focus of this study, is a myxobacterial secondary metabolite whose rare mode of action as RNA-polymerase inhibitor, good antibacterial activity towards, *e.g.* MSRA and *Wolbachia* and low toxicity, qualify it as a promising candidate for pre-clinical evaluation (Erol et al., 2010; Schäberle et al., 2014b).

5.2 Biosynthesis of myxobacterial natural products focussing on corallopyronin A

Understanding the biosynthetic process of bioactive natural products is of importance for their further development, e.g. sustaining their supply, bioengineering of derivatives. Myxobacterial secondary metabolites such as corallopyronin A are characterized by a high structural complexity including multiple chiral centres, ring formations and functional groups. The basic structure of most of these diverse compounds is synthesized by large multi enzymes, *i.e.* polyketide synthases (PKS), non-ribosomal peptide synthases (NRPS) and mixed-type PKS/NRPS systems (Wenzel and Müller, 2009). Post-NRPS or post-PKS enzymes like glycosyl transferases, methyltransferases, acylases, cyclases and oxidative enzymes further modify these basic structures (Staunton and Wilkinson, 1998).

Corallopyronin A is the product of a type 1 PKS/NRPS, which produces pre-corallopyronin A, while further enzymes perform post-PKS/NRPS reactions. The latter include, e.g. the isomerisation of the double-bond Δ^{26} to Δ^{25} putatively mediated by CorN and the incorporation of a hydroxyl moiety at C-25 probably catalyzed by the cytochrome P450 oxidase CorO (**figure 4-1**).

In modular PKS and linear NRPS systems such as the one responsible for corallopyronin A biosynthesis a one-to-one correspondence between the architecture of the PKS or NRPS assembly line and the backbone of the assembled intermediate exists. This correlation is named “co-linearity rule” and in the case of corallopyronin A it helped in the identification and characterization of the biosynthetic gene cluster.

Corallopyronin A biosynthesis, however, also shows some non-canonical features, (i) the core structure is formed by head to head connection of two separate chains derived from a PKS and a NRPS/PKS system, respectively, (ii) two of the methyl groups are incorporated by a β-branching cassette, (iii) the ER functionality is encoded in *trans*-position as a bifunctional enzyme together with the *trans*-AT. Additionally, the starter unit was surprisingly shown to be hydrogen carbonate. Therefore, not all processes of this biosynthesis are easily predictable since the classical co-linearity rule does not apply (Piel, 2010).

Such an exception to the co-linearity rule in corallopyronin A biosynthesis is the position of the C-11/C-12 carbon-carbon double-bond, representing a rare β,γ pattern (**figure 4-6**). The usual PKS-NRPS machinery places such double-bonds in α,β position by elimination of water from the respective β-hydroxy intermediate. Similar cases are exemplified in very few other polyketides, *e.g.* rhizoxin (Kusebauch et al., 2010), ansamitocin (Taft et al., 2009) and bacillaene (Moldenhauer et al., 2010). Concerning ansamitocin an unusual but functional DH domain was assumed to place the double-bond in β,γ position (Taft et al., 2009). A yet different mechanism was recently found to occur in the biosynthesis of bacillaene and rhizoxin. By the construction of thioesterase knockout mutants, late-pathway intermediates had been identified in which double-bonds were present in α,β and in the shifted β,γ position (Kusebauch et al., 2010; Moldenhauer et al., 2010). These experiments showed that isomerisation is taking place during polyketide assembly, and due to the structure of the intermediates the timing of the isomerisation reaction was assigned to specific modules of the assembly line. Thus, for rhizoxin it was shown that the double-bond Δ^8 was shifted to Δ^9 after elongation of the nascent polyketide chain by a downstream to the respective PKS module encoded “shift module (including DH*)” (Kusebauch et al., 2010). We proposed a similar process for corallopyronin A biosynthesis and provide here evidence that a distinct domain of the respective assembly line is responsible for the double-bond shift.

The current study describes two different *in vitro* assays to prove the functional role of the CorJ DH* domain within the respective shift module of the corallopyronin A biosynthesis cluster. For this purpose the respective protein domains (CorJ DH* and CorJ ACP, **figure 4-11**) involved in corallopyronin A biosynthesis were heterologously

expressed, and a suitable substrate **1** for the isomerization reaction was synthesized as an *N*-acetylcysteamine (SNAC) thioester derivative (**figure 4-14**).

For the initial detection of a double-bond migration within the substrate the phosphopantetheine (PPant) ejection assay was used, which enables the analysis of carrier protein bound intermediates (Dorrestein et al., 2006; Meluzzi et al., 2008) (**figure 4-18**). To allow a mass spectroscopic monitoring of the CorJ DH* mediated double-bond shift the enzyme assay was performed in deuterated buffer to allow an H/D exchange correlating with the double-bond migration (**figure 4-17**). The corresponding increase in mass was observed by applying high resolution tandem MS technique. As expected a mass increase up to three could be observed in the obtained ions of the ACP-bound substrate and indicated thereby the catalytic activity of CorJ DH* (**figure 4-21**). However, non-enzymatical H/D exchange surely also occurred (**scheme 4-6**). Even though MS^4 experiments clearly pointed out the enzymatic reaction, we sought additional evidence using NMR spectroscopy.

For the NMR experiment the enzyme, i.e. CorJ DH* was incubated with substrate **1**. 1D and 2D NMR spectra, recorded of the educt of the enzyme-substrate reaction and of the product, clearly revealed that the double-bond had shifted to the β,γ position (**figure 4-24**). This provided a second proof of the double-bond isomerisation activity of CorJ DH*.

In order to get insight into the mechanisms of this double-bond migration, the protein CorJ DH* was mutated. It was assumed that one of the active site residues of the enzyme is a histidine, which is highly conserved within DH and DH* domains (**figure 4-7**). Both domain variants, i.e. DH and DH* have the same basic structure and the conserved residues in the same positions as was indicated by aligning and threading the sequences to the solved crystal structure of the DEBS DH (Keatinge-Clay, 2008; Kusebauch et al., 2010). To prove the involvement of the conserved histidine (H) residue a mutational exchange to alanine (A) was performed in CorJ DH* to give CorJ DH*H47A. This enzyme was likewise expressed and assayed as CorJ DH* using the masspectrometric assay. Indeed, the only H/D exchange which could be observed was unspecific and not at the site of the carbon double-bond (**table 4-6**). These results provided evidence that the histidine residue at position 47 is of major importance for the enzymatic reaction and possibly acts as a proton donor and acceptor in the course

of the back and forward isomerisation reaction. A further amino acid within the enzyme should function as a proton acceptor, *i.e.* it should be accepting the proton from the γ-position. We expected the conserved aspartic acid D211 in CorJ DH* to represent this proton acceptor, but the mutated enzyme containing an asparagine (N) instead of aspartic acid (D) CorJ DH*D211N retained the shifting activity (**table 4-7**).

Our experiments clearly evidenced that under assay conditions the carbon-carbon double-bond migration is reversible and resembles the described mechanism for DH domains (Keatinge-Clay, 2008). In the case of the CorJ DH* domain H47 serves as proton donor and a still unknown residue as acceptor. This is in agreement with the mechanism postulated earlier by Hertweck and co-workers (Kusebauch et al., 2010).

It is assumed that in PKS-systems KSs act as gatekeepers preventing incorporation of erroneous building blocks (Taft et al., 2009). This arrangement assures that only the correct substrate, in this case the rearranged β,γ double-bond, can be passed on for further processing. In line with this all corallopyronin-type molecules known to date possess the β,γ pattern. Only under *in vitro* conditions the isomerase-like CorJ DH* domain acts reversibly, since the equilibrium is not affected by further processing of the intermediates.

5.3 Outlook

I*n vitro* analysis of the enzymatic activity of wild type and mutated variants of CorJ DH* encoded within the corallopyronin A cluster provides evidence that this domain is responsible for the unusual carbon-carbon double bond migration during the biosynthesis of this antibiotic. Our experiments thus clarified the genetic and biochemical basis underlying double-bond isomerisations in polyketide biosynthesis. This will allow a better prediction of polyketide structures from DNA sequence information, which is of major importance considering the increasing number of sequenced microbial genomes and biosynthetic gene clusters, and will enlarge the tool box for the rational design of metabolites in genetic engineering.

Future studies will focus on the crystallization of the respective proteins, which will aid to reveal the molecular basis for the double bond migration reaction, in particular the still unknown proton acceptor within the enzyme.

6 Summary

Corallopyronin A is a myxobacterial compound, which was isolated in our lab from the strain *Corallococcus coralloides* B035. It is a potent *in vivo* active antibiotic, which is currently undergoing preclinical studies. Regarding its biosynthesis, corallopyronin A was found to originate from two chains, one being solely PKS- and the other NRPS/PKS dervived.

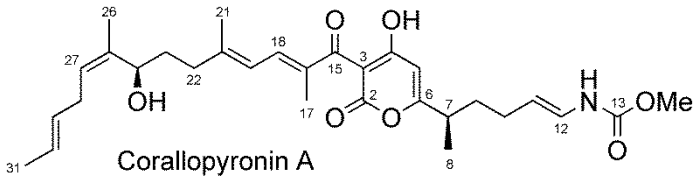

Corallopyronin A

Scheme 6-1. Corallopyronin A

In polyketide biosynthesis the reduction of β-carbonyl groups to an alkene moiety usually results in a α,β positioned double-bond. However, in a few polyketides the rare case of such a carbon-carbon double-bond in β,γ position is depicted, *e.g.* in the biosynthesis of ansamitocin (Taft et al., 2009), bacillaene (Moldenhauer et al., 2010) and rhizoxin (Kusebauch et al., 2010). For rhizoxin it was shown that the respective double-bond (Δ^8) was shifted to the β,γ position after elongation of the nascent polyketide chain by a distinct "shift module" including an unusual dehydratase-like domain (DH*) downstream in the PKS assembly line (Kusebauch et al., 2010). We proposed a similar process for the antibiotic corallopyronin A and provided here evidence that a distinct domain (CorJ DH*) catalyses the carbon-carbon double-bond shift from α,β to β,γ position during corallopyronin A biosynthesis.

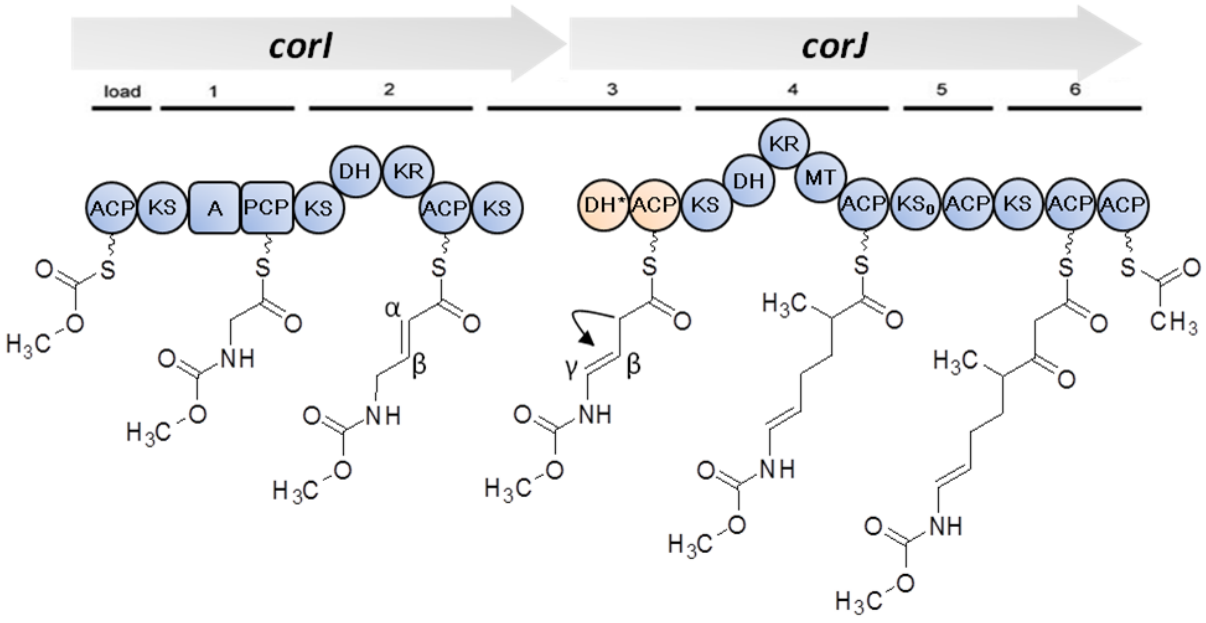

Figure 6-1. Section of the corallopyronin A biosynthetic assembly line focussing on the "shift module" marked in orange. The shift domain CorJ DH* catalyses the double-bond migration from α,β → to β,γ position within the nascent polyketide backbone of corallopyronin A.

In this study the *in vitro* analysis of the enzyme domain (CorJ DH*) responsible for this double-bond isomerisation was analysed. This "shift domain" was heterologously expressed and assayed with its acyl carrier protein bound substrate **2**. To facilitate this analysis the biosynthetic corallopyronin A intermediate was chemically synthesized as a *N*-acetylcysteamine-thioester **1**.

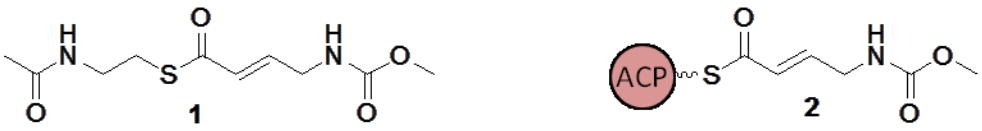

Figure 6-2. *N*-acetylcysteamine activated substrate 1 for the shift domain (CorJ DH*) and ACP-bound intermediate 2 of the corallopyronin A biosynthetic pathway.

Enzyme activity was analyzed by NMR and high-resolution MS measurements, the latter were possible by performing the assay in deuterated buffer, thereby observing a proton/deuterium exchange reaction. The here reported *in vitro* experiments clearly demonstrated that CorJ DH* acts as double-bond migrating enzyme in corallopyronin

A biosynthesis. Mutated enzyme variants (CorJ DH*H47A and CorJ DH*D211N) gave first experimental evidence for the essential amino acids involved in double-bond migration. It could be shown that the amino acid histidine in position 47 (H47) plays a major role in the double-bond isomerisation in that it serves as proton donor. A still unknown residue must function as acceptor, which is in agreement with the mechanism postulated earlier by Hertweck and co-workers (Kusebauch et al., 2010).

These results provide evidence for the genetic and enzymatic basis of carbon-carbon double-bond migrations in polyketides. Furthermore, they support the partly still hypothetical corallopyronin A biosynthetic process, and widen the understanding of PKS systems in general as the tool box for the rational design of metabolites in genetic engineering (Lohr et al., 2013).

7 References

Ahn, J.-W., Jang, K.H., Chung, S.-C., Oh, K.-B., and Shin, J. (2008). Sorangiadenosine, a new sesquiterpene adenoside from the myxobacterium *Sorangium cellulosum*. Org. Lett. *10*, 1167–1169.

Akey, D.L., Razelun, J.R., Tehranisa, J., Sherman, D.H., Gerwick, W.H., and Smith, J.L. (2010). Crystal structures of dehydratase domains from the curacin polyketide biosynthetic pathway. Structure *18*, 94–105.

Alhamadsheh, M.M., Palaniappan, N., DasChouduri, S., and Reynolds, K.A. (2007). Modular polyketide synthases and cis double-bond formation: establishment of activated cis -3-cyclohexylpropenoic acid as the diketide intermediate in phoslactomycin biosynthesis. J. Am. Chem. Soc. *129*, 1910–1911.

Altendorfer, M., Irschik, H., and Menche, D. (2012). Design, synthesis and biological evaluation of simplified side chains of the macrolide antibiotic etnangien. Bioorg. Med. Chem. Lett. *22*, 5731–5734.

Altendorfer, M., Raja, A., Sasse, F., Irschik, H., and Menche, D. (2013). Modular synthesis of polyene side chain analogues of the potent macrolide antibiotic etnangien by a flexible coupling strategy based on hetero-bis-metallated alkenes. Org. Biomol. Chem. *11*, 2116–2139.

Apel, C., Barg, A., Rheinberg, A., Conrads, G., and Wagner-Döbler, I. (2013). Dental composite materials containing carolacton inhibit biofilm growth of Streptococcus mutans. Dent. Mater. *29*, 1188–1199.

Arora, P., Vats, A., Saxena, P., Mohanty, D., and Gokhale, R.S. (2005). Promiscuous fatty acyl CoA ligases produce acyl-CoA and acyl-SNAC precursors for polyketide biosynthesis. J. Am. Chem. Soc. *127*, 9388–9389.

Artsimovitch, I., Seddon, J., and Sears, P. (2012). Fidaxomicin Is an Inhibitor of the initiation of bacterial RNA synthesis. Clin. Infect. Dis. *55*, S127–S131.

Augustiniak, H., Höfle, G., Irschik, H., and Reichenbach, H. (1996). Antibiotics from gliding bacteria, LXXVIII. Ripostatin A, B, and C: isolation and structure and structure elucidation of novel metabolites from Sorangium cellulosum. Liebigs Ann. *1996*, 1657–1663.

Ayele, W.Y., Neill, S.D., Zinsstag, J., Weiss, M.G., and Pavlik, I. (2004). Bovine tuberculosis: an old disease but a new threat to Africa. Int. J. Tuberc. Lung Dis. *8*, 924–937.

Banu, L.D., Conrads, G., Rehrauer, H., Hussain, H., Allan, E., and van der Ploeg, J.R. (2010). The Streptococcus mutans serine/threonine kinase, PknB, regulates competence development, bacteriocin production, and cell wall metabolism. Infect. Immun. *78*, 2209–2220.

References

Belogurov, G.A., Vassylyeva, M.N., Sevostyanova, A., Appleman, J.R., Xiang, A.X., Lira, R., Webber, S.E., Klyuyev, S., Nudler, E., Artsimovitch, I., et al. (2008). Transcription inactivation through local refolding of the RNA polymerase structure. Nature *457*, 332–335.

Bergeron, R.J., and Phanstiel, O. (1992). The total synthesis of nannochelin: a novel cinnamoyl hydroxamate-containing siderophore. J. Org. Chem. *57*, 7140–7143.

Bock, M., Buntin, K., Müller, R., and Kirschning, A. (2008). Stereochemical determination of thuggacins A–C, highly active antibiotics from the myxobacterium Sorangium cellulosum. Angew. Chem. Int. Ed. *47*, 2308–2311.

Buedenbender, S., Rachid, S., Müller, R., and Schulz, G.E. (2009). Structure and action of the myxobacterial chondrochloren halogenase CndH: a new variant of FAD-dependent halogenases. J. Mol. Biol. *385*, 520–530.

Buntin, K., Irschik, H., Weissman, K.J., Luxenburger, E., Blöcker, H., and Müller, R. (2010). Biosynthesis of thuggacins in myxobacteria: comparative cluster analysis reveals basis for natural product structural diversity. Chem. Biol. *17*, 342–356.

Buurman, E.T., Foulk, M.A., Gao, N., Laganas, V.A., McKinney, D.C., Moustakas, D.T., Rose, J.A., Shapiro, A.B., and Fleming, P.R. (2012). Novel rapidly diversifiable antimicrobial RNA polymerase switch region inhibitors withconfirmed mode of action in Haemophilus influenzae. J. Bacteriol. *194*, 5504–5512.

Campbell, E.A., Pavlova, O., Zenkin, N., Leon, F., Irschik, H., Jansen, R., Severinov, K., and Darst, S.A. (2005). Structural, functional, and genetic analysis of sorangicin inhibition of bacterial RNA polymerase. EMBO J. *24*, 674–682.

Chen, X.-H., Vater, J., Piel, J., Franke, P., Scholz, R., Schneider, K., Koumoutsi, A., Hitzeroth, G., Grammel, N., Strittmatter, A.W., et al. (2006). Structural and functional characterization of three polyketide synthase geneclusters in Bacillus amyloliquefaciens FZB 42. J. Bacteriol. *188*, 4024–4036.

Chopra, I. (2007). Bacterial RNA polymerase: A promising target for the discovery of new antimicrobial agents. Curr. Opin. Investig. Drugs 600–607.

Chowdhury, G., Sarkar, U., Pullen, S., Wilson, W.R., Rajapakse, A., Fuchs-Knotts, T., and Gates, K.S. (2012). DNA strand cleavage by the phenazine di- *N* -oxide natural product myxin under both aerobic and anaerobic conditions. Chem. Res. Toxicol. *25*, 197–206.

Content, S., Dutton, C.J., and Roberts, L. (2003). Myxovirescin analogues via macrocyclic ring-closing metathesis. Bioorg. Med. Chem. Lett. *13*, 321–325.

Cortina, N.S., Revermann, O., Krug, D., and Müller, R. (2011). Identification and characterization of the althiomycin biosynthetic gene cluster in Myxococcus xanthus DK897. ChemBioChem *12*, 1411–1416.

Crimmins, M.T., Haley, M.W., and O'Bryan, E.A. (2011). Formal synthesis of (+)-sorangicin A. Org. Lett. *13*, 4712–4715.

Datsenko, K.A., and Wanner, B.L. (2000). One-step inactivation of chromosomal genes in Escherichia coli K-12 using PCR products. Proc. Natl. Acad. Sci. *97*, 6640–6645.

Donadio, S., Brandi, L., Monciardini, P., Sosio, M., and Gualerzi, C.O. (2007). Novel assays and novel strains ? Promising routes to new antibiotics? Expert Opin. Drug Discov. *2*, 789–798.

Dorrestein, P.C., Bumpus, S.B., Calderone, C.T., Garneau-Tsodikova, S., Aron, Z.D., Straight, P.D., Kolter, R., Walsh, C.T., and Kelleher, N.L. (2006). Facile detection of acyl and peptidyl intermediates on thiotemplate carrier domains via phosphopantetheinyl elimination reactions during tandem mass spectrometry. Biochemistry (Mosc.) *45*, 12756–12766.

Doundoulakis, T., Xiang, A.X., Lira, R., Agrios, K.A., Webber, S.E., Sisson, W., Aust, R.M., Shah, A.M., Showalter, R.E., Appleman, J.R., et al. (2004). Myxopyronin B analogs as inhibitors of RNA polymerase, synthesis and biological evaluation. Bioorg. Med. Chem. Lett. *14*, 5667–5672.

Erol, Ö., Schäberle, T.F., Schmitz, A., Rachid, S., Gurgui, C., El Omari, M., Lohr, F., Kehraus, S., Piel, J., Müller, R., et al. (2010). Biosynthesis of the myxobacterial antibiotic corallopyronin A. ChemBioChem *11*, 1253–1265.

Felder, S., Kehraus, S., Neu, E., Bierbaum, G., Schäberle, T.F., and König, G.M. (2013a). Salimyxins and enhygrolides: antibiotic, sponge-related metabolites from the obligate marine myxobacterium Enhygromyxa salina. ChemBioChem *14*, 1363–1371.

Felder, S., Dreisigacker, S., Kehraus, S., Neu, E., Bierbaum, G., Wright, P.R., Menche, D., Schäberle, T.F., and König, G.M. (2013b). Salimabromide: unexpected chemistry from the obligate marine myxobacterium Enhygromxya salina. Chem. - Eur. J. *19*, 9319–9324.

Fujimoto, H., Kinoshita, T., Suzuki, H., and Umezawa, H. (1970). Studiess in the mode of action of althiomycin. J. Antibiot. (Tokyo) *23*, 271–275.

Fürstner, A., Bonnekessel, M., Blank, J.T., Radkowski, K., Seidel, G., Lacombe, F., Gabor, B., and Mynott, R. (2007). Total Ssynthesis of myxovirescin A1. Chem. - Eur. J. *13*, 8762–8783.

Gerc, A.J., Song, L., Challis, G.L., Stanley-Wall, N.R., and Coulthurst, S.J. (2012). The insect pathogen Serratia marcescens Db10 uses a hybrid Non-Ribosomal Peptide Synthetase-Polyketide Synthase to produce the antibiotic althiomycin. PLoS ONE *7*, e44673.

Gerth, K., Irschik, H., Reichenbach, H., and Trowitzsch, W. (1982). The myxovirescins, a family of antibiotics from Myxococcus virescens (Myxobacterales). J. Antibiot. (Tokyo) *35*, 1454–1459.

Giddens, A.C., Nielsen, L., Boshoff, H.I., Tasdemir, D., Perozzo, R., Kaiser, M., Wang, F., Sacchettini, J.C., and Copp, B.R. (2008). Natural product inhibitors of fatty acid biosynthesis: synthesis of the marine microbial metabolites pseudopyronines A and B and evaluation of their anti-infective activities. Tetrahedron *64*, 1242–1249.

Gieseler, M.T., and Kalesse, M. (2013). Synthesis of angiolam A. Org. Lett. *16*, 548–551.

Glaus, F., and Altmann, K.-H. (2012). Total synthesis of the bacterial RNA polymerase inhibitor ripostatin B. Angew. Chem. Int. Ed. *51*, 3405–3409.

Guo, H., Naser, S.A., Ghobrial, G., and Phanstiel (2002). Synthesis and biological evaluation of new citrate-based siderophores as potential probes for the mechanism of Iron uptake in mycobacteria. J. Med. Chem. *45*, 2056–2063.

Guo, X., Liu, T., Valenzano, C.R., Deng, Z., and Cane, D.E. (2010). Mechanism and stereospecificity of a fully saturating polyketide synthase module: nanchangmycin synthase module 2 and its dehydratase domain. J. Am. Chem. Soc. *132*, 14694–14696.

Gust, B., Challis, G.L., Fowler, K., Kieser, T., and Chater, K.F. (2003). PCR-targeted streptomyces gene replacement identifies a protein domain needed for biosynthesis of the sesquiterpene soil odor geosmin. Proc. Natl. Acad. Sci. *100*, 1541–1546.

Haebich, D., and von Nussbaum, F. (2009). Lost in transcription-inhibition of RNA polymerase. Angew. Chem. Int. Ed. *48*, 3397–3400.

Herrmann, M., Böhlendorf, B., Irschik, H., Reichenbach, H., and Höfle, G. (1998). Maracin and maracen: new types of ethynyl vinyl ether andα-chloro divinyl ether antibiotics from Sorangium cellulosum with specific activity against mycobacteria. Angew. Chem. Int. Ed. *37*, 1253–1255.

Hertweck, C. (2009). The biosynthetic logic of polyketide diversity. Angew. Chem. Int. Ed. *48*, 4688–4716.

Ho, M.X., Hudson, B.P., Das, K., Arnold, E., and Ebright, R.H. (2009). Structures of RNA polymerase–antibiotic complexes. Curr. Opin. Struct. Biol. *19*, 715–723.

Höfle, G. (1998). Sci. Annu. Rep. of the GBF.

Höfle, G., and Kunze, B. (2008). Biosynthesis of aurachins A−L in *Stigmatella aurantiaca* : a feeding study. J. Nat. Prod. *71*, 1843–1849.

Höfle, G., Böhlendorf, B., Fecker, T., Sasse, F., and Kunze, B. (2008). Semisynthesis and antiplasmodial activity of the quinoline alkaloid aurachin E. J. Nat. Prod. *71*, 1967–1969.

Höfling, S.B., Hultsch, C., Wester, H.-J., and Heinrich, M.R. (2008). Radiochemical ^{18}F-fluoroarylation of unsaturated α-, β- and γ-amino acids, application to a radiolabelled analogue of baclofen. Tetrahedron *64*, 11846–11851.

Hu, T., Schaus, J.V., Lam, K., Palfreyman, M.G., Wuonola, M., Gustafson, G., and Panek, J.S. (1998). Total Synthesis and Preliminary Antibacterial Evaluation of the RNA Polymerase Inhibitors (±)-Myxopyronin A and B. J. Org. Chem. *63*, 2401–2406.

Hutchings, M.I., Palmer, T., Harrington, D.J., and Sutcliffe, I.C. (2009). Lipoprotein biogenesis in Gram-positive bacteria: knowing when to hold ‘em, knowing when to fold ‘em. Trends Microbiol. *17*, 13–21.

Inami, K., and Shiba, T. (1986). Syntheses of althiomycin analogs in relation to antibacterial activities. Bull. Chem. Soc. Jpn. *59*, 2185–2189.

Irschik, H., and Reichenbach, H. (1985). The mechanism of action of myxovalargin A, a peptide antibiotic from Myxococcus fulvus. J. Antibiot. (Tokyo) *38*, 1237–1245.

Irschik, H., Gerth, K., Höfle, G., Kohl, W., and Reichenbach, H. (1983a). The myxopyronins, new inhibitors of bacterial RNA synthesis from Myxococcus fulvus (Myxobacterales). J. Antibiot. (Tokyo) *36*, 1651–1658.

Irschik, H., Gerth, K., Kemmer, T., Steinmetz, H., and Reichenbach, H. (1983b). The myxovalargins, new peptide antibiotics from Myxococcus fulvus (myxobacterales). I. cultivation, isolation, and some chemical and biological properties. J. Antibiot. (Tokyo) *36*, 6–12.

Irschik, H., Jansen, R., Höfle, G., Gerth, K., and Reichenbach, H. (1985). The corallopyronins, new inhibitors of bacterial RNA synthesis from Myxobacteria. J. Antibiot. (Tokyo) *38*, 145–152.

Irschik, H., Jansen, R., Gerth, K., Höfle, G., and Reichenbach, H. (1987). The sorangicins, novel and powerful inhibitors of eubacterial RNA polymerase isolated from myxobacteria. J. Antibiot. (Tokyo) *40*, 7–13.

Irschik, H., Augustiniak, H., Gerth, K., HöFle, G., and Reichenbach, H. (1995). Antibiotics from gliding bacteria. No. 68. The Ripostatins, Novel Inhibitors of Eubacterial RNA Polymerase Isolated from myxobacteria. J. Antibiot. (Tokyo) *48*, 787–792.

Irschik, H., Schummer, D., Höfle, G., Reichenbach, H., Steinmetz, H., and Jansen, R. (2007a). Etnangien, a macrolide-polyene antibiotic from *Sorangium cellulosum* that inhibits nucleic acid polymerases. J. Nat. Prod. *70*, 1060–1063.

Irschik, H., Reichenbach, H., Höfle, G., and Jansen, R. (2007b). The thuggacins, novel antibacterial macrolides from Sorangium cellulosum acting against selected Gram-positive bacteria. J. Antibiot. (Tokyo) *60*, 733–738.

Irschik, H., Kopp, M., Weissman, K.J., Buntin, K., Piel, J., and Müller, R. (2010). Analysis of the sorangicin gene cluster reinforces the utility of a combined phylogenetic/retrobiosynthetic analysis for deciphering natural product assembly by trans-AT PKS. ChemBioChem *11*, 1840–1849.

Ishihara, M., Iizuka, T., Fudou, R., Yamanaka, S., Ojika, M., Suzuki, Y., and Sakagami, Y. (2002). Macrolide fungicides manufacture with Sorangium. Patent WO 2002099113 A1.

Jansen, R., Höfle, G., Irschik, H., and Reichenbach, H. (1985). Antibiotika aus gleitenden Bakterien, XXIV. Corallopyronin A, B und C – drei neue Antibiotika ausCorallococcus coralloides Cc c127 (Myxobacterales). Liebigs Ann. Chem. *1985*, 822–836.

Jansen, R., Höfle, G., Irschik, H., Reichenbach, H., and Wray, V. (1989a). Antibiotika aus gleitenden Bakterien, XXXVIII. Natürliche Strukturvarianten von sorangicin A aus Sorangium cellulosum, So ce12. Liebigs Ann. Chem. *1989*, 213–222.

Jansen, R., Höfle, G., Irschik, H., Reichenbach, H., and Wray, V. (1989b). Antibiotika aus gleitenden Bakterien, XXXIX. Biosynthese von Sorangicin A insorangium cellulosum, So ce12. Liebigs Ann. Chem. *1989*, 309–313.

Jansen, R., Kunze, B., Reichenbach, H., and Höfle, G. (2003). Chondrochloren A and B, new β-amino styrenes from chondromyces crocatus (Myxobacteria). Eur. J. Org. Chem. *2003*, 2684–2689.

Jansen, R., Irschik, H., Huch, V., Schummer, D., Steinmetz, H., Bock, M., Schmidt, T., Kirschning, A., and Müller, R. (2010). Carolacton - a macrolide ketocarbonic acid that reduces biofilm formation by the caries- and endocarditis-associated bacterium Streptococcus mutans. Eur. J. Org. Chem. *2010*, 1284–1289.

Jansen, R., Kunze, B., and Irschik, H. (2012). Thuggacin-type macrolide antibiotics and their use as antimycobacterial agents. Patent EP2089025 B1.

Jiang, Z.-D., and Gerwick, W.H. (1997). Novel oxylipins from the temperate red alga Polyneura latissima: Evidence for an arachidonate 9(S)-lipoxygenase. Lipids *32*, 231–235.

Jünemann, S., Wrigglesworth, J.M., and Rich, P.R. (1997). Effects of decyl-aurachin d and reversed electron transfer in cytochrome bd. Biochemistry (Mosc.) *36*, 9323–9331.

Katsuyama, Y., Harmrolfs, K., Pistorius, D., Li, Y., and Müller, R. (2012). A semipinacol rearrangement directed by an enzymatic system featuring dual-function fad-dependent monooxygenase. Angew. Chem. Int. Ed. *51*, 9437–9440.

Keatinge-Clay, A. (2008). Crystal structure of the erythromycin polyketide synthase dehydratase. J. Mol. Biol. *384*, 941–953.

Kelleher, N.L., Lin, H.Y., Valaskovic, G.A., Aaserud, D.J., Fridriksson, E.K., and McLafferty, F.W. (1999). Top down versus bottom up protein characterization by tandem high-resolution mass spectrometry. J. Am. Chem. Soc. *121*, 806–812.

Kirst, H.A., Szymanski, E.F., Dorman, D.E., Occolowitz, J.L., Jones, N.D., Chaney, M.O., Hamill, R.L., and Hoehn, M.M. (1975). Structure of althiomycin. J. Antibiot. (Tokyo) *28*, 286–291.

Kitagawa, W., Ozaki, T., Nishioka, T., Yasutake, Y., Hata, M., Nishiyama, M., Kuzuyama, T., and Tamura, T. (2013). Cloning and heterologous expression of the aurachin RE biosynthesis gene cluster afford a new cytochrome p450 for quinoline N-hydroxylation. ChemBioChem *14*, 1085–1093.

Kitsche, A., and Kalesse, M. (2013). Configurational assignment of secondary hydroxyl groups and methyl branches in polyketide natural products through bioinformatic analysis of the ketoreductase domain. ChemBioChem *14*, 851–861.

Kohl, W., Irschik, H., Reichenbach, H., and Höfle, G. (1983). Antibiotika aus gleitenden Bakterien, XVII. Myxopyronin A und B – zwei neue Antibiotika ausMyxococcus fulvus Stamm Mx f50. Liebigs Ann. Chem. *1983*, 1656–1667.

Kohl, W., Irschik, H., Reichenbach, H., and Höfle, G. (1984). Antibiotika aus gleitenden Bakterien, XXII. Die Biosynthese des Antibiotikums Myxopyronin A ausMyxococcus fulvus Stamm Mx f50. Liebigs Ann. Chem. *1984*, 1088–1093.

Kohl, W., Witte, B., Höfle, G., Kunze, B., Reichenbach, H., Wray, V., and Schomburg, D. (1985). Antibiotika aus gleitenden Bakterien, XXVII. Angiolam A – ein neues Antibiotikum aus Angiococcus disciformis (Myxobacterales). Liebigs Ann. Chem. *1985*, 2088–2097.

Kopp, M., Rupprath, C., Irschik, H., Bechthold, A., Elling, L., and Müller, R. (2007). SorF: a glycosyltransferase with promiscuous donor substrate specificity in vitro. ChemBioChem *8*, 813–819.

Kovacs-Simon, A., Titball, R.W., and Michell, S.L. (2011). Lipoproteins of bacterial pathogens. Infect. Immun. *79*, 548–561.

Krug, D., and Müller, R. (2009). Discovery of additional members of the tyrosine aminomutase enzyme family and the mutational analysis of CmdF. ChemBioChem *10*, 741–750.

Kubota, T., Brünjes, M., Frenzel, T., Xu, J., Kirschning, A., and Floss, H.G. (2006). Determination of the cryptic stereochemistry of the first PKS chain-extension step in ansamitocin biosynthesis by Actinosynnema pretiosum. ChemBioChem *7*, 1221–1225.

Kunze, B., Reichenbach, H., Augustiniak, H., and HöFle, G. (1982). Isolation and identification of althiomycin from Cystobacter fuscus (Myxobacterales). J. Antibiot. (Tokyo) *35*, 635–636.

Kunze, B., Kohl, W., HOFLE, G., and REICHENBACH, H. (1985). Antibiotics from gliding bacteria - production, isolation, physicochemical and biological properties of angiolam-a, a new antibiotic from Angiococcus-disciformis (myxobacterales). J. Antibiot. (Tokyo) *38*, 1649–1654.

Kunze, B., HöFle, G., and Reichenbach, H. (1987). The aurachins, new quinoline antibiotics from myxobacteria : production, physico-chemical and biological properties. J. Antibiot. (Tokyo) *40*, 258–265.

Kunze, B., Trowitzsch-Kienast, W., HöFle, G., and Reichenbach, H. (1992). Nannochelins A, B and C, new iron-chelating compounds from Nannocystis exedens (myxobacteria). production, isolation,physico-chemical and biological properties. J. Antibiot. (Tokyo) *45*, 147–150.

Kunze, B., Reck, M., Dötsch, A., Lemme, A., Schummer, D., Irschik, H., Steinmetz, H., and Wagner-Döbler, I. (2010). Damage of Streptococcus mutans biofilms by carolacton, a secondary metabolite from the myxobacterium Sorangium cellulosum. BMC Microbiol. *10*, 199.

Kusebauch, B., Busch, B., Scherlach, K., Roth, M., and Hertweck, C. (2010). Functionally distinct modules operate two consecutive α,β→β,γ double-bond shifts in the rhizoxin polyketide assembly line. Angew. Chem. Int. Ed. *49*, 1460–1464.

Lee, K., Kim, H., and Hong, J. (2012). Stereoselective synthesis of tetrahydropyrans through tandem and organocatalytic oxa-michael reactions: synthesis of the tetrahydropyran cores of ent-(+)-sorangicin A. Eur. J. Org. Chem. *2012*, 1025–1032.

Lewis, K. (2013). Platforms for antibiotic discovery. Nat. Rev. Drug Discov. *12*, 371–387.

Li, X.-W., Herrmann, J., Zang, Y., Grellier, P., Prado, S., Müller, R., and Nay, B. (2013). Synthesis and biological activities of the respiratory chain inhibitor aurachin D and new ring versus chain analogues. Beilstein J. Org. Chem. *9*, 1551–1558.

Lira, R., Xiang, A.X., Doundoulakis, T., Biller, W.T., Agrios, K.A., Simonsen, K.B., Webber, S.E., Sisson, W., Aust, R.M., Shah, A.M., et al. (2007). Syntheses of novel myxopyronin B analogs as potential inhibitors of bacterial RNA polymerase. Bioorg. Med. Chem. Lett. *17*, 6797–6800.

Lohr, F., Jenniches, I., Frizler, M., Meehan, M.J., Sylvester, M., Schmitz, A., Gütschow, M., Dorrestein, P.C., König, G.M., and Schäberle, T.F. (2013). α,β → β,γ double bond migration in corallopyronin A biosynthesis. Chem. Sci. *4*, 4175.

Magrini, V., Creighton, C., White, D., Hartzell, P.L., and Youderian, P. (1998). The aadA gene of plasmid R100 confers resistance to spectinomycin and streptomycin in Myxococcus xanthus. J. Bacteriol. *180*, 6757–6760.

Manor, A., Eli, I., Varon, M., Judes, H., and Rosenberg, E. (1989). Effect of adhesive antibiotic TA on plaque and gingivitis in man. J. Clin. Periodontol. *16*, 621–624.

Mariani, R., and Maffioli, S.I. (2009). Bacterial RNA polymerase inhibitors: an organized overview of their structure, derivatives, biological activity and current development status. Curr. Med. Chem. 430–454.

Mariner, K., McPhillie, M., Trowbridge, R., Smith, C., O'Neill, A.J., Fishwick, C.W.G., and Chopra, I. (2011). Activity of and development of resistance to corallopyronin a, an inhibitor of RNA polymerase. Antimicrob. Agents Chemother. *55*, 2413–2416.

Marsh, E.N.G., Patwardhan, A., and Huhta, M.S. (2004). S-Adenosylmethionine radical enzymes. Bioorganic Chem. *32*, 326–340.

Martinez, J.P., Hinkelmann, B., Fleta-Soriano, E., Steinmetz, H., Jansen, R., Diez, J., Frank, R., Sasse, F., and Meyerhans, A. (2013). Identification of myxobacteria-derived HIV inhibitors by a high-throughput two-step infectivity assay. Microb. Cell Factories *12*, 85.

McPhillie, M.J., Trowbridge, R., Mariner, K.R., O'Neill, A.J., Johnson, A.P., Chopra, I., and Fishwick, C.W.G. (2011). Structure-based ligand design of novel bacterial RNA polymerase inhibitors. ACS Med. Chem. Lett. *2*, 729–734.

Meluzzi, D., Zheng, W.H., Hensler, M., Nizet, V., and Dorrestein, P.C. (2008). Top-down mass spectrometry on low-resolution instruments: Characterization of phosphopantetheinylated carrier domains in polyketide and non-ribosomal biosynthetic pathways. Bioorg. Med. Chem. Lett. *18*, 3107–3111.

Menche, D., Arikan, F., Perlova, O., Horstmann, N., Ahlbrecht, W., Wenzel, S.C., Jansen, R., Irschik, H., and Müller, R. (2008). Stereochemical determination and complex biosynthetic assembly of etnangien, a highly potent RNA polymerase inhibitor from the myxobacterium Sorangium cellulosum. J. Am. Chem. Soc. *130*, 14234–14243.

Menche, D., Li, P., and Irschik, H. (2010). Design, synthesis and biological evaluation of simplified analogues of the RNA polymerase inhibitor etnangien. Bioorg. Med. Chem. Lett. *20*, 939–941.

Meunier, B., Madgwick, S.A., Reil, E., Oettmeier, W., and Rich, P.R. (1995). New inhibitors of the quinol oxidation sites of bacterial cytochromes bo and bd. Biochemistry (Mosc.) *34*, 1076–1083.

Milhous, W.K., Weatherly, N.F., Bowdre, J.H., and Desjardins, R.E. (1985). In vitro activities of and mechanisms of resistance to antifol antimalarial drugs. Antimicrob. Agents Chemother. *27*, 525–530.

Mogi, T., Akimoto, S., Endou, S., Watanabe-Nakayama, T., Mizuochi-Asai, E., and Miyoshi, H. (2006). Probing the ubiquinol-binding site in cytochrome bd by site-directed mutagenesis. Biochemistry (Mosc.) *45*, 7924–7930.

Mohapatra, D.K., Das, P.P., Pattanayak, M.R., and Yadav, J.S. (2010). Iodine-catalyzed highly diastereoselective synthesis of trans-2,6-disubstituted-3,4-dihydropyrans: application to concise construction of c28-c37 bicyclic core of (+)-sorangicin A. Chem. - Eur. J. *16*, 2072–2078.

Moldenhauer, J., Chen, X.-H., Borriss, R., and Piel, J. (2007). Biosynthesis of the antibiotic bacillaene, the product of a giant polyketide synthase complex of the trans-AT family. Angew. Chem. Int. Ed. *46*, 8195–8197.

Moldenhauer, J., Götz, D.C.G., Albert, C.R., Bischof, S.K., Schneider, K., Süssmuth, R.D., Engeser, M., Gross, H., Bringmann, G., and Piel, J. (2010). The final steps of bacillaene biosynthesis in Bacillus amyloliquefaciens FZB42: direct evidence for β,γ dehydration by a trans-acyltransferase polyketide synthase. Angew. Chem. *122*, 1507–1509.

Moy, T.I., Daniel, A., Hardy, C., Jackson, A., Rehrauer, O., Hwang, Y.S., Zou, D., Nguyen, K., Silverman, J.A., Li, Q., et al. (2011). Evaluating the activity of the RNA polymerase inhibitor myxopyronin B against Staphylococcus aureus: characterization of myxopyronin B in Staphylococcus aureus. FEMS Microbiol. Lett. *319*, 176–179.

Mukhopadhyay, J., Das, K., Ismail, S., Koppstein, D., Jang, M., Hudson, B., Sarafianos, S., Tuske, S., Patel, J., Jansen, R., et al. (2008). The RNA polymerase “switch region” is a target for inhibitors. Cell *135*, 295–307.

Nachtigall, J., Schneider, K., Nicholson, G., Goodfellow, M., Zinecker, H., Imhoff, J.F., Süssmuth, R.D., and Fiedler, H.-P. (2010). Two new aurachins from Rhodococcus sp. Acta 2259*. J. Antibiot. (Tokyo) *63*, 567–569.

Neises, B., and Steglich, W. (1978). Simple method for the esterification of carboxylic acids. Angew. Chem. Int. Ed. Engl. *17*, 522–524.

Norén, B., and Raper, K.B. (1962). Antibiotic activity of myxobacteria in relation to their bacteriolytic capacity. J. Bacteriol. *84*, 157–162.

O'Neill, A., Oliva, B., Storey, C., Hoyle, A., Fishwick, C., and Chopra, I. (2000). RNA polymerase inhibitors with activity against rifampin-resistant mutants of Staphylococcus aureus. Antimicrob. Agents Chemother. *44*, 3163–3166.

Onishi, N., Izaki, K., and Takahashi, H. (1984). A macrocyclic antibiotic M-230B produced by Myxococcus xanthus. isolation and characterization. J. Antibiot. (Tokyo) *37*, 13–19.

Oxford, A.E. (1947). Observations concerning the growth and metabolic activities of myxococci in a simple protein-free liquid medium. J. Bacteriol. *53*, 129–138.

Peach, K.C., Cheng, A.T., Oliver, A.G., Yildiz, F.H., and Linington, R.G. (2013). Discovery and biological characterization of the auromomycin chromophore as an inhibitor of biofilm formation in Vibrio cholerae. ChemBioChem *14*, 2209–2215.

Peterson, E.A., Gillespie, D.C., and Cook, F.D. (1966). A wide-spectrum antibiotic produced by a species of Sorangium. Can. J. Microbiol. *12*, 221–230.

Pfeifer, B.A., and Khosla, C. (2001). Biosynthesis of polyketides in heterologous hosts. Microbiol. Mol. Biol. Rev. *65*, 106–118.

Piel, J. (2010). Biosynthesis of polyketides by trans-AT polyketide synthases. Nat. Prod. Rep. *27*, 996.

Pistorius, D., Li, Y., Sandmann, A., and Müller, R. (2011). Completing the puzzle of aurachin biosynthesis in Stigmatella aurantiaca Sg a15. Mol. Biosyst. *7*, 3308–3315.

Quade, N., Huo, L., Rachid, S., Heinz, D.W., and Müller, R. (2011). Unusual carbon fixation gives rise to diverse polyketide extender units. Nat. Chem. Biol. *8*, 117–124.

Quadri, L.E.N., Weinreb, P.H., Lei, M., Nakano, M.M., Zuber, P., and Walsh, C.T. (1998). Characterization of Sfp, a *Bacillus subtilis* phosphopantetheinyl transferase for peptidyl carrier protein domains in peptide synthetases. Biochemistry (Mosc.) *37*, 1585–1595.

Rachid, S., Krug, D., Kunze, B., Kochems, I., Scharfe, M., Zabriskie, T.M., Blöcker, H., and Müller, R. (2006). Molecular and biochemical studies of chondramide formation—highly cytotoxic natural products from Chondromyces crocatus Cm c5. Chem. Biol. *13*, 667–681.

Rachid, S., Scharfe, M., Blöcker, H., Weissman, K.J., and Müller, R. (2009). Unusual chemistry in the biosynthesis of the antibiotic chondrochlorens. Chem. Biol. *16*, 70–81.

Rachid, S., Revermann, O., Dauth, C., Kazmaier, U., and Muller, R. (2010). Characterization of a novel type of oxidative decarboxylase involved in the biosynthesis of the styryl moiety of chondrochloren from an acylated tyrosine. J. Biol. Chem. *285*, 12482–12489.

Reck, M., Rutz, K., Kunze, B., Tomasch, J., Surapaneni, S.K., Schulz, S., and Wagner-Dobler, I. (2011). The biofilm inhibitor carolacton disturbs membrane integrity and cell division of Streptococcus mutans through the serine/threonine protein kinase PknB. J. Bacteriol. *193*, 5692–5706.

Rentsch, A., and Kalesse, M. (2012). The total synthesis of corallopyronin A and myxopyronin B. Angew. Chem. Int. Ed. *51*, 11381–11384.

Roblot, G., Wylde, R., Martin, A., and Parello, J. (1993). Regioselective synthesis of inhibitors of histone acetyl transferase covalently linking spermidine to the s-terminus of coenzyme a and fragments. Tetrahedron *49*, 6381–6398.

Rosenberg, E., and Dworkin, M. (1996). Autocides and a paracide, antibiotic TA, produced by Myxococcus xanthus. J. Ind. Microbiol. Biotechnol. *17*, 424–431.

Rosenberg, E., Porter, J.M., Nathan, P.N., Manor, A., and Varon, M. (1984). Antibiotic TA: an adherent antibiotic. Bio/Technology *2*, 796–799.

Sahner, J.H., Groh, M., Negri, M., Haupenthal, J., and Hartmann, R.W. (2013). Novel small molecule inhibitors targeting the “switch region” of bacterial RNAP: structure-based optimization of a virtual screening hit. Eur. J. Med. Chem. *65*, 223–231.

Sakakibara, H., Naganawa, H., Ohno, M., Maeda, K., and Umezawa, H. (1974). The structure of althiomycin. J. Antibiot. (Tokyo) *27*, 897–899.

Sakamoto, T., Li, H., and Kikugawa, Y. (1996). A total synthesis of nannochelin a. a short route to optically active N^{ω}-hydroxy-α-amino acid derivatives. J. Org. Chem. *61*, 8496–8499.

Sandmann, A., Dickschat, J., Jenke-Kodama, H., Kunze, B., Dittmann, E., and Müller, R. (2007). A type II polyketide synthase from the gram-negative bacteriumstigmatella aurantiaca is involved in aurachin alkaloid biosynthesis. Angew. Chem. Int. Ed. *46*, 2712–2716.

Sanger, F., Nicklen, S., and Coulson, A.R. (1977). DNA sequencing with chain-terminating inhibitors. Proc. Natl. Acad. Sci. *74*, 5463–5467.

Schäberle, T.F., and Hack, I.M. (2014). Overcoming the current deadlock in antibiotic research. Trends Microbiol. *22*, 165–167.

Schäberle, T.F., Mir Mohseni, M., Lohr, F., Schmitz, A., and Konig, G.M. (2014a). Function of the loading module in cori and of the o-methyltransferase corh in vinyl carbamate biosynthesis of the antibiotic corallopyronin A. Antimicrob. Agents Chemother. *58*, 950–956.

Schäberle, T.F., Schiefer, A., Schmitz, A., König, G.M., Hoerauf, A., and Pfarr, K. (2014b). Corallopyronin A – a promising antibiotic for treatment of filariasis. Int. J. Med. Microbiol. *304*, 72–78.

Schäberle, T.F., Lohr, F., Schmitz, A., König, G.M. (2014c). Antibiotics from myxobacteria. DOI:10.1039/C4NP00011K

Schiefer, A., Schmitz, A., Schaberle, T.F., Specht, S., Lammer, C., Johnston, K.L., Vassylyev, D.G., Konig, G.M., Hoerauf, A., and Pfarr, K. (2012). Corallopyronin A specifically targets and depletes essential obligate wolbachia endobacteria from filarial nematodes in vivo. J. Infect. Dis. *206*, 249–257.

Schleicher, K.D., and Jamison, T.F. (2013). A reductive coupling strategy towards ripostatin A. Beilstein J. Org. Chem. *9*, 1533–1550.

Schmidt, T., and Kirschning, A. (2012). Total synthesis of carolacton, a highly potent biofilm inhibitor. Angew. Chem. Int. Ed. *51*, 1063–1066.

Schmitz, A. (2013). The corallopyronin A and the corallorazines from the myxobacterium Corallococcus coalloides 035. PhD thesis.

Schmitz, A., Felder, S., Höver, T., Kehraus, S., Neu, E., Lohr, F., König, G.M., and Schäberle, T.F. (2013). Antibiotics from gliding bacteria. Phytochem. Rev. *12*, 507–516.

Silakowski, B., Nordsiek, G., Kunze, B., Blöcker, H., and Müller, R. (2001). Novel features in a combined polyketide synthase/non-ribosomal peptide synthetase: the myxalamid biosynthetic gene cluster of the myxobacterium Stigmatella aurantiaca Sga1511. Chem. Biol. *8*, 59–69.

Simunovic, V., and Müller, R. (2007a). 3-Hydroxy-3-methylglutaryl-coA-like synthases direct the formation of methyl and ethyl side groups in the biosynthesis of the antibiotic myxovirescin A. ChemBioChem *8*, 497–500.

Simunovic, V., and Müller, R. (2007b). Mutational analysis of the myxovirescin biosynthetic gene cluster reveals novel insights into the functional elaboration of polyketide backbones. ChemBioChem *8*, 1273–1280.

Simunovic, V., Zapp, J., Rachid, S., Krug, D., Meiser, P., and Müller, R. (2006). Myxovirescin A biosynthesis is directed by hybrid polyketide synthases/nonribosomal peptide synthetase, 3-hydroxy-3-methylglutaryl-coA synthases, and trans-acting acyltransferases. ChemBioChem *7*, 1206–1220.

Smith, A.B., Dong, S., Brenneman, J.B., and Fox, R.J. (2009). Total synthesis of (+)-sorangicin A. J. Am. Chem. Soc. *131*, 12109–12111.

Spiteller, P., Bai, L., Shang, G., Carroll, B.J., Yu, T.-W., and Floss, H.G. (2003). The post-polyketide synthase modification steps in the biosynthesis of the antitumor agent ansamitocin by *Actinosynnema p retiosum*. J. Am. Chem. Soc. *125*, 14236–14237.

Srivastava, A., Talaue, M., Liu, S., Degen, D., Ebright, R.Y., Sineva, E., Chakraborty, A., Druzhinin, S.Y., Chatterjee, S., Mukhopadhyay, J., et al. (2011). New target for inhibition of bacterial RNA polymerase: “switch region.”Curr. Opin. Microbiol. *14*, 532–543.

Staunton, J., and Wilkinson, B. (1998). The biosynthesis of aliphatic polyketides.

Stec, E., Pistorius, D., Müller, R., and Li, S.-M. (2011). AuaA, a membrane-bound farnesyltransferase from stigmatella aurantiaca, catalyzes the prenylation of 2-methyl-4-hydroxyquinoline in the biosynthesis of aurachins. ChemBioChem *12*, 1724–1730.

Steinmetz, H., Irschik, H., Kunze, B., Reichenbach, H., Höfle, G., and Jansen, R. (2007). Thuggacins, macrolide antibiotics active against mycobacterium tuberculosis: isolation from myxobacteria, structure elucidation, conformation analysis and biosynthesis. Chem. - Eur. J. *13*, 5822–5832.

Steinmetz, H., Mohr, K.I., Zander, W., Jansen, R., Gerth, K., and Müller, R. (2012). Indiacens A and B: prenyl indoles from the myxobacterium Sandaracinus amylolyticus. J. Nat. Prod. *75*, 1803–1805.

Stephan, S., Heinzle, E., Wenzel, S.C., Krug, D., Müller, R., and Wittmann, C. (2006). Metabolic physiology of Pseudomonas putida for heterologous production of myxochromide. Process Biochem. *41*, 2146–2152.

Sucipto, H., Wenzel, S.C., and Müller, R. (2013). Exploring chemical diversity of α-pyrone antibiotics: molecular basis of myxopyronin biosynthesis. ChemBioChem *14*, 1581–1589.

Taft, F., Knobloch, T., Floss, H.G., and Kirschning, A. (2009). Timing of the $\Delta^{10,12}$-$\Delta^{11,13}$ double bond migration during ansamitocin biosynthesis in Actinosynnema pretiosum. J. Am. Chem. Soc. *131*, 3812–3813.

Takayama, S., Yamanaka, S., Miyashiro, S., Yokokawa, Y., and Shibai, H. (1988). Novel macrocyclic antibiotics: megovalicins A, B, C, D, G and H. II. isolation and chemical structures of megovalicins. J. Antibiot. (Tokyo) *41*, 439–445.

Tang, W., and Prusov, E.V. (2012a). Total synthesis of RNA-polymerase inhibitor ripostatin B and 15-deoxyripostatin A. Angew. Chem. Int. Ed. *51*, 3401–3404.

Tang, W., and Prusov, E.V. (2012b). Total synthesis of ripostatin A. Org. Lett. *14*, 4690–4693.

Taylor, M.J., Hoerauf, A., and Bockarie, M. (2010). Lymphatic filariasis and onchocerciasis. The Lancet *376*, 1175–1185.

Thompson, C.A. (2007). FDA approves new breast cancer treatment. Am. J. Health. Syst. Pharm. *64*, 2406–2406.

Tjalsma, H. (1999). The role of lipoprotein processing by signal peptidase II in the Gram-positive eubacterium bacillus subtilis. signal peptidase II is required for the efficient secretion of alpha -amylase, a non-lipoprotein. J. Biol. Chem. *274*, 1698–1707.

Trowitzsch-Kienast, W., Schober, K., Wray, V., Gerth, K., Reichenbach, H., and Höfle, G. (1989). Antibiotika aus gleitenden Bakterien, XLI. Zur Konstitution der myxovirescine B - T und Biogenese des myxovirescins A. Liebigs Ann. Chem. *1989*, 345–355.

Vergnolle, O., Hahn, F., Baerga-Ortiz, A., Leadlay, P.F., and Andexer, J.N. (2011). Stereoselectivity of isolated dehydratase domains of the borrelidin polyketide synthase: implications for cis double-bond formation. ChemBioChem *12*, 1011–1014.

Villain-Guillot, P., Bastide, L., Gualtieri, M., and Leonetti, J.-P. (2007). Progress in targeting bacterial transcription. Drug Discov. Today *12*, 200–208.

Walsh, C.T., Chen, H., Keating, T.A., Hubbard, B.K., Losey, H.C., Luo, L., Marshall, C.G., Miller, D.A., and Patel, H.M. (2001). Tailoring enzymes that modify nonribosomal peptides during and after chain elongation on NRPS assembly lines. Curr. Opin. Chem. Biol. *5*, 525–534.

Wehrli, W., and Staehelo, M. (1971). Actions of rifamycins. Bacteriol. Rev. *35*, 290–309.

Weissman, K.J., and Müller, R. (2009). A brief tour of myxobacterial secondary metabolism. Bioorg. Med. Chem. *17*, 2121–2136.

Wenzel, S.C., Zhang, Y., Fu, J., Stewart, A.F., Müller, R. (2005). Heterologous Expression of a Myxobacterial Natural Products Assembly Line in Pseudomonads via Red/ET Recombineering Chem. Biol. *12*, 349–356

Wenzel, S.C., and Müller, R. (2009). The impact of genomics on the exploitation of the myxobacterial secondary metabolome. Nat. Prod. Rep. *26*, 1385–1407.

Winter, P., Hiller, W., and Christmann, M. (2012). Access to skipped polyene macrolides through ring-closing metathesis: total synthesis of the RNA polymerase inhibitor ripostatin B. Angew. Chem. Int. Ed. *51*, 3396–3400.

Wu, J., Zaleski, T.J., Valenzano, C., Khosla, C., and Cane, D.E. (2005). Polyketide double-bond biosynthesis. mechanistic analysis of the dehydratase-containing module 2 of the picromycin/methymycin polyketide synthase. J. Am. Chem. Soc. *127*, 17393–17404.

Xiao, Y., Gerth, K., Muller, R., and Wall, D. (2012). Myxobacterium-produced antibiotic TA (myxovirescin) inhibits type II signal peptidase. Antimicrob. Agents Chemother. *56*, 2014–2021.

Xu, M., Zhou, Y.N., Goldstein, B.P., and Jin, D.J. (2005). Cross-resistance of Escherichia coli RNA polymerases conferring rifampin resistance to different antibiotics. J. Bacteriol. *187*, 2783–2792.

Yakushiji, F., Miyamoto, Y., Kunoh, Y., Okamoto, R., Nakaminami, H., Yamazaki, Y., Noguchi, N., and Hayashi, Y. (2013). Novel hybrid-type antimicrobial agents targeting the switch region of bacterial RNA polymerase. ACS Med. Chem. Lett. *4*, 220–224.

Yamaguchi, H., Nakayama, Y., Takeda, K., Tawara, K., Maeda, K., Takeuchi, T., and Umezawa, H. (1957). A new antibiotic, althiomycin. J. Antibiot. (Tokyo) *10*, 195–200.

Zander, W., Gerth, K., Mohr, K.I., Kessler, W., Jansen, R., and Müller, R. (2011). Roimatacene: an antibiotic against Gram-negative bacteria isolated from Cystobacter ferrugineus Cb G35 (myxobacteria). Chem. - Eur. J. *17*, 7875–7881.

Zander, W., Irschik, H., Augustiniak, H., Herrmann, M., Jansen, R., Steinmetz, H., Gerth, K., Kessler, W., Kalesse, M., Höfle, G., et al. (2012). Sulfangolids, macrolide sulfate esters from Sorangium cellulosum. Chem. - Eur. J. *18*, 6264–6271.

Zarantonello, P., Leslie, C.P., Ferritto, R., and Kazmierski, W.M. (2002). Total synthesis and semi-synthetic approaches to analogues of antibacterial natural product althiomycin. Bioorg. Med. Chem. Lett. *12*, 561–565.

Zhou, H., Qiao, K., Gao, Z., Meehan, M.J., Li, J.W.-H., Zhao, X., Dorrestein, P.C., Vederas, J.C., and Tang, Y. (2010). Enzymatic synthesis of resorcylic acid lactones by cooperation of fungal iterative polyketide synthases involved in hypothemycin biosynthesis. J. Am. Chem. Soc. *132*, 4530–4531.

Annual report 2012 of the German Centre for Infection Research.

8 Appendix

8.1 Primer sequences

Table 8-1. Primers used for the knock-out approach of the *trans*-AT in the corallopyronin A gene cluster in *Corallococcus coralloides* B035. Template for λ_AT and λ_apra primers: DNA of plasmid pIJ773 and pIJ778 (Gust et al., 2003). Template for Δ_AT_Nachweis primers: DNA of cosmid FJF or genomic DNA of *C. coralloides* B035.

Primer	Sequence (5'–3')	Amplification product
λ_AT_for	AGTGCGCTGTCCTACCTGAAGAGTCAGG AGGCGGGCGTGACTAGTAAAATGCCGGCCTTTGAATG	*aadA*
λ_AT_rev	CATTTCCATGCTCCGGACAGGAAAAGACA CTGCTTAAACACTAGTAAATGTAGGCTGGAGCTGCTTC	
λ_apra_for2	AGTGCGCTGTCCTACCTGAAGAGTCAGGA GGCGGGCGTGGCCGTATTTGCAGTACC	*aac(3)IV*
λ_apra_rev2	CATTTCCATGCTCCGGACAGGAAAAGACA CTGCTTAAACCCGGGCTGCAGGAATTCG	
Δ_AT_Nachweis_for	CAGGGAGCCCAATCGAAAGG	*corA AT* locus
Δ_AT_Nachweis_rev	CCGGAGGCAGGTCGTATTTC	

Table 8-2. Primers used for the heterologous expression approach of the eastern chain of corallopyronin A in Pseudomonas putida KT2440. Template for λ_EcoRV_3 and λ_SpeI_3 primers: DNA of plasmid pIJ778 (Gust et al., 2003). Amplification product *aadA*_EcoRV/SpeI was used to be integrated into cosmid FJ7 by Lamda Red recombineering. Template for Apra_SpeI and Pm_EcoRV primers: DNA of the construct pIB861_apra. Amplification product *pm/xylS/aac(3)IV*_EcoRV/SpeI was used to be integrated into the restricted cosmid FJ7_aadA_EcoRV/SpeI by ligation. Template for λ_for_tet_3 and λ_for_trpE_3 primers: DNA of the cloning construct pGEMT_trpE_tetA. Amplification product *tetA/trpE* was used to be integrated into the recombinant construct FJ7_pm/xylS by Lamda Red recombineering to give the finished construct FJ7_pm/xylS/trpE (54 kb).

Primer	**Sequence (5'–3')**	**Amplification product**
λ_EcoRV_3	TGACTCTTCAGGTAGGACAGCGCACTGAC GACGTACAGCGATATCTGGCGAGCGGCATCTTATTTG	*aadA*
λ_SpeI_3	CGCGATTGACATGTTCACTGGCGGTCAGT ATGGATTGCGACTAGTGACGCCGTTGGATACACCAAGG	
Apra_SpeI_for	ACTAGTTACGGCCCACAGAATG	*pm/xylS/*
Pm_EcoRV_rev	GATATCGCCGCAATTCACATGTTC	*aac(3)IV*
λ_for_tet_3	ATGATTGAACAAGATGGATTGCACGCAG GTTCTCCGGCCGCTTGGCGCCAAGCTATTTAGGTG	*tetA/trpE*
λ_rev_trpE_3	TCAGAAGAACTCGTCAAGAAGGCGATAG AAGGCGATGCGCTGCGAATCACTATAGGGCGAATTGGG	

Table 8-3. Primers used for amplification of the sequences encoding for the proteins CorJ DH*ACP, CorJ ACP, CorJ DH*, CorJ DH*H47A ACP, CorJ DH* D211N ACP. Template: DNA of cosmid FJ7.

Primer	Sequence (5'–3')	Amplification product
corJ_start	TAGAATTCATGACCGTGGAGTCCGACAAGG	*corJ* DH*ACP
corJ_end_ACP	ATAAGCTTTAATGCGGGAGGGAGGGCGCGAA	
ACP_1_upstream	TAGAATTCCCGGTTGCACCGCTCTC	*corJ* ACP
corJ_end_ACP	ATAAGCTTTAATGCGGGAGGGAGGGCGCGAA	
corJ_start	TAGAATTCATGACCGTGGAGTCCGACAAGG	*corJ* DH*
DH_shift_neu	GAAGCTTAATGCACCACGATGCGCTCCAC	
corJ_start	TAGAATTCATGACCGTGGAGTCCGACAAGG	*corJ* DH*H47A ACP
H47A_rev	CCGAGGACGGTGGCGTCCCTCAG	(sequential PCR 1a)
corJ_end_ACP	ATAAGCTTTAATGCGGGAGGGAGGGCGCGAA	*corJ* DH*H47A ACP
H47A_for_neu	CTGAGGGACCACACCGTCCTCGG	(sequential PCR 1b)
corJ_start	TAGAATTCATGACCGTGGAGTCCGACAAGG	*corJ* DH*D211N ACP
DtoN1	CCTCCAGCGCTCCTGAACGGCGTCATCGTCG	(sequential PCR 1a)
corJ_end_ACP	ATAAGCTTTAATGCGGGAGGGAGGGCGCGAA	*corJ* DH*D211N ACP
DtoN2	CGACGATGACGCCGTTCAGGAGCGCTGGAGG	(sequential PCR 1b)

8.2 Protein sequences

8.2.1 Protein sequence of CorJ ACP

MGSSHHHHHHSSGLVPRGSHMASMTGGQQMGRGSEFPVAPLSAGDEVARGVERRLRERVAA
KLGVSVEQVDPARTFMEAGLSSVALVELMTALGTELGAALSPTLVFEFQSPRALALHLAREHAPA
FAPSLP

8.2.2 Protein sequence of CorJ DH*

MGSSHHHHHHSSGLVPRGSHMASMTGGQQMGRGSEFMTVESDKVTTVSSSPGGLLTRRALR
VVGARREDGFTLTHDDPALRDHTVLGQRVLLGVTYASWVLEAGRRHFQDRPPVGLRDLLFHQP
LVLGPGEAARVTVSVRDASFEVSFQLGADAPPVRCATGTFLFDAGAGPTPATLDVARFQREAAR
TTDGVRVYERMRQVAVAYGPALFTVQRTFHRDGEVLGELAVAEEASVGSDWLVPPALLNGVIV
AGAFEPLAARGRPCIPMFVERIVVHQAPGPRCLASSRVRLSNDEVLVLDARLHDASGRTLVELTG
VTLKNVPALGNPFSSSAVAAPPPARAPVAPLSAGDEVARGVERRLRERVAAKLGVSVEQVDPAR
TFMEAGLSSVALVELMTALGTELGAALSPTLVFEFQSPRALALHLAREHAPAFAPSLPH

8.2.3 Protein sequence of CorJ DH*ACP

MGSSHHHHHHSSGLVPRGSHMASMTGGQQMGRGSEFMTVESDKVTTVSSSPGGLLTRRALR
VVGARREDGFTLTHDDPALRDHTVLGQRVLLGVTYASWVLEAGRRHFQDRPPVGLRDLLFHQP
LVLGPGEAARVTVSVRDASFEVSFQLGADAPPVRCATGTFLFDAGAGPTPATLDVARFQREAAR
TTDGVRVYERMRQVAVAYGPALFTVQRTFHRDGEVLGELAVAEEASVGSDWLVPPALLDGVIV
AGAFEPLAARGRPCIPMFVERIVVHQAPGPRCLASSRVRLSNDEVLVLDARLHDASGRTLVELTG
VTLKNVPALGNPFSSSAVAAPPPARAPVAPLSAGDEVARGVERRLRERVAAKLGVSVEQVDPAR
TFMEAGLSSVALVELMTALGTELGAALSPTLVFEFQSPRALALHLAREHAPAFAPSLPH

8.2.4 Protein sequence of CorJ DH*H47A ACP

MGSSHHHHHHSSGLVPRGSHMASMTGGQQMGRGSEFMTVESDKVTTVSSSPGGLLTRRALR
VVGARREDGFTLTHDDPALRDATVLGQRVLLGVTYASWVLEAGRRHFQDRPPVGLRDLLFHQPL
VLGPGEAARVTVSVRDASFEVSFQLGADAPPVRCATGTFLFDAGAGPTPATLDVARFQREAART
TDGVRVYERMRQVAVAYGPALFTVQRTFHRDGEVLGELAVAEEASVGSDWLVPPALLDGVIVA
GAFEPLAARGRPCIPMFVERIVVHQAPGPRCLASSRVRLSNDEVLVLDARLHDASGRTLVELTGV
TLKNVPALGNPFSSSAVAAPPPARAPVAPLSAGDEVARGVERRLRERVAAKLGVSVEQVDPARTF
MEAGLSSVALVELMTALGTELGAALSPTLVFEFQSPRALALHLAREHAPAFAPSLP

8.2.5 Protein sequence of CorJ DH*D211N ACP

MGSSHHHHHHSSGLVPRGSHMASMTGGQQMGRGSEFMTVESDKVTTVSSSPGGLLTRRALR
VVGARREDGFTLTHDDPALRDHTVLGQRVLLGVTYASWVLEAGRRHFQDRPPVGLRDLLFHQP
LVLGPGEAARVTVSVRDASFEVSFQLGADAPPVRCATGTFLFDAGAGPTPATLDVARFQREAAR
TTDGVRVYERMRQVAVAYGPALFTVQRTFHRDGEVLGELAVAEEASVGSDWLVPPALLNGVIV
AGAFEPLAARGRPCIPMFVERIVVHQAPGPRCLASSRVRLSNDEVLVLDARLHDASGRTLVELTG
VTLKNVPALGNPFSSSAVAAPPPARAPVAPLSAGDEVARGVERRLRERVAAKLGVSVEQVDPAR
TFMEAGLSSVALVELMTALGTELGAALSPTLVFEFQSPRALALHLAREHAPAFAPSLPH

8.3 Analytical data of compounds 1, 6, 7, 8, 10, 11 and 12

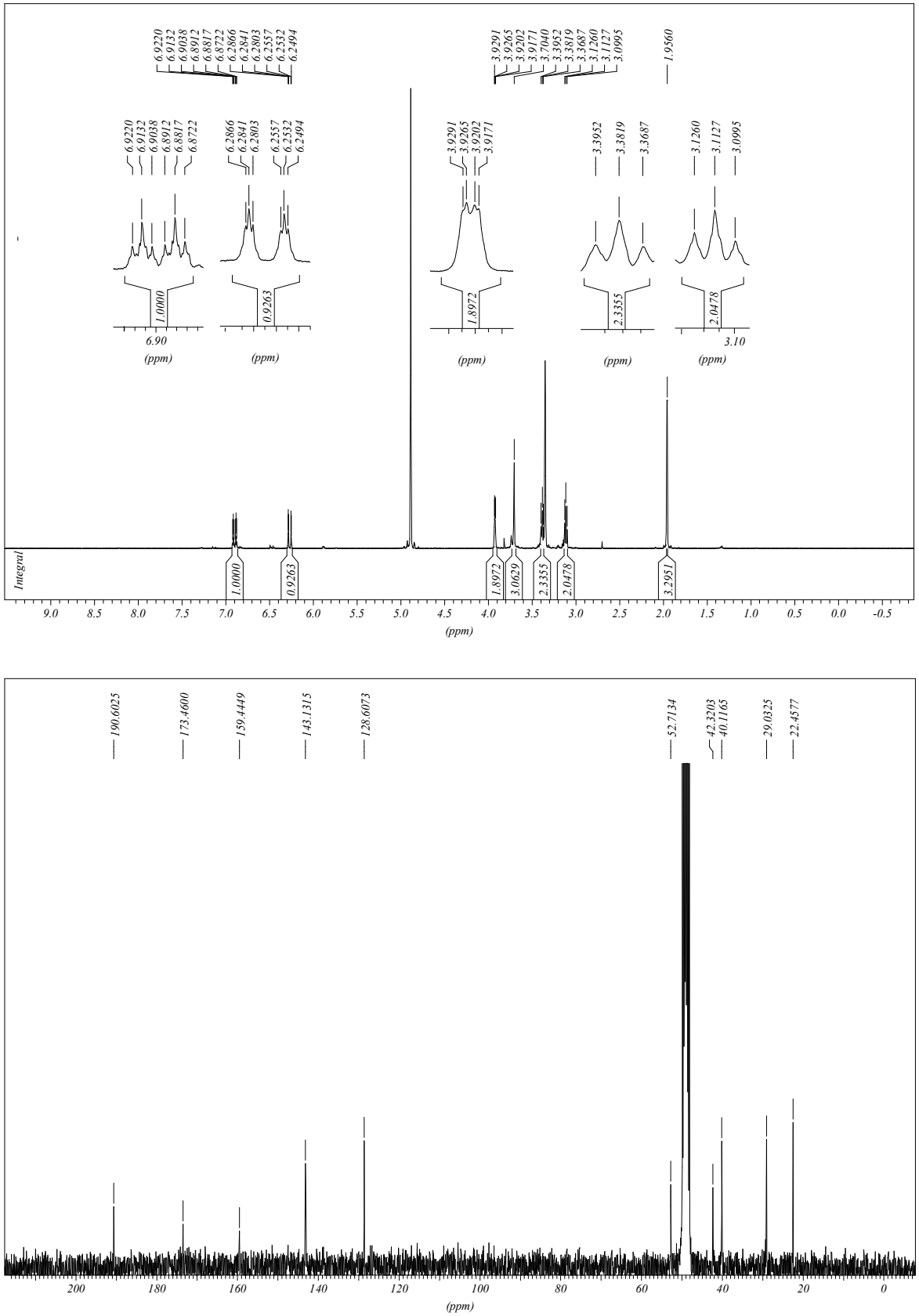

Figure 8-1. ^{1}H and ^{13}C NMR spectra of (*E*)-*S*-2-Acetamidoethyl 4-(methoxycarbonylamino)but-2-enethioate (**1**).

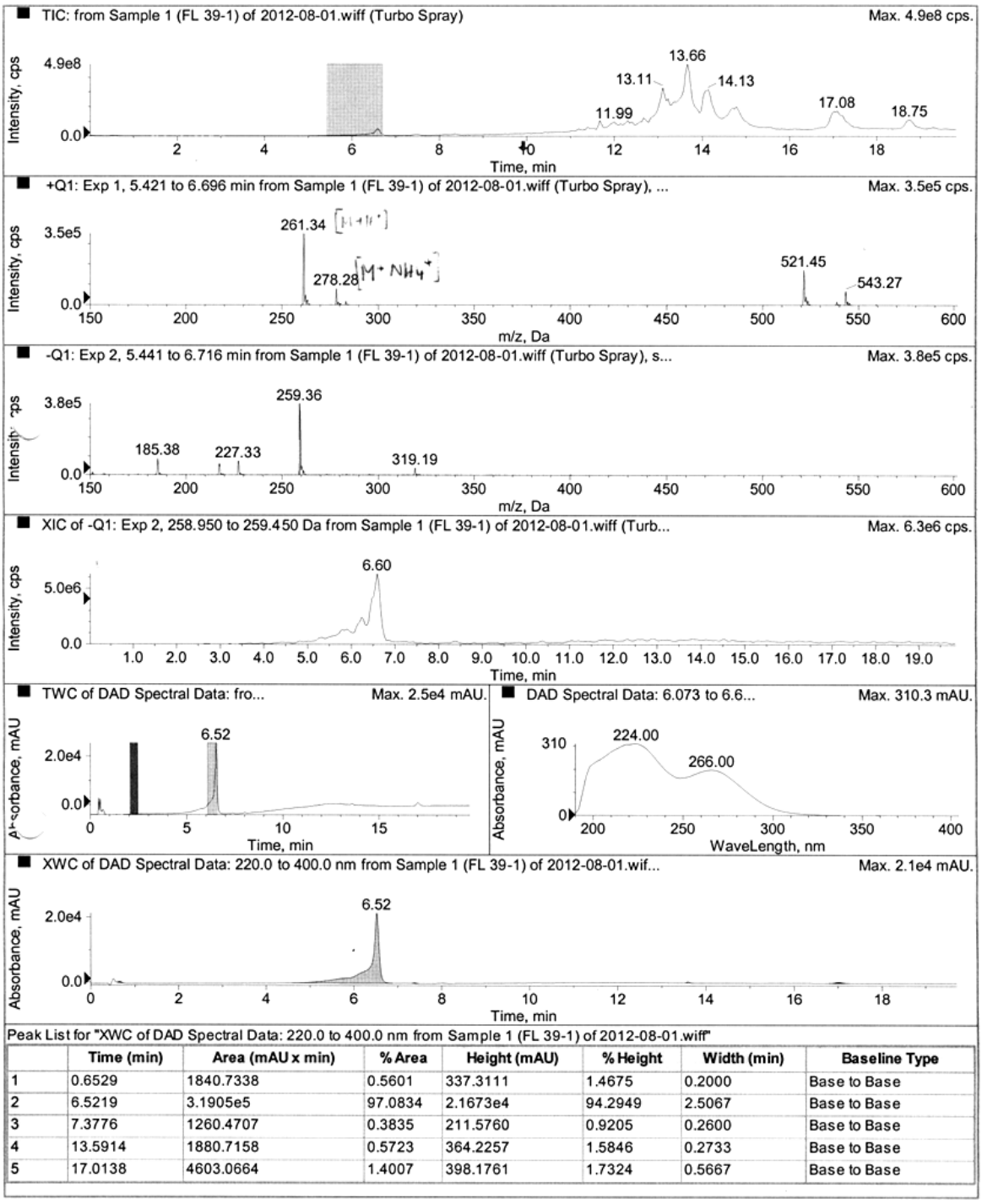

Peak List for "XWC of DAD Spectral Data: 220.0 to 400.0 nm from Sample 1 (FL 39-1) of 2012-08-01.wiff"

	Time (min)	Area (mAU x min)	% Area	Height (mAU)	% Height	Width (min)	Baseline Type
1	0.6529	1840.7338	0.5601	337.3111	1.4675	0.2000	Base to Base
2	6.5219	3.1905e5	97.0834	2.1673e4	94.2949	2.5067	Base to Base
3	7.3776	1260.4707	0.3835	211.5760	0.9205	0.2600	Base to Base
4	13.5914	1880.7158	0.5723	364.2257	1.5846	0.2733	Base to Base
5	17.0138	4603.0664	1.4007	398.1761	1.7324	0.5667	Base to Base

Figure 8-2. Compound **1**, LC-MS(ESI) (90 % H2O to 100 % MeOH in 10 min, then 100% MeOH to 20 min, DAD 220.0– 400.0 nm).

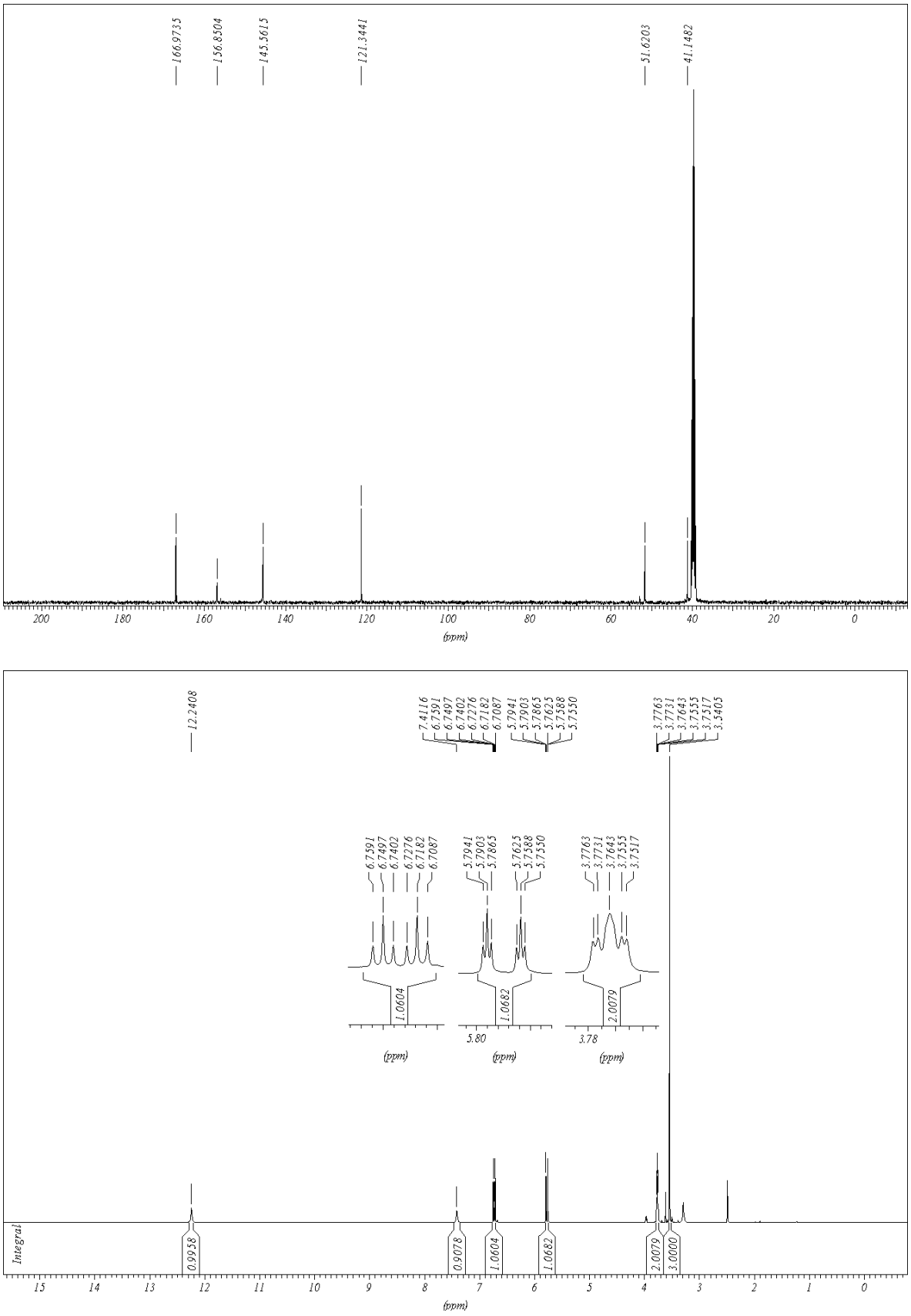

Figure 8-3. ^{1}H and ^{13}C NMR spectra of (E)-4-Methoxycarbonylaminobut 2-enoic acid (**6**) ([D_4]MeOH, 500 MHz).

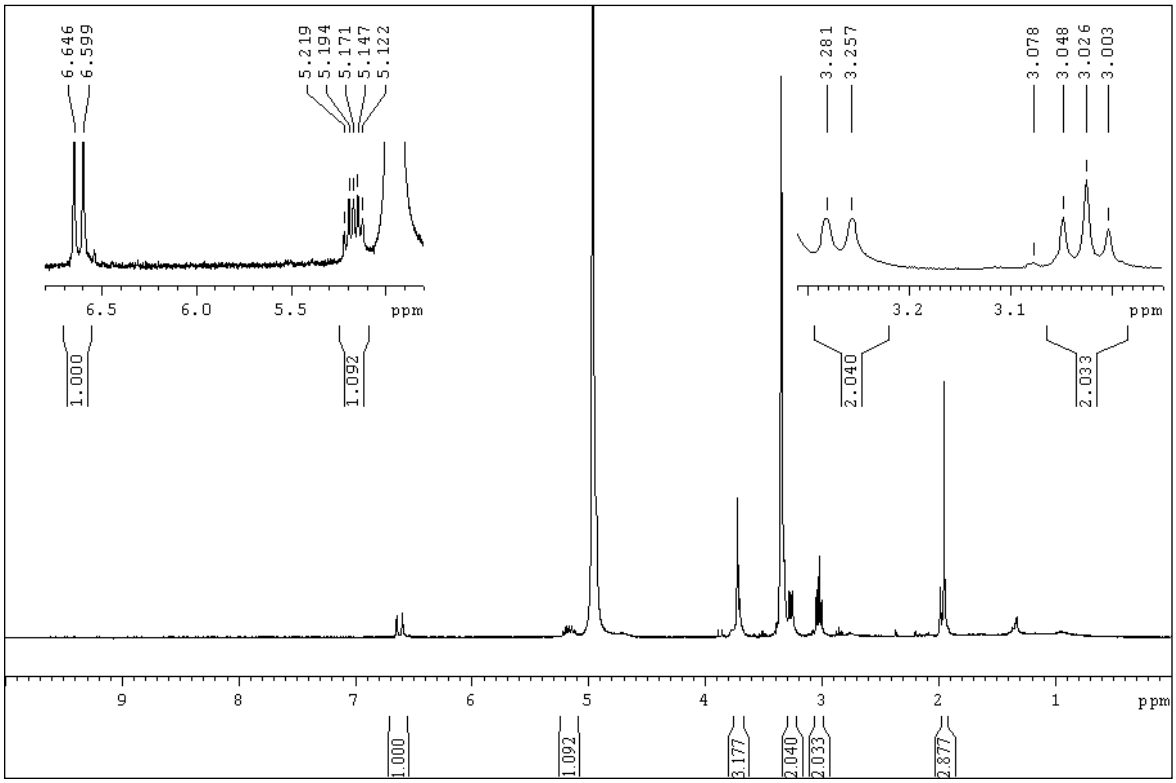

Figure 8-4. ^{1}H spectrum of (E)-S-2-Acetamidoethyl 4-(methoxycarbonylamino)but-3-enethioate (**7**). ([D_4]MeOH, 300 MHz).

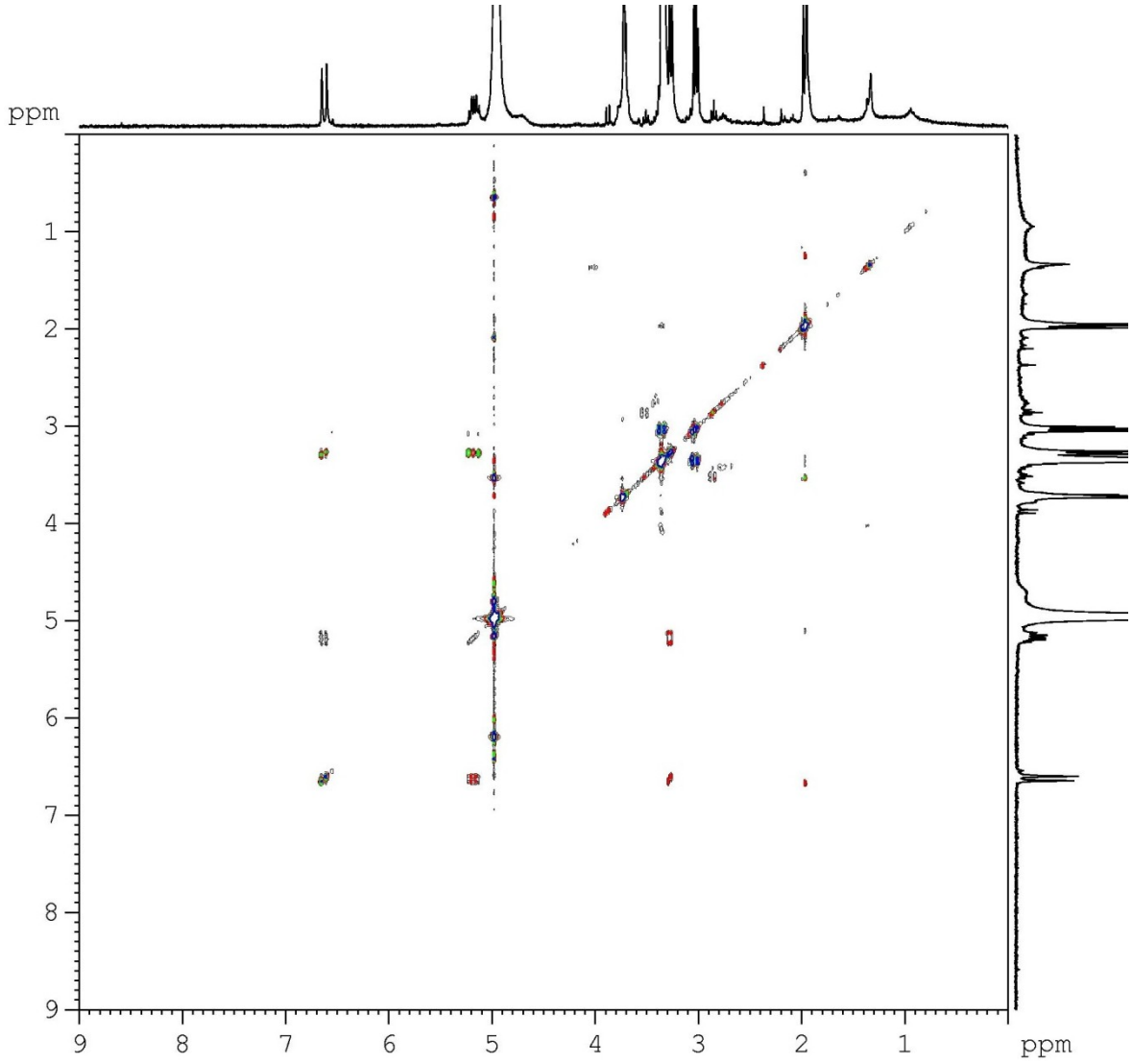

Figure 8-5. Compound **7**, ^{1}H-^{1}H COSY measurement. ([D_4]MeOH, 300 MHz).

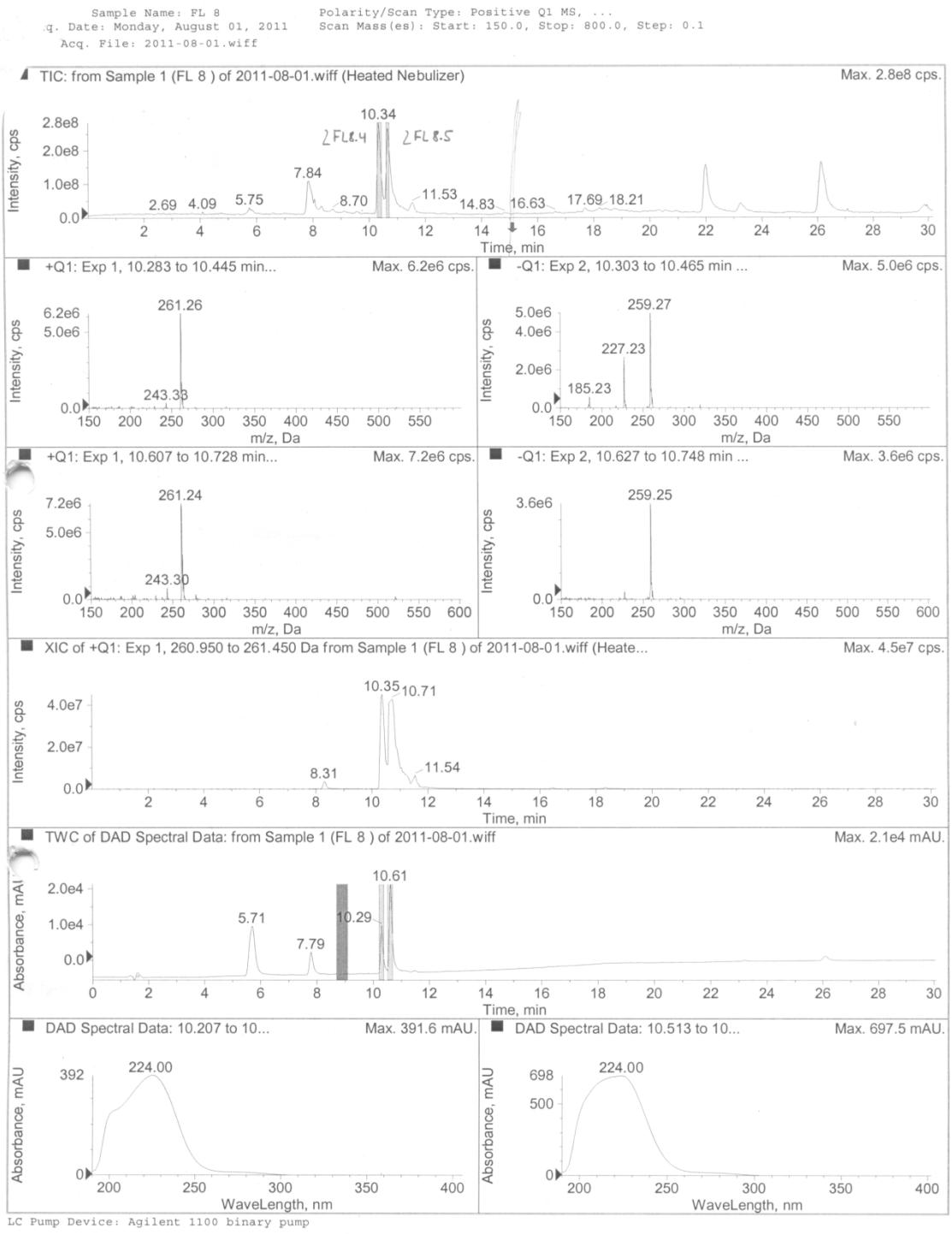

Figure 8-6. LC-MS (ESI) of compound **7**. Column: Phenomenex Luna® 3 µm C18(2); linear gradient from 90 % H_2O to 100 % MeOH in 10 min, then 100 % MeOH to 20 min.

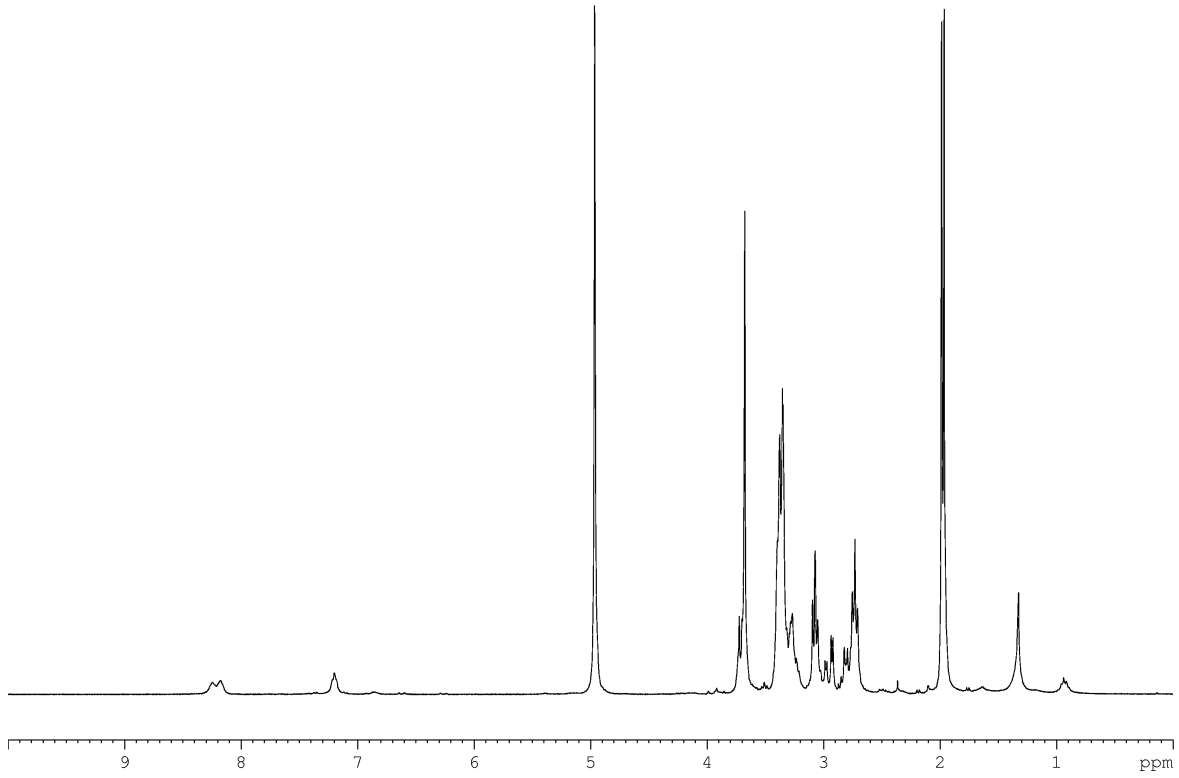

Figure 8-7. ^{1}H and spectrum of **8.** ([D_4]MeOH, 300 MHz).

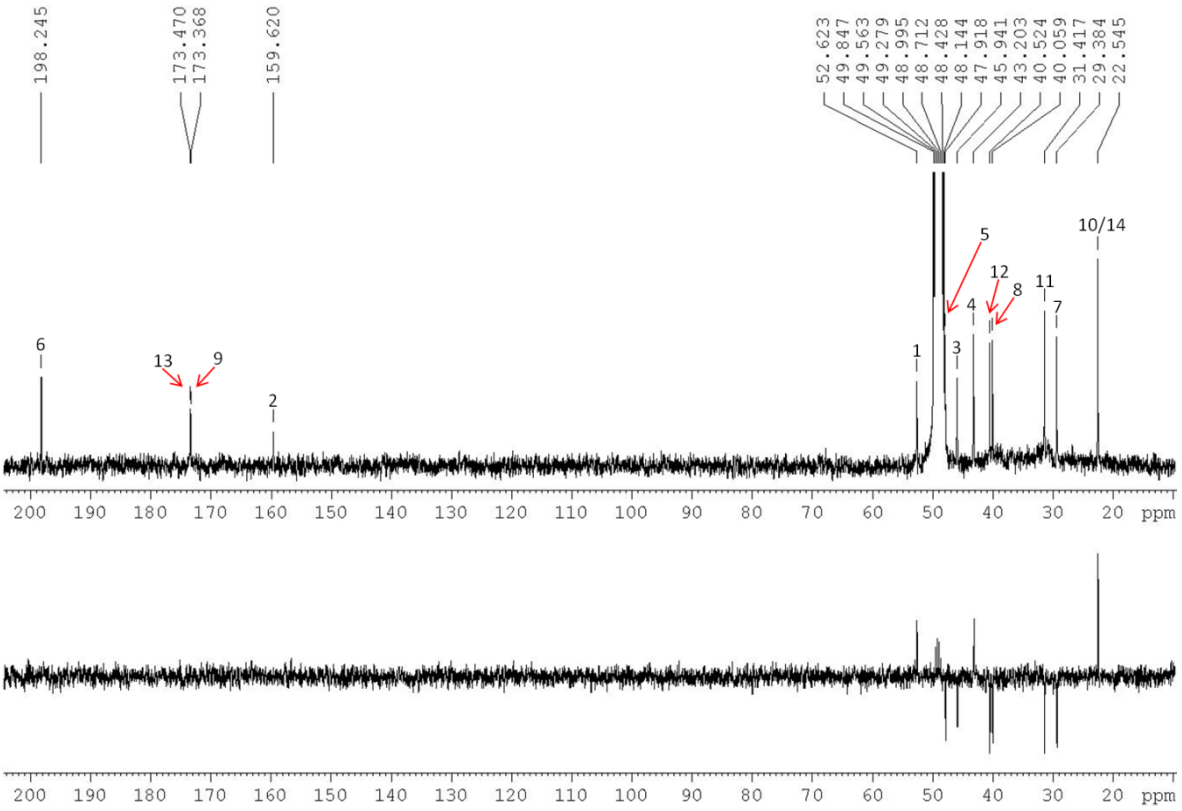

Figure 8-8. Compound **8**, ^{13}C NMR and Dept-135 NMR measurement. ([D_4]MeOH, 300 MHz). Numbers 1–14 represent the carbon atoms in molecule **8**.

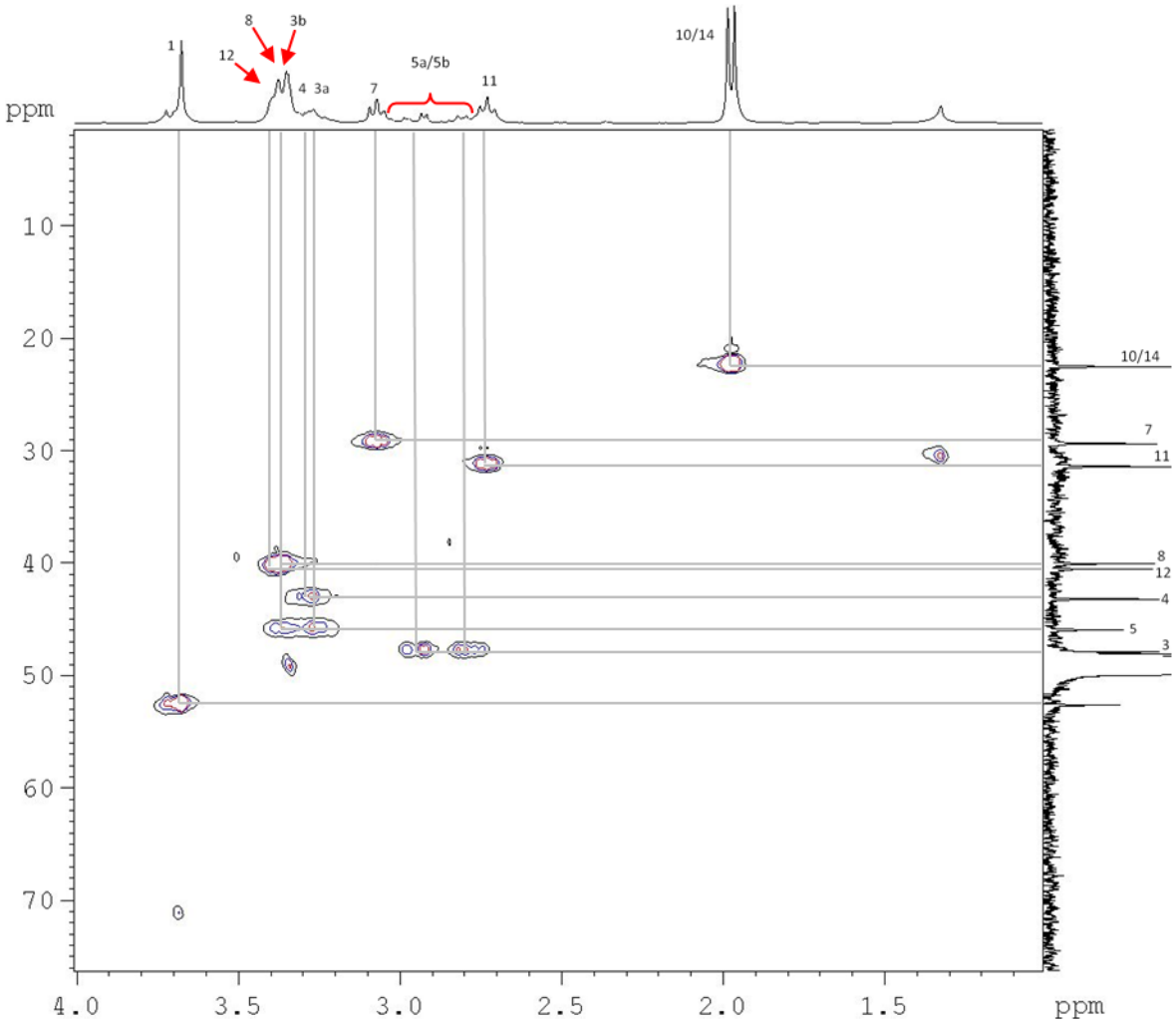

Figure 8-9. Compound **8**, ^{1}H-^{13}C HSQC measurement. ([D_4]MeOH, 300 MHz).

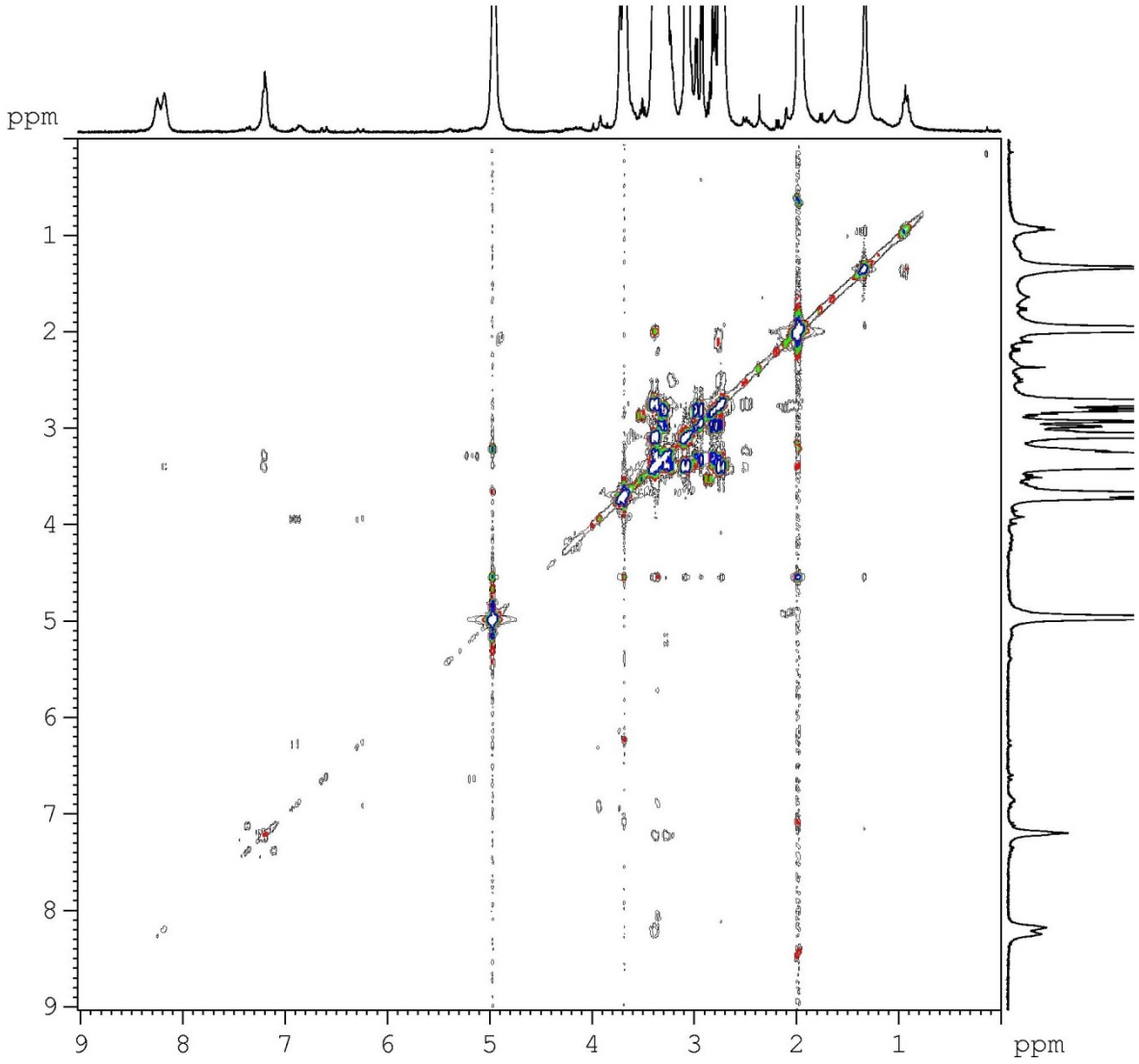

Figure 8-10. Compound **8**, ^{1}H-^{1}H COSY measurement. ([D_4]MeOH, 300 MHz).

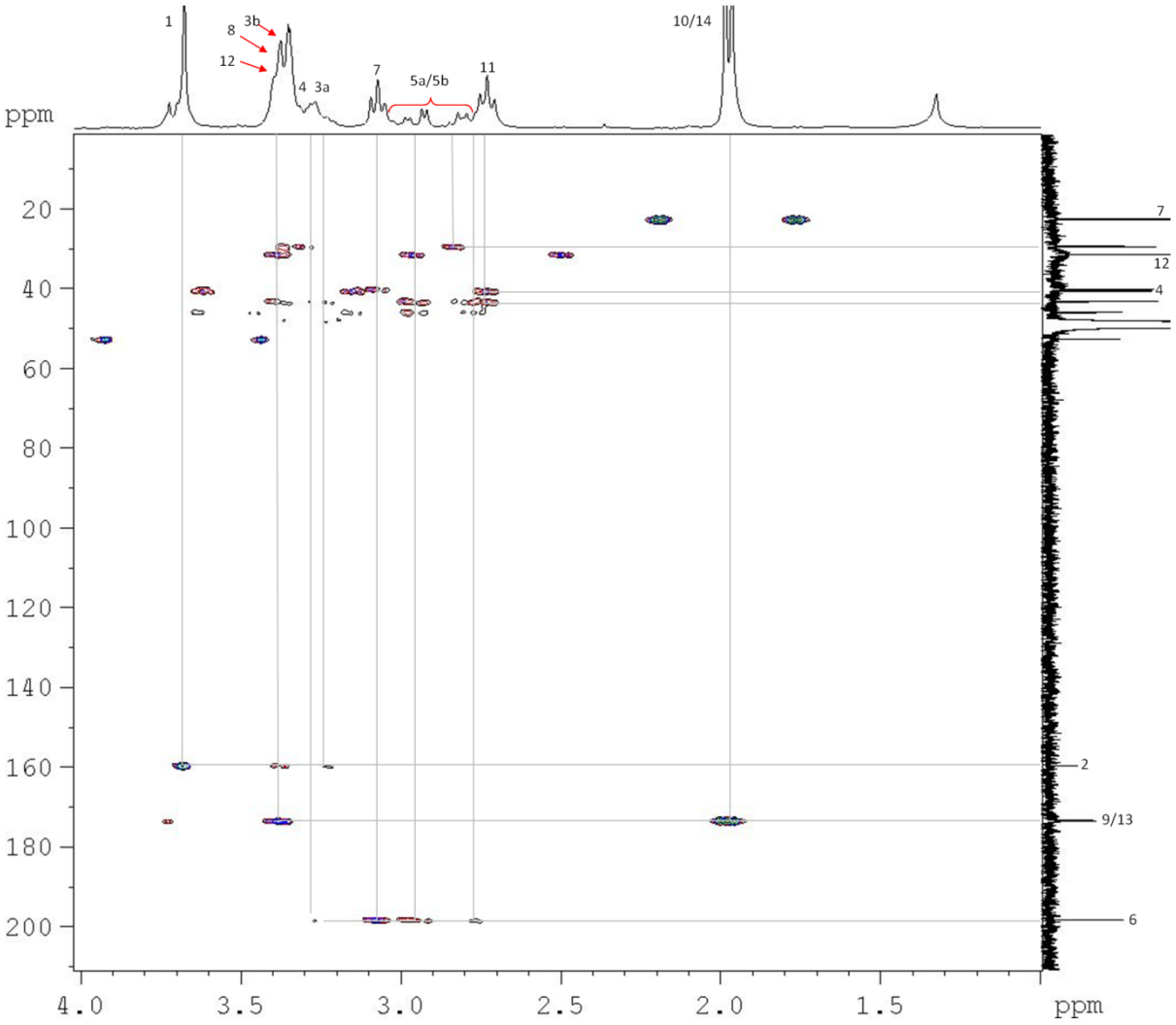

Figure 8-11. Compound **8**, ^{1}H-^{13}C HMBC measurement. ([D_4]MeOH, 300 MHz).

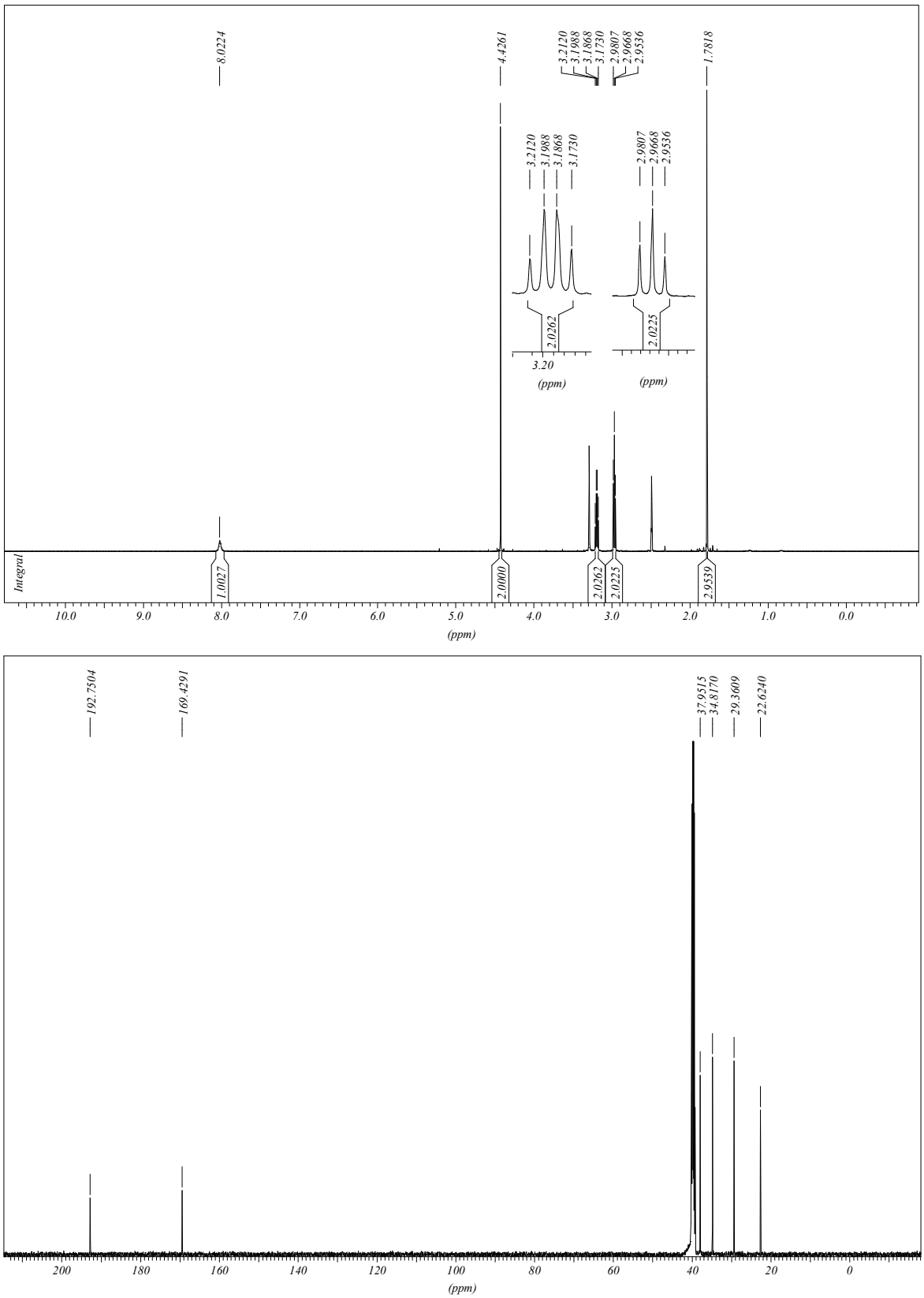

Figure 8-12. ^{1}H and ^{13}C NMR spectra of *S*-2-Acetamidoethyl 2-bromoethanethioate (**10**).

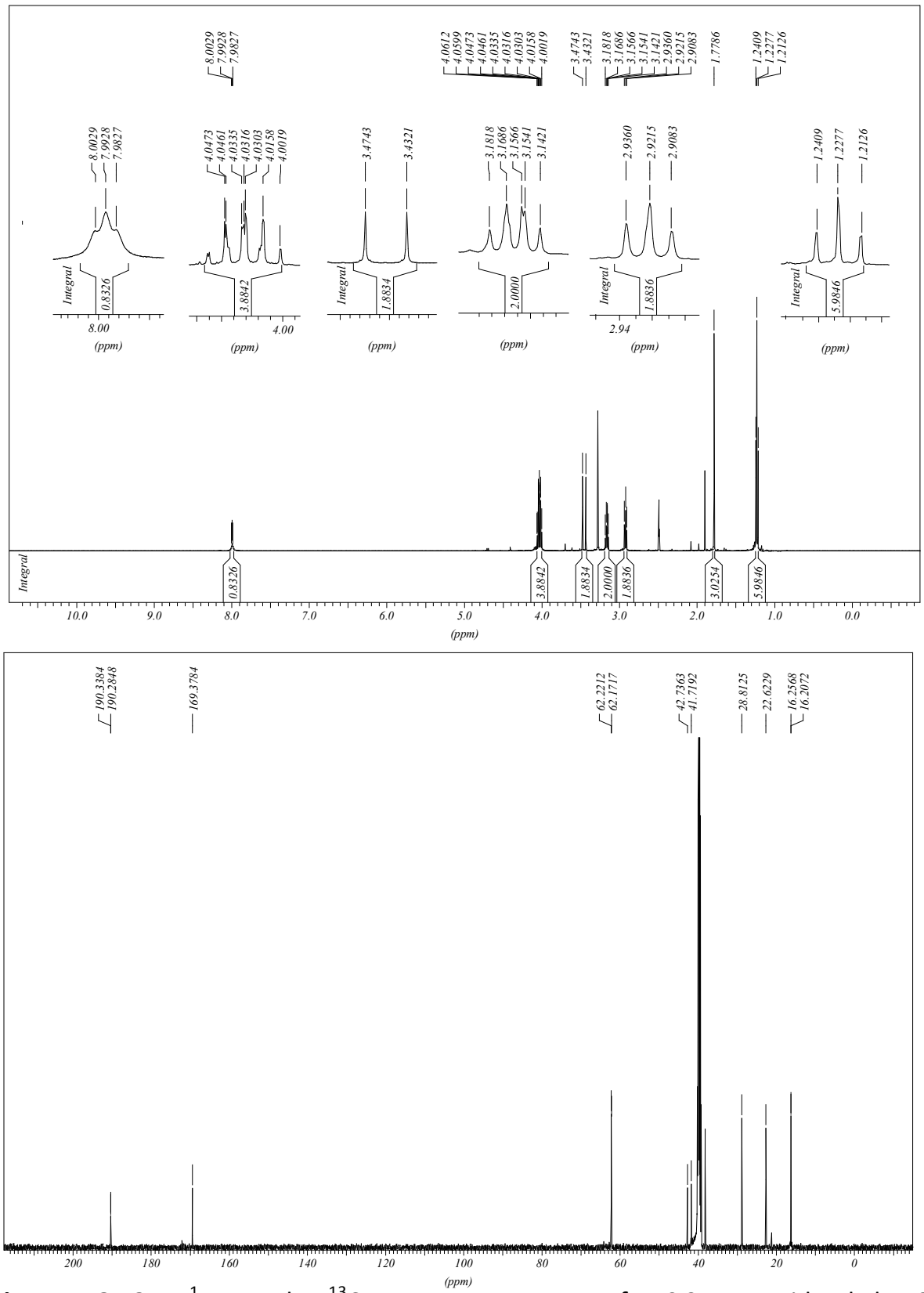

Figure 8-13. ^{1}H and ^{13}C NMR spectra of *S*-2-Acetamidoethyl 2-(diethoxyphosphoryl)ethanethioate (**11**).

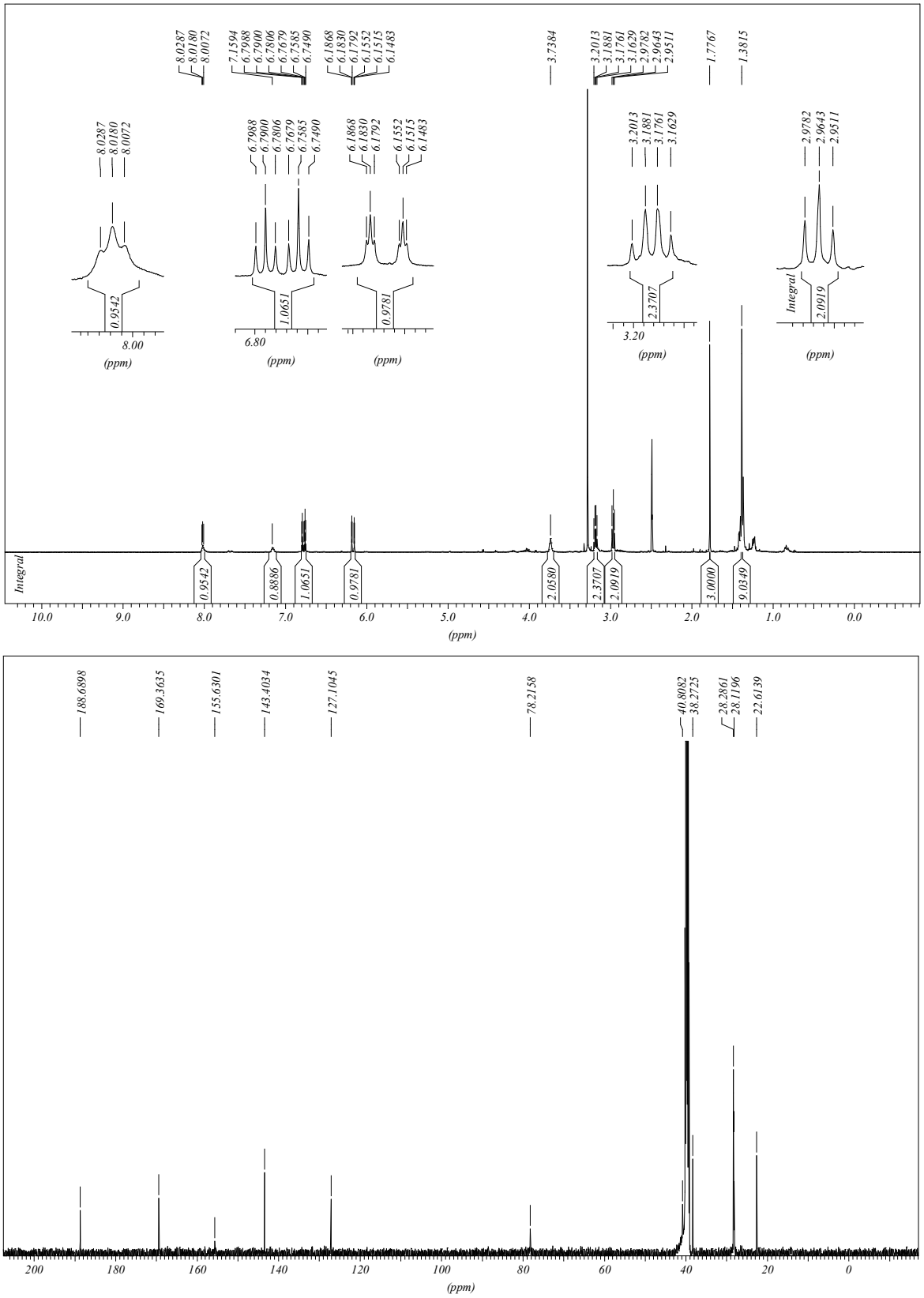

Figure 8-14. ^{1}H and ^{13}C NMR spectra of (*E*)-*S*-2-Acetamidoethyl 4-(tert-butyloxycarbonylamino)but-2-enethioate (**12**).